1
Introduction

1.1 A short history of computer simulation

What is a liquid? As you read this book, you may be mixing up, drinking down, sailing on, or swimming in, a liquid. Liquids flow, although they may be very viscous. They may be transparent or they may scatter light strongly. Liquids may be found in bulk, or in the form of tiny droplets. They may be vaporized or frozen. Life as we know it probably evolved in the liquid phase, and our bodies are kept alive by chemical reactions occurring in liquids. There are many fascinating details of liquid-like behaviour, covering thermodynamics, structure, and motion. Why do liquids behave like this?

The study of the liquid state of matter has a long and rich history, from both the theoretical and experimental standpoints. From early observations of Brownian motion to recent neutron-scattering experiments, experimentalists have worked to improve the understanding of the structure and particle dynamics that characterize liquids. At the same time, theoreticians have tried to construct simple models which explain how liquids behave. In this book, we concentrate exclusively on atomic and molecular models of liquids, and their analysis by computer simulation. For excellent accounts of the current status of liquid science, the reader should consult the standard references (Barker and Henderson, 1976; Rowlinson and Widom, 1982; Barrat and Hansen, 2003; Hansen and McDonald, 2013).

Early models of liquids (Morrell and Hildebrand, 1936) involved the physical manipulation and analysis of the packing of a large number of gelatine balls, representing the molecules; this resulted in a surprisingly good three-dimensional picture of the structure of a liquid, or perhaps a random glass, and later applications of the technique have been described (Bernal and King, 1968). Assemblies of metal ball bearings, kept in motion by mechanical vibration (Pieranski et al., 1978), have been used as models of granular materials and show some analogies with molecular systems (Olafsen and Urbach, 2005). Clearly, the use of large numbers of macroscopic physical objects to represent molecules can be very time-consuming; there are obvious limitations on the types of interactions between them, and the effects of gravity are difficult to eliminate. However, modern research on colloidal suspensions, where the typical particle size lies in the range 1 nm–1000 nm, with the ability to manipulate individual particles and study large-scale collective behaviour, has greatly revitalized the field (Pusey and van Megen, 1986; Ebert et al., 2009; Lekkerkerker and Tuinier, 2011; Bechinger et al., 2013).

Computer Simulation of Liquids. Second Edition. M. P. Allen and D. J. Tildesley.
© M. P. Allen and D. J. Tildesley 2017. Published in 2017 by Oxford University Press.

The natural extension of this approach is to use a mathematical, rather than a physical, model, and to perform the analysis by computer. It is now over 60 years since the first computer simulation of a liquid was carried out at the Los Alamos National Laboratories in the United States (Metropolis et al., 1953). The Los Alamos computer, called MANIAC, was at that time one of the most powerful available; it is a measure of the continuing rapid advance in computer technology that handheld devices of comparable power are now available to all at modest cost.

Rapid development of computer hardware means that computing power continues to increase at an astonishing rate. Using modern parallel computer architectures, we can expect to enjoy exaflop computing by 2020 (an exaflop is 10^{18} floating-point operations per second). This is matched by the enormous increases in data storage available to researchers and the general public. Computer simulations, of the type we describe in this book, are possible on most machines from laptops to continental supercomputers, and we provide an overview of some opportunities with respect to architecture and computing languages, as they relate to the field, in Appendix A.

The very earliest work (Metropolis et al., 1953) laid the foundations of modern Monte Carlo simulation (so-called because of the role that random numbers play in the method). The precise technique employed in this study is still widely used, and is referred to simply as 'Metropolis Monte Carlo'. The original models were highly idealized representations of molecules, such as hard spheres and disks, but, within a few years, Monte Carlo (MC) simulations were carried out on the Lennard-Jones interaction potential (Wood and Parker, 1957) (see Section 1.3). This made it possible to compare data obtained from experiments on, for example, liquid argon, with the computer-generated thermodynamic data derived from a model.

A different technique is required to obtain the dynamic properties of many-particle systems. Molecular dynamics (MD) is the term used to describe the solution of the classical equations of motion (Newton's equations) for a set of molecules. This was first accomplished, for a system of hard spheres, by Alder and Wainwright (1957; 1959). In this case, the particles move at constant velocity between perfectly elastic collisions, and it is possible to solve the dynamic problem without making any approximations, within the limits imposed by machine accuracy. It was several years before a successful attempt was made to solve the equations of motion for a set of Lennard-Jones particles (Rahman, 1964). Here, an approximate, step-by-step procedure is needed, since the forces change continuously as the particles move. Since that time, the properties of the Lennard-Jones model have been thoroughly investigated (Verlet, 1967; 1968; Johnson et al., 1993).

After this initial groundwork on atomic systems, computer simulation developed rapidly. An early attempt to model a diatomic molecular liquid (Harp and Berne, 1968; Berne and Harp, 1970) using molecular dynamics was quickly followed by two ambitious attempts to model liquid water, first by MC (Barker and Watts, 1969), and then by MD (Rahman and Stillinger, 1971). Water remains one of the most interesting and difficult liquids to study by simulation (Morse and Rice, 1982; McCoustra et al., 2009; Lynden-Bell, 2010; Lin et al., 2012). From early studies of small rigid molecules (Barojas et al., 1973) and flexible hydrocarbons (Ryckaert and Bellemans, 1975), simulations have developed to model more complicated systems such as polymers (Binder, 1995), proteins, lipids, nucleic acids, and carbohydrates (Monticelli and Salonen, 2013). Simulations containing half a

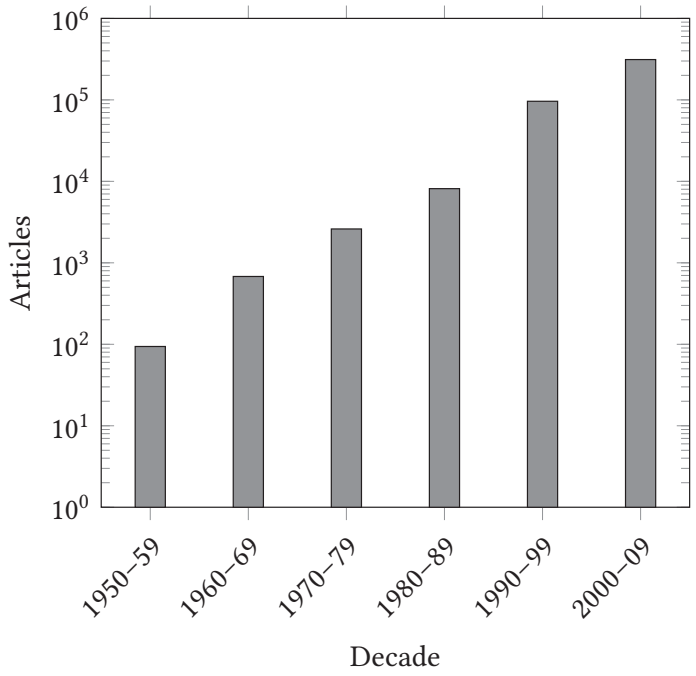

Fig. 1.1 The approximate number of articles concerning the computer simulation of condensed phases published in each complete decade. The search was carried out using the Web of Science® by searching on Monte Carlo, molecular dynamics, Brownian dynamics, lattice Boltzmann, dynamical density functional theory, Car–Parrinello, QM/MM in both the TITLE and TOPIC search fields.

million atoms have been conducted for 50 million timesteps to study the surface tension of a small liquid droplet (van Giessen and Blokhuis, 2009) and the massive parallel molecular dynamics code, ls1 mardyn, has been used to simulate a trillion Lennard-Jones atoms (Niethammer et al., 2014). It is now possible to follow the folding of a solvated protein using simulations in the microsecond-to-millisecond range (ca. 10^9–10^{12} timesteps) on a special purpose computer (Piana et al., 2014).

The growth of the field of computer simulation over the last 60 years, as evidenced by the number of publications in refereed journals, has been dramatic. In Fig. 1.1, we have attempted to calculate the number of papers published in this field during each complete decade. While bibliometric exercises of this kind will fail to capture some important papers and will often include some unwanted papers in related disciplines, the overall trend in the number of articles is clear.

This is, in part, due to the continuing and substantial increase in computing power, which follows the celebrated Moore's law curve over this period (see Appendix A). It is also due to the application of these methods to a wide range of previously intractable problems in the materials and life sciences. However, it is also, in no small part, due to the ingenuity of its practitioners in extending the early methods to areas such as: the calculation of free energies and phase diagrams (Chapter 9); the simulation of rare events (Chapter 10); the development of nonequilibrium methods for calculating transport coefficients (Chapter 11); the development of coarse-grained methods to extend the length and timescales that can be simulated (Chapter 12); and in the extension to include

quantum mechanical effects (Chapter 13). This level of activity points to the proposition that computer simulation now sits alongside experiment and theory as a third and equally important tool in modern science. We start by asking: what is a computer simulation? How does it work? What can it tell us?

1.2 Computer simulation: motivation and applications

Some problems in statistical mechanics are exactly soluble. By this, we mean that a complete specification of the microscopic properties of a system (such as the Hamiltonian of an idealized model like the perfect gas or the Einstein crystal) leads directly, and perhaps easily, to a set of useful results or macroscopic properties (such as an equation of state like $PV = Nk_{\mathrm{B}}T$). There are only a handful of non-trivial, exactly soluble problems in statistical mechanics (Baxter, 1982); the two-dimensional Ising model is a famous example.

Some problems in statistical mechanics, while not being exactly soluble, succumb readily to an analysis based on a straightforward approximation scheme. Computers may have an incidental, calculational, part to play in such work; for example, in the evaluation of cluster integrals in the virial expansion for dilute, imperfect gases (Rosenbluth and Rosenbluth, 1954; Wheatley, 2013). The problem is that, like the virial expansion, many 'straightforward' approximation schemes simply do not work when applied to liquids. For some liquid properties, it may not even be clear how to begin constructing an approximate theory in a reasonable way. The more difficult and interesting the problem, the more desirable it becomes to have exact results available, both to test existing approximate methods and to point the way towards new approaches. It is also important to be able to do this without necessarily introducing the additional question of how closely a particular model (which may be very idealized) mimics a real liquid, although this may also be a matter of interest. Computer simulations have a valuable role to play in providing essentially exact results for problems in statistical mechanics which would otherwise only be soluble by approximate methods, or might be quite intractable. In this sense, computer simulation is a test of theories and, historically, simulations have indeed discriminated between well-founded approaches, such as integral equation theories (Hansen and McDonald, 2013), and ideas that are plausible but, in the event, less successful, such as the old cell theories of liquids (Lennard-Jones and Devonshire, 1939a,b). The results of computer simulations may also be compared with those of real experiments. In the first place, this is a test of the underlying model used in a computer simulation. Eventually, if the model is a good one, the simulator hopes to offer insights to the experimentalist, and assist in the interpretation of new results. This dual role of simulation, as a bridge between models and theoretical predictions on the one hand, and between models and experimental results on the other, is illustrated in Fig. 1.2. Because of this connection role, and the way in which simulations are conducted and analysed, these techniques are often termed 'computer experiments'.

Computer simulation provides a direct route from the microscopic details of a system (the masses of the atoms, the interactions between them, molecular geometry, etc.) to macroscopic properties of experimental interest (the equation of state, transport coefficients, structural order parameters, and so on). As well as being of academic interest, this type of information is technologically useful. It may be difficult or impossible to carry out experiments under extremes of temperature and pressure, while a computer simulation

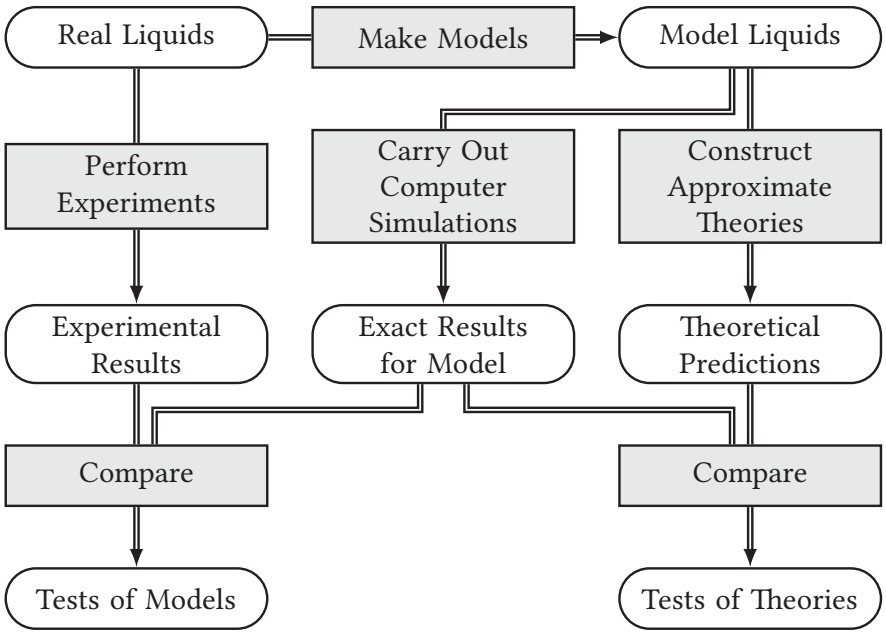

Fig. 1.2 The connection between experiment, theory, and computer simulation.

of the material in, say, a shock wave, a high-temperature plasma, a nuclear reactor, or a planetary core, would be perfectly feasible. Quite subtle details of molecular motion and structure, for example in heterogeneous catalysis, fast ion conduction, or enzyme action, are difficult to probe experimentally but can be extracted readily from a computer simulation. Finally, while the speed of molecular events is itself an experimental difficulty it represents no hindrance to the simulator. A wide range of physical phenomena, from the molecular scale to the galactic (Hockney and Eastwood, 1988), may be studied using some form of computer simulation.

In most of this book, we will be concerned with the details of carrying out simulations (the central box in Fig. 1.2). In the rest of this chapter, however, we deal with the general question of how to put information in (i.e. how to define a model of a liquid) while in Chapter 2 we examine how to get information out (using statistical mechanics).

1.3 Model systems and interaction potentials

1.3.1 Introduction

In most of this book, the microscopic state of a system may be specified in terms of the positions and momenta of a constituent set of particles: the atoms and molecules. Within the Born–Oppenheimer (BO) approximation (see also Chapter 13), it is possible to express the Hamiltonian of a system as a function of the nuclear variables, the (rapid) motion of the electrons having been averaged out. Making the additional approximation that a classical description is adequate, we may write the Hamiltonian $\mathcal{H}$ of a system of N molecules as a sum of kinetic- and potential-energy functions of the set of coordinates $\mathbf{q}_i$

and momenta $\mathbf{p}_i$ of each molecule i. Adopting a condensed notation

$$\mathbf{q} = (\mathbf{q}_1, \mathbf{q}_2, \cdots, \mathbf{q}_N) \tag{1.1a}$$

$$\mathbf{p} = (\mathbf{p}_1, \mathbf{p}_2, \cdots, \mathbf{p}_N) \tag{1.1b}$$

we have

$$\mathcal{H}(\mathbf{q}, \mathbf{p}) = \mathcal{K}(\mathbf{p}) + \mathcal{V}(\mathbf{q}). \tag{1.2}$$

Usually, the Hamiltonian will be equal to the total internal energy E of the system. The generalized coordinates $\mathbf{q}_i$ may simply be the set of Cartesian coordinates $\mathbf{r}_i$ of each atom (or nucleus) in the system, but, as we shall see, it is sometimes useful to treat molecules as rigid bodies, in which case $\mathbf{q}$ will consist of the Cartesian coordinates of each molecular centre of mass together with a set of variables $\boldsymbol{\Omega}_i$ that specify molecular orientation. In any case, $\mathbf{p}$ stands for the appropriate set of conjugate momenta. For a simple atomic system, the kinetic energy $\mathcal{K}$ takes the form

$$\mathcal{K} = \sum_{i=1}^{N} \sum_{\alpha} p_{i\alpha}^2 / 2m_i \tag{1.3}$$

where m_i is the molecular mass, and the index α runs over the different (x, y, z) components of the momentum of atom i. The potential energy $\mathcal{V}$ contains the interesting information regarding intermolecular interactions: assuming that $\mathcal{V}$ is fairly sensibly behaved, it will be possible to construct, from $\mathcal{H}$, an equation of motion (in Hamiltonian, Lagrangian, or Newtonian form) which governs the entire time-evolution of the system and all its mechanical properties (Goldstein, 1980). Solution of this equation will generally involve calculating, from $\mathcal{V}$, the forces $\mathbf{f}_i$ and torques $\boldsymbol{\tau}_i$ acting on the molecules (see Chapter 3). The Hamiltonian also dictates the equilibrium distribution function for molecular positions and momenta (see Chapter 2). Thus, generally, it is $\mathcal{H}$ (or $\mathcal{V}$) which is the basic input to a computer simulation program. The approach used almost universally in computer simulation is to separate the potential energy into terms involving pairs, triplets, etc. of molecules. In the following sections we shall consider this in detail.

Recently, there has been a spectacular growth in the number of simulation studies which avoid the use of effective potentials by considering the electrons explicitly using density functional theory (Martin, 2008). In an early approach, the electron density was represented by an extension of the electron gas theory (LeSar and Gordon, 1982; 1983; LeSar, 1984). In most of the current work, the electronic degrees of freedom are explicitly included in the description. The electrons, influenced by the external field of the nuclei, are allowed to evolve during the course of the simulation by an auxiliary set of dynamical equations (Car and Parrinello, 1985). This method, known as *ab initio* molecular dynamics (Marx and Hutter, 2012), is now sufficiently well developed that it may become the method of choice for simulations in materials and the life sciences as the speed of computers increases. We will consider this approach in more detail in Chapter 13.

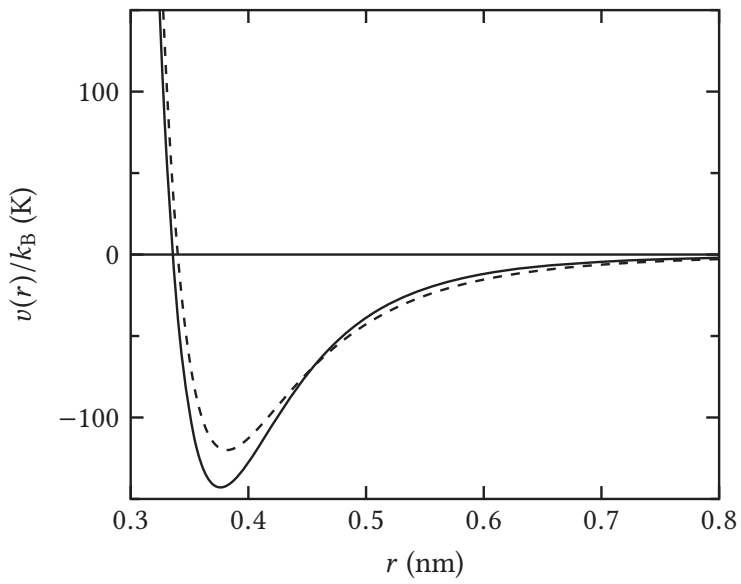

Fig. 1.3 Argon pair potentials. We illustrate (solid line) a recent pair potential for argon calculated by *ab initio* methods (see Patkowski and Szalewicz, 2010). Also shown is the Lennard-Jones 12–6 potential (dashed line) used in computer simulations of liquid argon.

1.3.2 Atomic systems

Consider first the case of a system containing N atoms. The potential energy may be divided into terms depending on the coordinates of individual atoms, pairs, triplets, etc.:

$$\mathcal{V} = \sum_i v_1(\mathbf{r}_i) + \sum_i \sum_{j>i} v_2(\mathbf{r}_i, \mathbf{r}_j) + \sum_i \sum_{j>i} \sum_{k>j} v_3(\mathbf{r}_i, \mathbf{r}_j, \mathbf{r}_k) + \ldots . \tag{1.4}$$

The $\sum_i \sum_{j>i}$ notation indicates a summation over all distinct pairs i and j without counting any pair twice (i.e. as ij and ji); the same care must be taken for triplets. The first term in eqn (1.4), $v_1(\mathbf{r}_i)$, represents the effect of an external field (including, e.g. the container walls) on the system. The remaining terms represent particle interactions. The second term, v_2, the pair potential, is the most important. The pair potential depends only on the magnitude of the pair separation $r_{ij} = |\mathbf{r}_{ij}| = |\mathbf{r}_i - \mathbf{r}_j|$, so it may be written $v_2(r_{ij})$. Figure 1.3 shows one of the more recent estimates for the pair potential between two argon atoms, as a function of separation (Patkowski and Szalewicz, 2010). This potential was determined by fitting to very accurate *ab initio* calculations for the argon dimer. The potential provides a position for the minimum and a well-depth that are very close to the experimental values. It can be used to calculate the spectrum of the isolated argon dimer and it produces a rotational constant and dissociation energy that are in excellent agreement with experiment (Patkowski et al., 2005). In fact, the computed potential is accurate enough to cast some doubt on the recommended, experimental, values of the second virial coefficient of argon at high temperatures (Dymond and Smith, 1980).

The potential shows the typical features of intermolecular interactions. There is an attractive tail at large separations, essentially due to correlation between the electron clouds surrounding the atoms ('van der Waals' or 'London' dispersion). In addition, for

charged species, Coulombic terms would be present. There is a negative well, responsible for cohesion in condensed phases. Finally, there is a steeply rising repulsive wall at short distances, due to non-bonded overlap between the electron clouds.

The v_3 term in eqn (1.4), involving triplets of molecules, is undoubtedly significant at liquid densities. Estimates of the magnitudes of the leading, triple-dipole, three-body contribution (Axilrod and Teller, 1943) have been made for inert gases in their solid-state face centred cubic (FCC) lattices (Doran and Zucker, 1971; Barker and Henderson, 1976). It is found that up to 10 % of the lattice energy of argon (and more in the case of more polarizable species) may be due to these non-additive terms in the potential; we may expect the same order of magnitude to hold in the liquid phase. Four-body (and higher) terms in eqn (1.4) are expected to be small in comparison with v_2 and v_3.

Despite the size of three-body terms in the potential, they are only rarely included in computer simulations (Barker et al., 1971; Attard, 1992; Marcelli and Sadus, 2012). This is because, as we shall see shortly, the calculation of any quantity involving a sum over triplets of molecules will be very time-consuming on a computer. In most cases, the pairwise approximation gives a remarkably good description of liquid properties because the average three-body effects can be partially included by defining an 'effective' pair potential. To do this, we rewrite eqn (1.4) in the form

$$\mathcal{V} \approx \sum_i v_1(\mathbf{r}_i) + \sum_i \sum_{j>i} v_2^{\text{eff}}(r_{ij}). \tag{1.5}$$

The pair potentials appearing in computer simulations are generally to be regarded as effective pair potentials of this kind, representing all the many-body effects; for simplicity, we will just use the notation $v(r_{ij})$, or $v(r)$. A consequence of this approximation is that the effective pair potential needed to reproduce experimental data may turn out to depend on the density, temperature, etc., while the true two-body potential $v_2(r_{ij})$, of course, does not.

Now we turn to the simpler, more idealized, pair potentials commonly used in computer simulations. These reflect the salient features of real interactions in a general, often empirical, way. Illustrated, with the accurate argon pair potential, in Fig. 1.3 is a simple Lennard-Jones 12–6 potential

$$v^{\text{LJ}}(r) = 4\epsilon\left[(\sigma/r)^{12} - (\sigma/r)^{6}\right] \tag{1.6}$$

which provides a reasonable description of the properties of argon, via computer simulation, if the parameters ϵ and σ are chosen appropriately. The potential has a long-range attractive tail of the form $-1/r^6$, a negative well of depth ϵ, and a steeply rising repulsive wall at distances less than $r \sim \sigma$. The well-depth is often quoted in units of temperature as ϵ/k_{B}, where k_{B} is Boltzmann's constant; values of $\epsilon/k_{\text{B}} = 120\,\text{K}$ and $\sigma = 0.34\,\text{nm}$ provide reasonable agreement with the experimental properties of liquid argon. Once again, we must emphasize that these are not the values which would apply to an isolated pair of argon atoms, as is clear from Fig. 1.3.

For the purposes of investigating general properties of liquids, and for comparison with theory, highly idealized pair potentials may be of value. In Fig. 1.4, we illustrate three

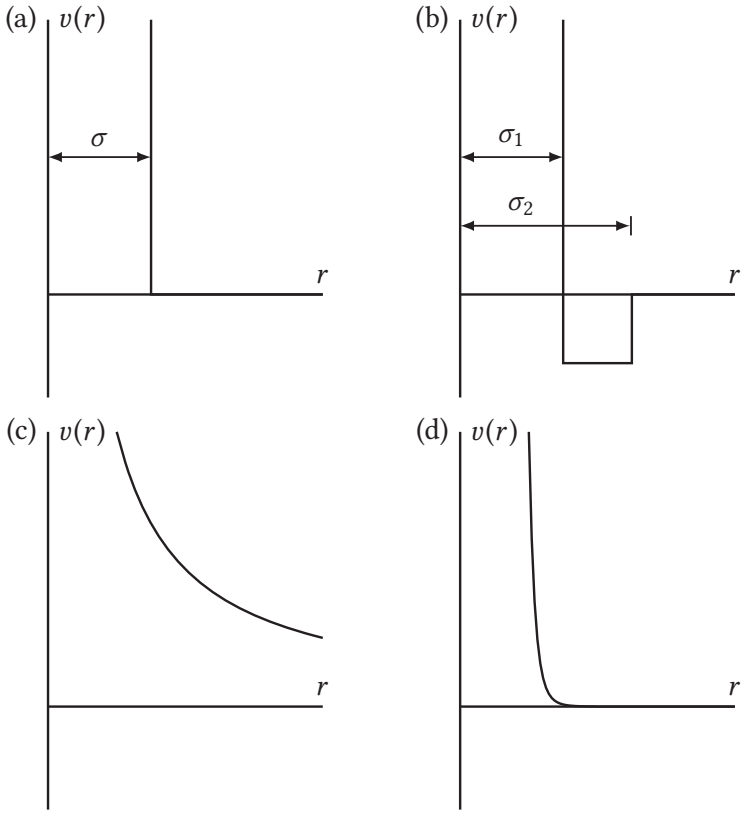

Fig. 1.4 Idealized pair potentials. (a) The hard-sphere potential; (b) the square-well potential; (c) The soft-sphere potential with repulsion parameter $\nu = 1$; (d) The soft-sphere potential with repulsion parameter $\nu = 12$. Vertical and horizontal scales are arbitrary.

forms which, although unrealistic, are very simple and convenient to use in computer simulation and in liquid-state theory. These are: the hard-sphere potential

$$v^{\mathrm{HS}}(r) = \begin{cases} \infty & \text{if } r < \sigma \\ 0 & \text{if } \sigma \leq r; \end{cases} \tag{1.7}$$

the square-well potential

$$v^{\mathrm{SW}}(r) = \begin{cases} \infty & \text{if } r < \sigma_1 \\ -\epsilon, & \text{if } \sigma_1 \leq r < \sigma_2 \\ 0, & \text{if } \sigma_2 \leq r; \end{cases} \tag{1.8}$$

and the soft-sphere potential

$$v^{\mathrm{SS}}(r) = \epsilon(\sigma/r)^{\nu} = ar^{-\nu}, \tag{1.9}$$

where ν is a parameter, often chosen to be an integer. The soft-sphere potential becomes progressively 'harder' as ν is increased. Soft-sphere potentials contain no attractive part. It is often useful to divide more realistic potentials into separate attractive and repulsive

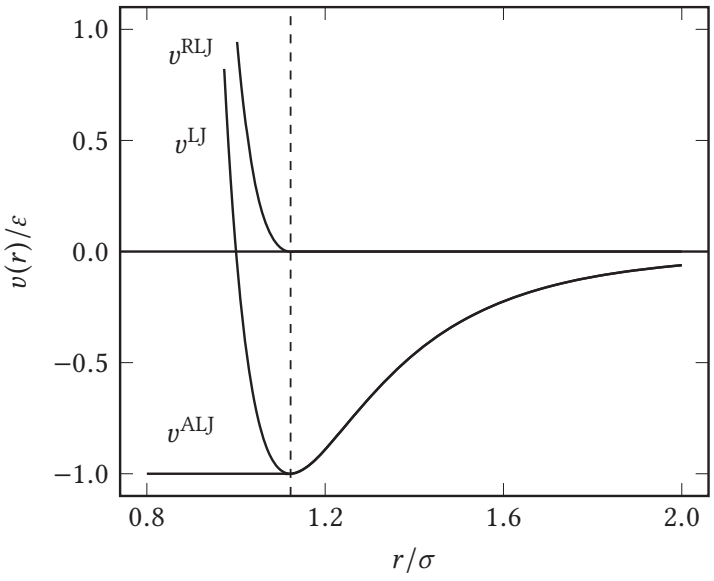

Fig. 1.5 The separation of the Lennard-Jones potential v^{LJ} into attractive and repulsive components, v^{ALJ} and v^{RLJ}, respectively. The vertical dashed line shows the position of r_{min}.

components, and the separation proposed by Weeks et al. (1971) involves splitting the potential at the minimum. For the Lennard-Jones potential, the repulsive and attractive parts are, as illustrated in Fig. 1.5,

$$v^{\mathrm{RLJ}}(r) = \begin{cases} v^{\mathrm{LJ}}(r) + \epsilon & \text{if } r < r_{\mathrm{min}} \\ 0 & \text{if } r_{\mathrm{min}} \leq r \end{cases} \tag{1.10a}$$

$$v^{\mathrm{ALJ}}(r) = \begin{cases} -\epsilon & \text{if } r < r_{\mathrm{min}} \\ v^{\mathrm{LJ}}(r) & \text{if } r_{\mathrm{min}} \leq r, \end{cases} \tag{1.10b}$$

where $r_{\mathrm{min}} = 2^{1/6}\sigma \approx 1.12\sigma$. In perturbation theory (Weeks et al., 1971), a hypothetical fluid of molecules interacting via the repulsive potential v^{RLJ} is treated as a reference system and the attractive part v^{ALJ} is the perturbation. It should be noted that the potential v^{RLJ} is significantly harder than the inverse twelfth power soft-sphere potential, which is also sometimes thought of as the 'repulsive' part of $v^{\mathrm{LJ}}(r)$.

For ions, of course, these potentials are not sufficient to represent the long-range interactions. A simple approach is to supplement one of these pair potentials with the Coulomb charge–charge interaction

$$v^{qq}(r_{ij}) = \frac{q_i q_j}{4\pi\epsilon_0 r_{ij}} \tag{1.11}$$

where q_i, q_j are the charges on ions i and j and ϵ_0 is the permittivity of free space (not to be confused with ϵ in eqns (1.6)–(1.10)). For ionic systems, induction interactions are important: the ionic charge induces a dipole on a neighbouring ion. This term is not pairwise additive and hence is difficult to include in a simulation. The shell model is a crude attempt to account for this polarizability (Dixon and Sangster, 1976; Lindan, 1995).

Each ion is represented as a core surrounded by a shell. Part of the ionic charge is located on the shell and the rest in the core. This division is always arranged so that the shell charge is negative (it represents the electronic cloud). The interactions between ions are just sums of the Coulombic shell–shell, core–core, and shell–core contributions. The shell and core of a given ion are coupled by a harmonic spring potential. The shells are taken to have zero mass. During a simulation, their positions are adjusted iteratively to zero the net force acting on each shell: this process makes the simulations expensive. We shall return to the simulation of polarizable systems in Section 1.3.3.

When a potential depends upon just a few parameters, such as ϵ and σ, it may be possible to choose an appropriate set of units in which these parameters take values of unity. This results in a simpler description of the properties of the model, and there may also be technical advantages within a simulation program. For Coulomb systems, the factor $4\pi\epsilon_0$ in eqn (1.11) is often omitted, and this corresponds to choosing a non-standard unit of charge. We discuss such reduced units in Appendix B. Reduced densities, temperatures, etc. are often denoted by an asterisk, that is, ρ^*, T^* etc.

1.3.3 Molecular systems

In principle, there is no reason to abandon the atomic approach when dealing with molecular systems: chemical bonds are simply interatomic potential-energy terms (Chandler, 1982). Ideally, we would like to treat all aspects of chemical bonding, including the reactions which form and break bonds, in a proper quantum mechanical fashion. This difficult task has not yet been accomplished but there are two common simplifying approaches. We might treat the bonds as classical harmonic springs (or Morse oscillators) or we could treat the molecule as a rigid or semi-rigid unit, with fixed bond lengths and, sometimes, fixed bond angles and torsion angles.

Bond vibrations are of very high frequency (and hence difficult to handle, certainly in a classical simulation). It quite possible that a high-frequency vibration will not be in thermal equilibrium with the fluid that surrounds it. These vibrations are also of low amplitude (and are therefore unimportant for many liquid properties). For these reasons, we prefer the approach of constraining the bond lengths to their equilibrium values. Thus, a diatomic molecule with a strongly binding interatomic potential-energy surface might be replaced by a dumb-bell with a rigid interatomic bond.

The interaction between the nuclei and electronic charge clouds of a pair of molecules i and j is clearly a complicated function of relative positions $\mathbf{r}_i$, $\mathbf{r}_j$ and orientations Ω_i, Ω_j (Gray and Gubbins, 1984). One way of modelling a molecule is to concentrate on the positions and sizes of the constituent atoms (Eyring, 1932). The much simplified 'atom–atom' or 'site–site' approximation for diatomic molecules is illustrated in Fig. 1.6. The total interaction is a sum of pairwise contributions from distinct sites a in molecule i, at position $\mathbf{r}_{ia}$, and b in molecule j, at position $\mathbf{r}_{jb}$:

$$v(\mathbf{r}_{ij},\ \Omega_i,\ \Omega_j) = \sum_a \sum_b v_{ab}(r_{ab}). \tag{1.12}$$

Here a, b take the values 1, 2, v_{ab} is the pair potential acting between sites a and b, and r_{ab} is shorthand for the inter-site separation $r_{ab} = |\mathbf{r}_{ab}| = |\mathbf{r}_{ia} - \mathbf{r}_{jb}|$. The interaction sites are usually centred, more or less, on the positions of the nuclei in the real molecule, so as to

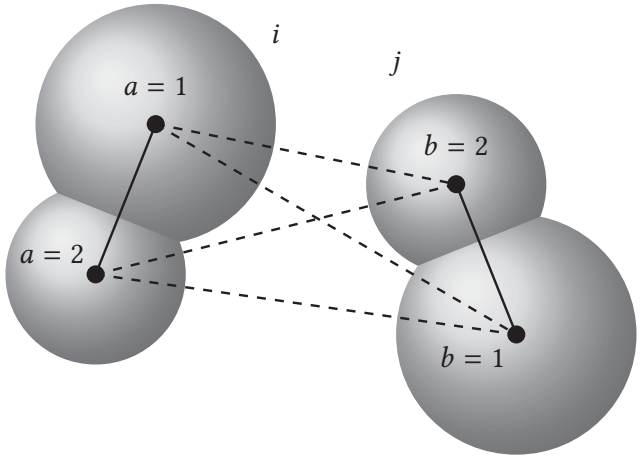

Fig. 1.6 The atom–atom model of a diatomic molecule. The total interaction is a sum of terms involving the distances $|\mathbf{r}_{ia} - \mathbf{r}_{jb}|$, indicated by dashed lines.

represent the basic effects of molecular 'shape'. A very simple extension of the hard-sphere model is to consider a diatomic composed of two hard spheres fused together (Streett and Tildesley, 1976), but more realistic models involve continuous potentials. Thus, nitrogen, fluorine, chlorine, etc. have been depicted as two 'Lennard-Jones atoms' separated by a fixed bond length (Barojas et al., 1973; Cheung and Powles, 1975; Singer et al., 1977).

The description of the molecular charge distribution may be improved somewhat by incorporating point multipole moments at the centre of charge (Streett and Tildesley, 1977). These multipoles may be equal to the known (isolated molecule) values, or may be 'effective' values chosen simply to yield a better description of the liquid structure and thermodynamic properties. A useful collection of the values of multipole moments is given in Gray and Gubbins (1984). Price et al. (1984) have developed an efficient way of calculating the multipolar energy, forces and torques between molecules of arbitrary symmetry up to terms of $O(r_{ij}^{-5})$. However, it is now generally accepted that such a multipole expansion of the electrostatic potential based around the centre of mass of a molecule is not rapidly convergent.

A pragmatic alternative approach, for ionic and polar systems, is to use a set of fictitious 'partial charges' distributed 'in a physically reasonable way' around the molecule so as to reproduce the known multipole moments (Murthy et al., 1983). For example, the electrostatic part of the interaction between nitrogen molecules may be modelled using five partial charges placed along the axis, while for methane, a tetrahedral arrangement of partial charges is appropriate. These are illustrated in Fig. 1.7. For the case of N_2, taking the molecular axis to lie along z, the quadrupole moment Q is given by (Gray and Gubbins, 1984)

$$Q = \sum_{a=1}^{5} q_a z_a^2 \tag{1.13}$$

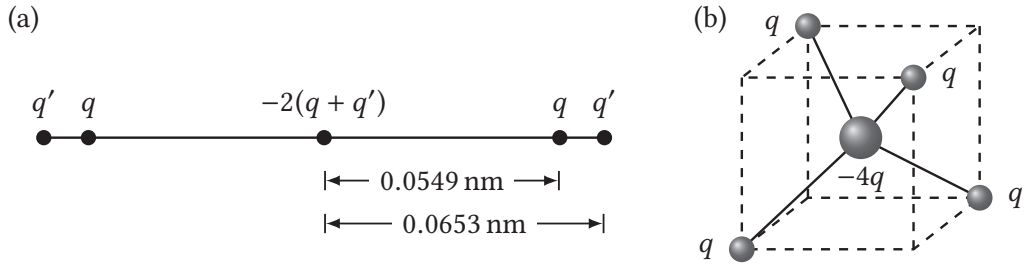

Fig. 1.7 Partial charge models: (a) A five-charge model for N_2. There is one charge at the bond centre, two at the positions of the nuclei, and two more displaced beyond the nuclei. Typical values (with $e = 1.602 \times 10^{-19}$ C): $q = +5.2366\,e$, $q' = -4.0469\,e$, giving $Q = -4.67 \times 10^{-40}$ C m^2 (Murthy et al., 1983). (b) A five-charge model for CH_4. There is one charge at the centre and four others at the positions of the hydrogen nuclei. Typical values are CH bond length 0.1094 nm, $q = 0.143\,e$ giving $O = 5.77 \times 10^{-50}$ C m^3 (Righini et al., 1981).

with similar expressions for the higher multipoles (all the odd ones vanish for N_2). The first non-vanishing moment for methane is the octopole O

$$O = \frac{5}{2}\sum_{a=1}^{5} q_a x_a y_a z_a \tag{1.14}$$

in a coordinate system aligned with the cube shown in Fig. 1.7. The aim of all these approaches is to approximate the complete charge distribution in the molecule. In a calculation of the potential energy, the interaction between partial charges on different molecules would be summed in the same way as the other site–site interactions.

The use of higher-order multipoles has enjoyed a renaissance in recent years. This is because we can obtain an accurate representation of the electrostatic potential by placing multipoles at various sites within the molecule. These sites could be at the atom positions, or at the centres of bonds or within lone pairs, and it is normally sufficient to place a charge, dipole and quadrupole at any particular site. This approach, known as a distributed multipole analysis (Stone, 1981; 2013, Chapter 7), is illustrated for N_2 and CO in Fig. 1.8. In the case of N_2 the multipoles are placed at the centre of the bond and on the two nitrogen atoms, with their z-axis along the bond. Each site has a charge and a quadrupole and, in addition, the two atoms have equal and opposite dipoles. These are calculated using an accurate density functional theory B3LYP (Martin, 2008). In atomic units (see Appendix B), the overall quadrupole of the molecule calculated from this distribution is $-1.170\,ea_0{}^2$ corresponding to the experimental estimate of $(-1.09 \pm 0.07)\,ea_0{}^2$. A similar calculation for CO produces charges, dipoles and quadrupoles on all three sites (the C and O atoms and the centre of the bond). The overall dipole and quadrupole moments from this distribution are $0.036\,ea_0$ and $-1.515\,ea_0{}^2$ respectively, compared with the experimental estimates of $0.043\,ea_0$ and $-1.4\,ea_0{}^2$. The electrostatic energy between two molecules is now the sum of the multipole interactions between the atoms or sites in different molecules. The energy of interaction between two sets of distributed multipoles $\{q_a, \boldsymbol{\mu}_a, \mathbf{Q}_a\}$ and $\{q_b, \boldsymbol{\mu}_b, \mathbf{Q}_b\}$,

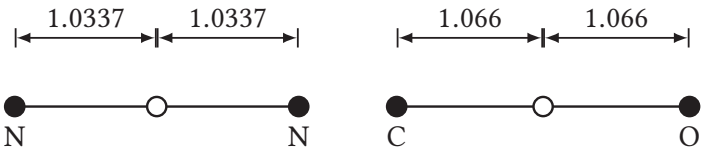

q	0.427	−0.854	0.427	0.556	−0.832	0.276
μ_z	0.947	0.0	−0.947	1.159	−0.030	−0.796
Q_{zz}	0.775	0.283	0.775	0.377	0.274	1.068

Fig. 1.8 The distributed multipoles required to represent the electrostatic potential of a N_2 and CO molecule calculated using a cc-p-VQZ basis set. Multipoles are placed at the positions of the atoms (black circles) and at the midpoint of the bond (white circles). The distances are in atomic units, $a_0 = 0.529\,\text{Å}$; charges, q, are in units of $e = 1.602 \times 10^{-19}\,\text{C}$; dipoles, μ, are in units of $ea_0 = 8.478 \times 10^{-30}\,\text{C m}$; and quadrupoles, Q, are in units of $ea_0{}^2 = 4.487 \times 10^{-40}\,\text{C m}^2$ (see Appendix B). Data from Stone (2013).

on atoms a and b at $\mathbf{r}_a$ and $\mathbf{r}_b$, is given by

$$\begin{aligned} v_{ab}^{\text{elec}} = {} & Tq_aq_b + T_\alpha(\mu_{a\alpha}q_b - q_a\mu_{b\alpha}) \\ & + T_{\alpha\beta}\left(\tfrac{1}{3}q_aQ_{b\alpha\beta} - \mu_{a\alpha}\mu_{b\beta} + \tfrac{1}{3}Q_{a\alpha\beta}\,q_b\right) \\ & + \tfrac{1}{3}T_{\alpha\beta\gamma}\left(\mu_{a\alpha}Q_{b\beta\gamma} - Q_{a\alpha\beta}\mu_{b\gamma}\right) + \tfrac{1}{9}T_{\alpha\beta\gamma\delta}Q_{a\alpha\beta}Q_{b\gamma\delta} \end{aligned} \tag{1.15}$$

where we take the sum over repeated Cartesian indices α, β etc. The interaction or 'T' tensors are given by

$$T_{\alpha,\beta\ldots\gamma} = (-1)^n\nabla_\alpha\nabla_\beta\ldots\nabla_\gamma\frac{1}{r_{ab}}, \tag{1.16}$$

where n is the order of the tensor. Thus

$$T = \frac{1}{r_{ab}}, \quad T_\alpha = \frac{(r_{ab})_\alpha}{r_{ab}^3}, \quad T_{\alpha\beta} = \frac{3(r_{ab})_\alpha(r_{ab})_\beta - r_{ab}^2\delta_{\alpha\beta}}{r_{ab}^5}, \tag{1.17}$$

and so on. Note that the T tensors are defined for $\mathbf{r}_{ab} = \mathbf{r}_a - \mathbf{r}_b$. This is a useful formulation of the electrostatic energy for a computer simulation where the T tensors are readily expressed in terms of the Cartesian coordinates of the atoms. In addition, it is also straightforward to evaluate the derivative of the potential to obtain the force (the field) or the field gradient. The electrostatic potential, ϕ, at a distance r from a charge q is $\phi(r) = q/r$ and the corresponding electric field is $\boldsymbol{\mathcal{E}} = -\boldsymbol{\nabla}\phi(r)$. The field is simply the force per unit charge. For example the field ($\boldsymbol{\mathcal{E}}$) and field gradient ($\boldsymbol{\mathcal{E}}'$) arising from a charge q_b at b are

$$\begin{aligned} \mathcal{E}_\alpha &= -\nabla_\alpha q_bT = q_bT_\alpha \\ \mathcal{E}'_{\alpha\beta} &= -\nabla_\alpha\nabla_\beta q_bT = -q_bT_{\alpha\beta}. \end{aligned} \tag{1.18}$$

The quadrupole tensor used in eqn (1.15) is defined to be traceless,

$$Q_{\alpha\beta} = \sum_a q_a\left(\tfrac{3}{2}(r_a)_\alpha(r_b)_\beta - \tfrac{1}{2}r_a^2\delta_{\alpha\beta}\right). \tag{1.19}$$

Code 1.1 Calculation of T tensors

This file is provided online. For a pair of linear molecules, electrostatic energies and forces are calculated using both the angles between the various vectors, and the T tensors.

```
! t_tensor.f90
! Electrostatic interactions: T-tensors compared with angles
PROGRAM t_tensor
```

The components of the dipole and quadrupole will initially be defined in an atom-fixed axis frame centred on an atom (or site) and at any given point in a simulation it will be necessary to transform these properties to the space-fixed axis system for use in eqn (1.15) (Dykstra, 1988; Ponder et al., 2010). This can be simply achieved with a rotation matrix which we discuss in Section 3.3.1. An example of the calculation of T tensors is given in Code 1.1.

Electronic polarization refers to the distortion of the electronic charge cloud by the electrostatic field from the other molecules. In a molecular fluid it can be an important contribution to the energy. It is inherently a many-body potential and unlike many of the interactions already discussed in this chapter, it cannot be broken down to a sum over pair interactions. For this reason, it is expensive to calculate and was often omitted from earlier simulations. In these cases, some compensation was obtained by enhancing the permanent electrostatic interactions in the model. For example, in early simulations of water, the overall permanent dipole of the molecule was set to ca. 2.2 D rather than the gas-phase value 1.85 D (where $1\,\mathrm{D} = 0.299\,79 \times 10^{-30}$ C m) in order to fit to the condensed phase properties in the absence of polarization (Watanabe and Klein, 1989). Nevertheless, polarization can be included explicitly in a model and there are three common approaches: the induced point multipole model; the fluctuating charge model; and the Drude oscillator model (Antila and Salonen, 2013; Rick and Stuart, 2003).

The induced multipole approach (Applequist et al., 1972) is based on a knowledge of the atomic dipole polarizability, $\alpha^a_{\alpha\beta}$, on a particular atom a. Consider a molecule containing a set of charges, q_a, on each atom. The induced dipole at a contains two terms

$$\Delta\mu^a_\gamma = \alpha^a_{\alpha\gamma}\left(\mathcal{E}^a_\alpha + \sum_{b\neq a} T_{\alpha\beta}\Delta\mu^b_\beta\right), \tag{1.20}$$

where we sum over repeated indices α, β. The first term in the field, $\boldsymbol{\mathcal{E}}$, comes from the permanent charges at the other atoms and the second term comes from the dipoles that have been induced at these atoms. We ignore contributions from the field gradient at atom a by setting the higher-order polarizabilities to zero. Eqn (1.20) can be formally solved for the induced dipoles

$$\Delta\mu^a_\alpha = \sum_{b\beta} A_{\alpha\beta}\mathcal{E}^b_\beta \tag{1.21}$$

Example 1.1 Water, water everywhere

The earliest simulations of molecular liquids focused on water (Barker and Watts, 1969; Rahman and Stillinger, 1971) and, since then, there have been over 80 000 published simulations of the liquid. Considerable effort and ingenuity have gone into developing models of the intermolecular potential between water molecules. There are three types of classical potential models in use: rigid, flexible, and polarizable.

The simplest rigid models use a single Lennard-Jones site to represent the oxygen atom and three partial charges: at the centre of the oxygen and the position of the hydrogen atoms. There are no specific dispersion interactions involving the H atoms and the charges are set to model the effective condensed-phase dipole moment of water, 2.2 D–2.35 D. Examples include the the SPC and the SPC/E models (Berendsen et al., 1981; 1987) used in the GROMOS force field, and the TIP3P model (Jorgensen et al., 1983) implemented in AMBER and CHARMM. The precise geometry and the size of the charges are different in each of these models. They predict the experimental liquid densities at a fixed pressure but tend to overestimate the diffusivity. The addition of a fourth negative charge along the bisector of the H–O–H bond creates the TIP4P model (Jorgensen et al., 1983) and its generalization TIP4P/2005 (Abascal and Vega, 2005). These models are capable of producing many of the qualitative features of the complicated water phase diagram. The TIP5P potential model (Mahoney and Jorgensen, 2000) supplements the three charges on the atoms with two negative charges at the position of the lone pairs. This model correctly predicts the density maximum near 4 °C at 1 bar, and the liquid structure obtained from diffraction experiments.

Flexibility can be included in models such as SPC/E using the intramolecular potential of Toukan and Rahman (1985), in which anharmonic oscillators are used to represent the O–H and H–H stretches. These flexible models predict many of the features of the vibrational spectrum of the liquid (Praprotnik et al., 2005).

A recent study by Shvab and Sadus (2013) indicates that rigid models underestimate the water structure and H-bond network at temperatures higher than 400 K and that none of the models so far discussed can predict the heat capacities or thermal expansion coefficients of the liquid. To improve on this position it is necessary to include polarization in the potential. Li et al. (2007a) show that the Matsuoka–Clementi–Yoshimine potential fitted from quantum calculations can be adapted to include three-body dispersion interactions for O atoms and fluctuating charges to create the more accurate MCYna model (Shvab and Sadus, 2013). These enhancements produce good agreement with experimental data over the entire liquid range of temperatures. Jones et al. (2013) have taken a different approach by embedding a quantum Drude oscillator (QDO) and using adiabatic path-integral molecular dynamics to simulate 4000 water molecules. Sokhan et al. (2015) show that this approach can produce accurate densities, surface tensions, and structure over a range of temperatures. Models of water in terms of pseudo-potentials to describe the nuclei and core electrons, and a model of the exchange correlation function to describe the non-classical electron repulsion between the valence electrons will be described in Chapter 13.

where the relay matrix $\mathbf{A} = \mathbf{B}^{-1}$ and

$$B_{\alpha\beta} = \begin{cases} (\alpha^a)^{-1} & \text{if } a = b \\ -T_{\alpha\beta} & \text{if } a \neq b. \end{cases} \tag{1.22}$$

Here **A** and **B** have dimensions of the number of sites involved in the polarization; this can be a large matrix, so practically eqn (1.20) is solved in a simulation by iterating the induced dipoles until convergence is achieved (Warshel and Levitt, 1976). This method can also be used with the distributed multipole analysis where the field at a polarizable atom might contain terms from the charge, dipole and quadrupole at a neighbouring atom, while the induction still occurs through the dipole polarizability (Ponder et al., 2010).

There is a well-known problem with these point polarizability models in which the elements of **A** diverge at short separations: the so-called polarization catastrophe. This is caused by the normal breakdown in the multipole expansion at these distances. It can be mitigated by smearing the charges on a particular site (Thole, 1981). The effect of this modification is to change the interaction tensor to

$$\tilde{T}_{\alpha\beta} = \frac{3f_t(r_{ab})_\alpha(r_{ab})_\beta - f_e r_{ab}^2 \delta_{\alpha\beta}}{4\pi\epsilon_0 r_{ab}^5} \tag{1.23}$$

where f_e and f_t are two, simple, damping functions. A useful discussion of the various possible choices for these damping functions is given by Stone (2013). The modified tensor $\tilde{T}_{\alpha\beta}$ can now be used in eqn (1.20) to calculate the induced moments. Once the induced dipole at atom a has been consistently determined then the induction energy associated with that atom is

$$v_a^{\text{ind}} = -\tfrac{1}{2}\mathcal{E}_\alpha^a \Delta\mu_\alpha^a. \tag{1.24}$$

The second method of including polarization in a model is the fluctuating charge model, sometimes referred to as the electronegativity equalization model. The partial charges are allowed to fluctuate as dynamical quantities. We can illustrate this approach by considering a model for water (Sprik, 1991). In addition to the three permanent charges normally used to represent the electrostatic moments, four additional fluctuating charges are disposed in a tetrahedron around the central oxygen atom (see Fig. 1.9). The magnitudes of the charges $q_i(t)$ fluctuate in time, but they preserve overall charge neutrality

$$\sum_{i=1}^{4} q_i(t) = 0 \tag{1.25}$$

and they produce an induced dipole

$$\Delta\boldsymbol{\mu} = \sum_{i=1}^{4} q_i(t)\mathbf{r}_i \tag{1.26}$$

where $\mathbf{r}_i$ are the vectors describing the positions of the tetrahedral charges with respect to the O atom. If $|\mathbf{r}_i| \ll r_{\text{OH}}$ then the higher moments of the fluctuating charge distribution can be neglected. The potential energy from the four charges is the sum of the electrostatic

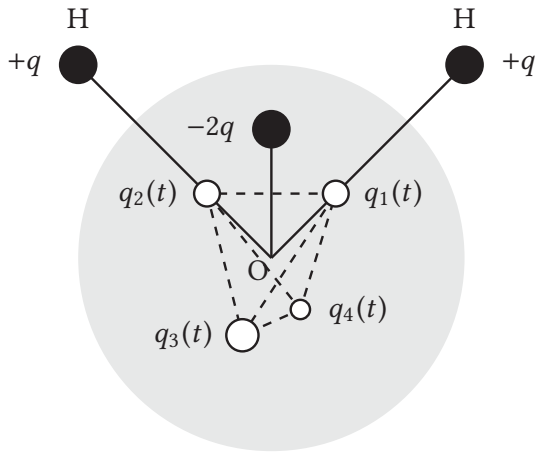

Fig. 1.9 A polarizable model for water (Sprik, 1991). The oxygen nucleus, O, is at the centre of the small tetrahedron. The three permanent charges $+q$, $+q$ and $-2q$, at the filled black spheres, are arranged to model the permanent electrostatic potential of water. The four fluctuating charges, $q_i(t)$, located at the white spheres, respond to the surrounding field and can be used to model the polarization of the molecule.

energy ($-\Delta\boldsymbol{\mu}\cdot\boldsymbol{\mathcal{E}}$) and a self energy term ($\Delta\mu^2/2\alpha_{\mathrm{O}}$) where α_{O} is the dipole polarizability associated with the oxygen atom. The fluctuating charges in this model can be determined by minimizing the potential energy in a given configuration subject to the constraint of charge neutrality, eqn (1.25),

$$\frac{\partial}{\partial q_i}\left(\frac{\left|\sum_{i=1}^{4} q_i\mathbf{r}_i\right|^2}{2\alpha_{\mathrm{O}}} - \sum_{i=1}^{4} q_i\mathbf{r}_i\cdot\mathcal{E}\right) = 0. \tag{1.27}$$

This approach can be extended to more complicated molecules by adding the appropriate number of fluctuating charges; and simplified to study spherical ions by including just two fluctuating charges within the spherical core. In these models, the fluctuating charges, q_i, are a crude representation of the electronic charge density and these can be usefully replaced by more realistic Gaussian charge distributions of width σ

$$\rho_i(\mathbf{r}) = q_i\left(\frac{1}{2\pi\sigma^2}\right)^{3/2}\exp\left(-\frac{\left|\mathbf{r}-\mathbf{r}_i\right|^2}{2\sigma^2}\right). \tag{1.28}$$

This improves the description of the polarization, particularly at short intermolecular separations (Sprik and Klein, 1988). We note that these models can be readily included in a molecular dynamics simulation by setting up separate equations of motions for the fluctuating charges (Sprik and Klein, 1988; Rick et al., 1994), and we shall consider this approach in Section 3.11.

The third approach is the Drude oscillator model or shell model. A polarizable site is represented as a heavy core particle of charge q_{d} and a massless or light shell particle of charge $-q_{\mathrm{d}}$. These two particles are connected by a harmonic spring with a spring constant k. The minimum in the spring potential is obtained when the core and shell are

coincident. The small charge q_d is in addition to the permanent charge at a particular site. The shell and core can separate to produce an induced dipole moment

$$\Delta\boldsymbol{\mu} = -q_\mathrm{d}\Delta\mathbf{r} \tag{1.29}$$

where $\Delta\mathbf{r}$ is the vector from the core to the shell. The repulsion–dispersion interactions associated with a particular site are normally centred on the shell part of the site.

In the adiabatic implementation the shell is massless and at each step of a simulation the positions of the shells are adjusted iteratively to achieve the minimum energy configuration. In the dynamic model the shells are given a low mass (0.5 u) and an extended Lagrangian approach is used to solve the dynamics for short timesteps. In this case the shell particles are coupled to a heat bath at a low temperature (see Section 3.11). For these models, the atomic polarizability is isotropic and given by $\alpha^a = q_\mathrm{d}^2/k$. Procedures are available for parameterizing the shell models to produce the correct molecular polarizabilities and electrostatic moments (Anisimov et al., 2005).

The model for water, shown in Fig. 1.9, begs the question as to whether we need to use a separate intermolecular potential to represent the hydrogen bond between two molecules. The hydrogen bond, between an H atom in one molecule and a strongly electronegative atom in another, is part permanent electrostatic interaction, part induced interaction, and some charge transfer. The evidence as reviewed by Stone (2013) indicates that the attractive electrostatic interaction is the most important term in determining the structure of the hydrogen-bonded dimer but that induced interactions will make an important contribution in condensed phases. It should be possible to avoid a separate hydrogen-bond potential by including an accurate representation of the electrostatic interactions (by using, for example, the distributed multipole approach) and by including polarization.

For larger molecules it may not be reasonable to 'fix' all the internal degrees of freedom. In particular, torsional motion about bonds, which gives rise to conformational interconversion in, for example, alkanes, cannot in general be neglected (since these motions involve energy changes comparable with normal thermal energies). An early simulation of n-butane, $CH_3CH_2CH_2CH_3$ (Ryckaert and Bellemans, 1975; Maréchal and Ryckaert, 1983), provides a good example of the way in which these features are incorporated in a simple model. Butane can be represented as a four-centre molecule, with fixed bond lengths and bond-bending angles, derived from known experimental (structural) data (see Fig. 1.10). A very common simplifying feature is built into this model: whole groups of atoms, such as CH_3 and CH_2, are condensed into spherically symmetric effective 'united atoms'. In fact, for butane, the interactions between such groups may be represented quite well by the ubiquitous Lennard-Jones potential, with empirically chosen parameters. In a simulation, the C_1–C_2, C_2–C_3 and C_3–C_4 bond lengths are held fixed by a method of constraints, which will be described in detail in Chapter 3. The angles θ and θ' may be fixed by additionally constraining the C_1–C_3 and C_2–C_4 distances; that is, by introducing 'phantom bonds'. If this is done, just one internal degree of freedom, namely the rotation about the C_2–C_3 bond, measured by the angle ϕ, is left unconstrained; for each molecule, an extra term in the potential energy, $v^{\mathrm{torsion}}(\phi)$, appears in the Hamiltonian. This potential would have a minimum at a value of ϕ corresponding to the *trans* conformer of butane, and secondary minima at the *gauche* conformations. It is easy to see how this approach

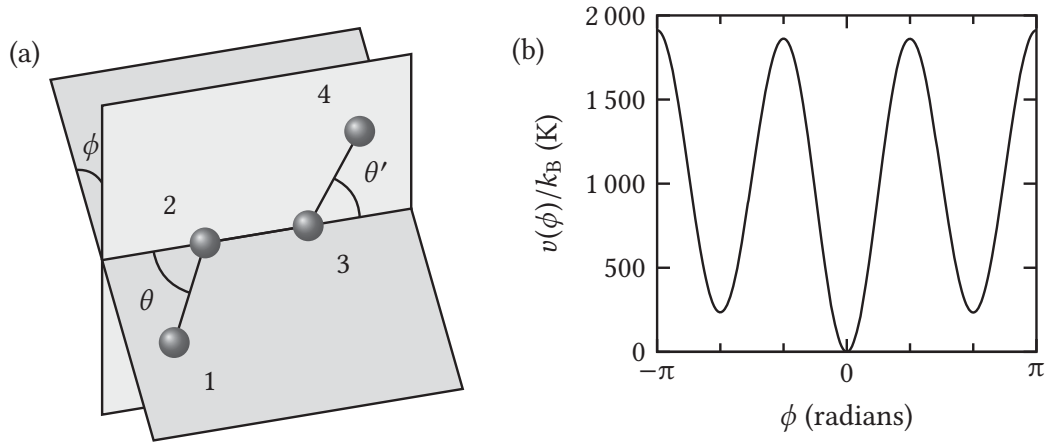

Fig. 1.10 (a) Geometry of a model of butane defining bending angles θ, θ' and the torsional angle ϕ (Ryckaert and Bellemans, 1975). (b) The torsional potential, in the AUA(2) model of Padilla and Toxvaerd (1991) as reviewed in Dysthe et al. (2000).

may be extended to much larger flexible molecules. The consequences of constraining bond lengths and angles will be treated in more detail in Chapters 2 and 4.

As the molecular model becomes more complicated, so too do the expressions for the potential energy, forces, and torques, due to molecular interactions. In Appendix C, we give some examples of these formulae, for rigid and flexible molecules, interacting via site–site pairwise potentials, including multipolar terms. We also show how to derive the forces from a simple three-body potential.

1.3.4 Coarse-grained potential models

Coarse graining a potential involves avoiding the full atomic representation of the molecules to find a description of the interaction at a longer or coarser length scale. We have already seen one simple example of this in the use of a united-atom potential for the methylene and methyl groups in butane. Coarse graining will reduce the number of explicit pairs that are needed for the calculation of the energy and force for a particular system and will reduce the computer time or, alternatively, allow us to study a much larger system. Normally an increase in the characteristic length scale in the model goes hand in hand with an increase in the timestep that we can use in a dynamical simulation of the problem. Coarse graining will allow us to use a longer timestep and to cover more 'real' time in our simulation.

One flavour of coarse-grained model has been widely used to study liquid crystalline systems, exhibiting some long-range orientational order. For example, for the nematogen quinquaphenyl, a large rigid molecule that forms a nematic phase, a substantial number of sites would be required to model the repulsive core. A crude model, which represented each of the five benzene rings as a single Lennard-Jones site, would necessitate 25 site–site interactions between each pair of molecules; sites based on each carbon atom would be more realistic but require 900 site–site interactions per pair. An alternative coarse-grained representation of intermolecular potential, introduced by Corner (1948), involves a single

site–site interaction between a pair of molecules, characterized by energy and length parameters that depend on the relative orientation of the molecules.

A version of this family of molecular potentials that has been used in computer simulation studies is the Gay–Berne potential (Gay and Berne, 1981). This is an extension of the Gaussian overlap model generalized to a Lennard-Jones form (Berne and Pechukas, 1972). The basic potential acting between two linear molecules is

$$v^{\mathrm{GB}}(\mathbf{r}_{ij}, \hat{\mathbf{e}}_i, \hat{\mathbf{e}}_j) = 4\epsilon(\hat{\mathbf{r}}, \hat{\mathbf{e}}_i, \hat{\mathbf{e}}_j)\Big[(\sigma_{\mathrm{s}}/\rho_{ij})^{12} - (\sigma_{\mathrm{s}}/\rho_{ij})^{6}\Big], \tag{1.30a}$$

$$\text{where} \qquad \rho_{ij} = r_{ij} - \sigma(\hat{\mathbf{r}}, \hat{\mathbf{e}}_i, \hat{\mathbf{e}}_j) + \sigma_{\mathrm{s}}. \tag{1.30b}$$

Here, r_{ij} is the distance between the centres of i and j, and $\hat{\mathbf{r}} = \mathbf{r}_{ij}/r_{ij}$ is the unit vector along $\mathbf{r}_{ij}$, while $\hat{\mathbf{e}}_i$ and $\hat{\mathbf{e}}_j$ are unit vectors along the axis of the molecules. The molecule can be considered (approximately) as an ellipsoid characterized by two diameters σ_{s} and σ_{e}, the separations at which the side-by-side potential, and the end-to-end potential, respectively, become zero. Thus

$$\sigma(\hat{\mathbf{r}}, \hat{\mathbf{e}}_i, \hat{\mathbf{e}}_j) = \sigma_{\mathrm{s}}\left[1 - \frac{\chi}{2}\left(\frac{(\hat{\mathbf{e}}_i \cdot \hat{\mathbf{r}} + \hat{\mathbf{e}}_j \cdot \hat{\mathbf{r}})^2}{1 + \chi(\hat{\mathbf{e}}_i \cdot \hat{\mathbf{e}}_j)} + \frac{(\hat{\mathbf{e}}_i \cdot \hat{\mathbf{r}} - \hat{\mathbf{e}}_j \cdot \hat{\mathbf{r}})^2}{1 - \chi(\hat{\mathbf{e}}_i \cdot \hat{\mathbf{e}}_j)}\right)\right]^{-1/2} \tag{1.31a}$$

$$\text{where} \quad \chi = \frac{\kappa^2 - 1}{\kappa^2 + 1}, \quad \text{and} \quad \kappa = \sigma_{\mathrm{e}}/\sigma_{\mathrm{s}}. \tag{1.31b}$$

κ is the elongation and χ is the shape anisotropy parameter ($\kappa = 1$, $\chi = 0$ for spherical particles, $\kappa \to \infty$, $\chi \to 1$ for very long rods, and $\kappa \to 0$, $\chi \to -1$ for very thin disks).

The energy term is the product of two functions

$$\epsilon(\hat{\mathbf{r}}, \hat{\mathbf{e}}_i, \hat{\mathbf{e}}_j) = \epsilon_0\, \epsilon_1^{\nu}(\hat{\mathbf{e}}_i, \hat{\mathbf{e}}_j)\, \epsilon_2^{\mu}(\hat{\mathbf{r}}, \hat{\mathbf{e}}_i, \hat{\mathbf{e}}_j) \tag{1.32a}$$

where

$$\epsilon_1(\hat{\mathbf{e}}_i, \hat{\mathbf{e}}_j) = \left(1 - \chi^2(\hat{\mathbf{e}}_i \cdot \hat{\mathbf{e}}_j)^2\right)^{-1/2} \tag{1.32b}$$

$$\epsilon_2(\hat{\mathbf{r}}, \hat{\mathbf{e}}_i, \hat{\mathbf{e}}_j) = 1 - \frac{\chi'}{2}\left(\frac{(\hat{\mathbf{e}}_i \cdot \hat{\mathbf{r}} + \hat{\mathbf{e}}_j \cdot \hat{\mathbf{r}})^2}{1 + \chi'(\hat{\mathbf{e}}_i \cdot \hat{\mathbf{e}}_j)} + \frac{(\hat{\mathbf{e}}_i \cdot \hat{\mathbf{r}} - \hat{\mathbf{e}}_j \cdot \hat{\mathbf{r}})^2}{1 - \chi'(\hat{\mathbf{e}}_i \cdot \hat{\mathbf{e}}_j)}\right) \tag{1.32c}$$

and the energy anisotropy parameter is

$$\chi' = \frac{\kappa'^{1/\mu} - 1}{\kappa'^{1/\mu} + 1}, \quad \text{where} \quad \kappa' = \epsilon_{\mathrm{ss}}/\epsilon_{\mathrm{ee}}. \tag{1.32d}$$

ϵ_{ss} and ϵ_{ee} are the well depths of the potentials in the side-by-side and end-to-end configurations respectively. The potential is illustrated for these arrangements, as well as for T-shaped and crossed configurations, in Fig. 1.11. The original model, with exponents $\mu = 2$, $\nu = 1$, and parameters $\kappa = 3$, $\kappa' = 5$, was used to mimic four collinear Lennard-Jones sites (Gay and Berne, 1981). The potential and corresponding force and torque can be readily evaluated and the functional form is rich enough to create mesogens of different shapes and energy anisotropies that will form the full range of nematic, smectic, and discotic liquid crystalline phases (Luckhurst et al., 1990; Berardi et al., 1993; Allen, 2006a;

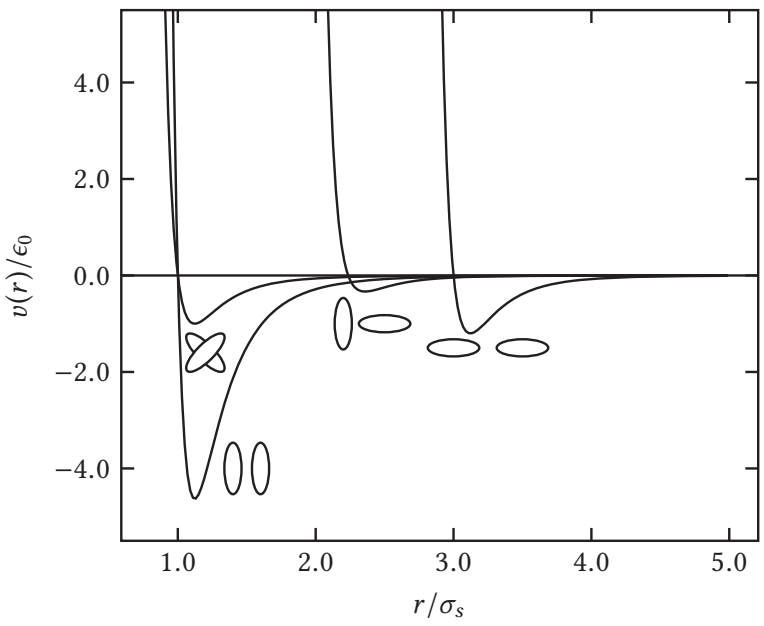

Fig. 1.11 The Gay-Berne potential, with parameters $\mu = 1$, $\nu = 3$, $\kappa = 3$, $\kappa' = 5$ (Berardi et al., 1993), as a function of centre–centre separation, for various molecular orientations.

Luckhurst, 2006). It is discussed further in Appendix C. Extensions of the potential, and its use in modelling liquid crystals, are discussed by Zannoni (2001).

The MARTINI approach is a coarse-grained potential developed for modelling lipid bilayers (Marrink et al., 2004; 2007) and proteins (Monticelli et al., 2008). In this model the bonded hydrogen atoms are included with their heavier partners, such as C, N, or O. These united atoms are then further combined using a 4:1 mapping to create larger beads (except in the case of rings where the mapping is normally 3:1). For these larger beads, there are four different bead types: charged (Q), polar (P), nonpolar (N), and apolar (C). Each of these types is further subdivided depending on the bead's hydrogen-bond forming propensities or its polarity. Overall there are 18 bead-types and each pair of beads interacts through a Lennard-Jones potential where the σ and ϵ parameters are specific to the atom types involved. Charged beads also interact through Coulombic potentials. The intramolecular interactions (bonds, angles, and torsions) are derived from atomistic simulations of crystal structures. This kind of moderate coarse graining has been successfully applied to simulations of the clustering behaviour of the membrane bound protein syntaxin-1A (van den Bogaart et al., 2011) and the simulation of the domain partitioning of membrane peptides (Schäfer et al., 2011).

It is possible to coarse grain potentials in a way that results in larger beads, that might contain 1–3 Kuhn chain-segments of a polymer or perhaps ten solvent molecules. We will consider this approach more fully in Chapter 12. However, at this point, we mention a very simple coarse-grained model of polymer chains due to Kremer and Grest (1990) and termed the finitely extensible nonlinear elastic (FENE) model. The bonds between beads

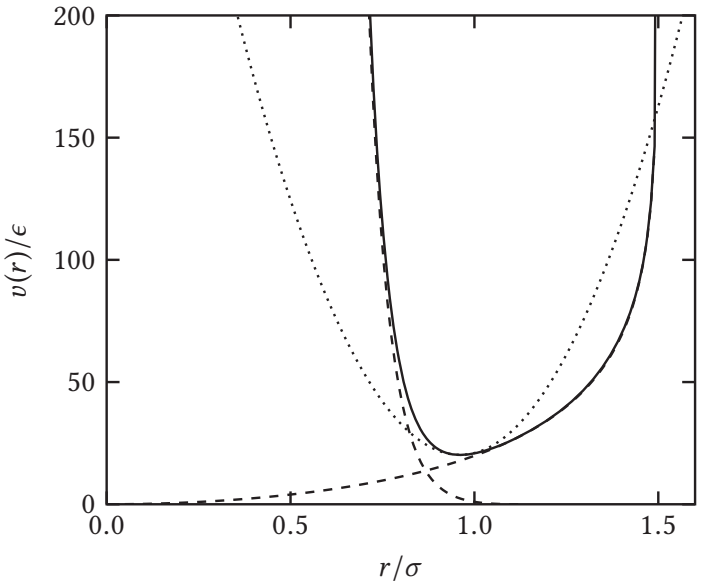

Fig. 1.12 The potential between bonded atoms in a coarse-grained polymer (solid line) together with its component parts (dashed lines): the attractive FENE potential, eqn (1.33) with $R_0 = 1.5\sigma$ and $k = 30\epsilon/\sigma^2$, and the repulsive Lennard-Jones potential, eqn (1.10a). Also shown (dotted line) is a harmonic potential, fitted to the curvature at the minimum. See Kremer and Grest (1990) for details.

within the chain are represented by the potential energy

$$v^{\mathrm{FENE}}(r) = \begin{cases} -\frac{1}{2}kR_0^2 \ln\left(1-(r/R_0)^2\right) & r < R_0 \\ \infty & r \geq R_0. \end{cases} \tag{1.33}$$

This is combined with the potential $v^{\mathrm{RLJ}}(r)$ of eqn (1.10a), representing the effects of excluded volume between every pair of beads (including those that are bonded together). The key feature of this potential is that it cannot be extended beyond $r = R_0$. This is important when studying entanglement effects: the simpler harmonic potential could, in principle, extend enough to let chains pass through one another, in some circumstances.

Finally, there has been considerable effort to develop a simple, single-site coarse-grained potential for water. One approach (Molinero and Moore, 2009; Moore and Molinero, 2011) has been to abandon the long-range electrostatics conventionally associated with hydrogen bonds, and use instead short-range directional interactions, of the kind previously used to model silicon (Stillinger and Weber, 1985). The resulting monatomic water (mW) model is very cheap to simulate but surprisingly successful in reproducing experimental structural and thermodynamic properties. Can one go further? It is difficult to imagine that a spherical, isotropic potential will be able to capture the strong association interactions in the fluid. Nevertheless, Lobanova et al. (2015) have used a Mie potential, a versatile form of the standard Lennard-Jones potential, where

$$v_{\mathrm{Mie}}(r) = C\epsilon\left[\left(\frac{\sigma}{r}\right)^n - \left(\frac{\sigma}{r}\right)^m\right], \quad \text{with} \quad C = \left(\frac{n}{n-m}\right)\left(\frac{n}{m}\right)^{m/(n-m)}. \tag{1.34}$$

A potential with $n = 8$ and $m = 6$ can be used with temperature-dependent energy and length parameters to represent the thermophysical properties of water over a broad range of conditions. However, a simpler form where ϵ and σ are independent of temperature can be used to represent water in the calculation of mixture phase diagrams such as CO_2/H_2O (Müller and Jackson, 2014). We briefly discuss this approach to coarse graining in Section 12.7.3. The examples just given are two amongst many attempts to model water in a coarse-grained way (for a review see Hadley and McCabe, 2012).

1.3.5 Calculating the potential

This is an appropriate point to introduce a piece of computer code, which illustrates the calculation of the potential energy in a system of Lennard-Jones atoms. Simulation programs are written in a range of languages: Fortran, C, and C++ are the most common, sometimes with a wrapper written in Python or Java. Here we shall use Fortran, which has a compact notation for arrays and array operations, and is simple enough to be read as a 'pseudo-code'. Appendix A contains some discussion of different programming approaches, and a summary of some of the issues affecting efficiency. We suppose that the coordinate vectors of our atoms are stored in an array `r` of rank two, with dimensions `(3,n)`, where the first index covers the x, y, and z components, and the second varies from `1` to `n` (equal to N, the number of particles). The potential energy will be stored in a variable `pot`, which is zeroed initially, and is then accumulated in a double loop over all distinct pairs of atoms, taking care to count each pair only once. This is shown in Code 1.2. The Lennard-Jones parameters ϵ and σ are assumed to be stored in the variables `epslj` and `sigma` respectively. The colon ':' is short for an implied loop over the corresponding index, so the statement `rij(:) = r(:,i) - r(:,j)` stands for the vector assignment $\mathbf{r}_{ij} = \mathbf{r}_i - \mathbf{r}_j$. The `SUM` function simply adds the components of its (array) argument, which in this case gives $r_{ij}^2 = x_{ij}^2 + y_{ij}^2 + z_{ij}^2$. Code 1.2 takes no account of periodic boundary conditions (we return to this in Section 1.6.2). Some measures have been taken here to avoid unnecessary use of computer time. The value of σ^2 is computed once beforehand, and stored in the variable `sigma_sq`; the factor 4ϵ, which appears in every pair potential term, is multiplied in once, at the very end. The aim is to avoid many unnecessary operations within the crucial 'inner loop' over index `j`. The more general questions of time-saving tricks in this part of the program are addressed in Chapter 5. The extension of this type of double loop to deal with other forms of the pair potential, and to compute forces in addition to potential terms, is straightforward, and examples will be given in later chapters. For molecular systems, the same general principles apply, but additional loops over the different sites or atoms in a molecule may be needed. For example, consider the site–site diatomic model of eqn (1.12) and Fig. 1.6. Then the intermolecular interactions might be computed as in Code 1.3. Note that, apart from the dependence of the range of the `j` loop on the index `i`, the order of nesting of loops is a matter of choice. Here, we have placed a loop over molecular indices innermost; assuming that `n` is relatively large, and depending on the machine architecture, this may improve the efficiency of fetching the relevant coordinates from memory (in Fortran, the arrays are stored so that the first indices vary rapidly, and the last indices vary slowly, so there is usually an advantage in accessing contiguous blocks of memory, or cache, in sequence). Simulations of molecular systems may also

Code 1.2 Double loop for Lennard-Jones potential

This code snippet illustrates the calculation of the potential energy for a system of Lennard-Jones atoms, using a double loop over the atomic indices. The declarations at the start are given just to remind us of the types and sizes of variables and arrays (some notes on precision of variables appear in Appendix A).

```
INTEGER               :: n, i, j
REAL, DIMENSION(3,n) :: r
REAL, DIMENSION(3)   :: rij
REAL                  :: epslj, sigma, sigma_sq
REAL                  :: pot, rij_sq, sr2, sr6, sr12
sigma_sq = sigma ** 2
pot = 0.0
DO i = 1, n-1
  DO j = i+1, n
    rij(:) = r(:,i) - r(:,j)
    rij_sq = SUM ( rij ** 2 )
    sr2    = sigma_sq / rij_sq
    sr6    = sr2 ** 3
    sr12   = sr6 ** 2
    pot    = pot + sr12 - sr6
  END DO
END DO
pot = 4.0 * epslj * pot
```

involve the calculation of intramolecular energies, which, for site–site potentials, will necessitate a triple summation (over `i`, `a`, and `b`).

These examples are essentially summations over pairs of interaction sites in the system. Any calculation of three-body interactions will, of course, entail triple summations over distinct triplets of indices `i`, `j`, and `k`; these will be much more time consuming than the double summations described here. Even for pairwise-additive potentials, the energy or force calculation is the most expensive part of a computer simulation. We will return to this crucial section of the program in Chapter 5.

1.4 Constructing an intermolecular potential from first principles

1.4.1 Introduction

There are two approaches to constructing an intermolecular potential for use in a simulation. For small, simple molecules and their mixtures, it is possible to customize a model, with considerable freedom in choosing the functional form of the potentials and in adjusting the parameters for the problem at hand. For larger molecules such as polymers, proteins, or DNA, either in solution or at a surface, or for multi-component mixtures

Code 1.3 Site–site potential energy calculation

The coordinates $\mathbf{r}_{ia}$ of site a in molecule i are stored in the elements `r(:,i,a)` of a rank-3 array; for a system of diatomic molecules `na=2`.

```
INTEGER                   :: n, i, j, a, b
REAL, DIMENSION(3,n,na) :: r
REAL, DIMENSION(3)      :: rij
DO a = 1, na
  DO b = 1, na
    DO i = 1, n - 1
      DO j = i + 1, n
        rij(:) = r(:,i,a) - r(:,j,b)
        ... calculate the i-j interaction ...
      END DO
    END DO
  END DO
END DO
```

containing many different types of molecule, then it will be more usual to employ one of the standard force fields (consisting of fixed functional forms for the potentials combined with parameters corresponding to the many different atom types in the simulation). We will cover the first aspect of model building in this section and consider force fields in Section 1.5.

There are essentially two stages in setting up a model for a realistic simulation of a given system. The first is 'getting started' by constructing a first guess at a potential model. This will allow some preliminary simulations to be carried out. The second is to use the simulation results, in comparison with experiment, to refine the potential model in a systematic way, repeating the process several times if necessary. We consider the two phases in turn.

1.4.2 Building the model potential

To illustrate the process of building up an intermolecular potential from first principles, we consider a small molecule, such as N_2, OCS, or CH_4, which can be modelled using the interaction site potentials discussed in Section 1.3. The essential features of this model will be an anisotropic repulsive core, to represent the shape, an anisotropic dispersion interaction, and some partial charges or distributed multipoles to model the permanent electrostatic effects. This crude effective pair potential can then be refined by using it to calculate properties of the gas, liquid, and solid, and comparing with experiment. Each short-range site–site interaction can be modelled using a Lennard-Jones potential. Suitable energy and length parameters for interactions between pairs of identical atoms in different molecules are available from a number of simulation studies. Some of these are given in Table 1.1. The energy parameter ϵ increases with atomic number as the polarizability goes up; σ also increases down a group of the Periodic Table, but decreases

Table 1.1 Atom–atom interaction parameters

Atom	Source	ϵ/k_B (K)	σ (nm)
H	Murad and Gubbins (1978)	8.6	0.281
He	Maitland et al. (1981)	10.2	0.228
C	Tildesley and Madden (1981)	51.2	0.335
N	Cheung and Powles (1975)	37.3	0.331
O	English and Venables (1974)	61.6	0.295
F	Singer et al. (1977)	52.8	0.283
Ne	Maitland et al. (1981)	47.0	0.272
S	Tildesley and Madden (1981)	183.0	0.352
Cl	Singer et al. (1977)	173.5	0.335
Ar	Maitland et al. (1981)	119.8	0.341
Br	Singer et al. (1977)	257.2	0.354
Kr	Maitland et al. (1981)	164.0	0.383

from left to right across a period with the increasing nuclear charge. For elements which do not appear in Table 1.1, a guide to ϵ and σ might be provided by the polarizability and van der Waals radius respectively. These values are only intended as a reasonable first guess: they take no regard of chemical environment and are not designed to be transferable. For example, the carbon atom parameters in CS_2 given in the table are quite different from the values appropriate to a carbon atom in graphite (Crowell, 1958).

Interactions between unlike atoms in different molecules can be approximated using the venerable Lorentz–Berthelot combining rules. For example, in CS_2 the cross-terms are

$$\sigma_{CS} = \tfrac{1}{2}\left(\sigma_{CC} + \sigma_{SS}\right), \quad \epsilon_{CS} = \left(\epsilon_{CC}\epsilon_{SS}\right)^{1/2}. \tag{1.35}$$

These rules are approximate; the ϵ cross-term expression, especially, is not expected to be appropriate in the majority of cases (Delhommelle and Millié, 2001; Haslam et al., 2008).

In tackling larger molecules, it may be necessary to model several atoms as a unified site. We have seen this for butane in Section 1.3, and a similar approach has been used in a model of benzene (Evans and Watts, 1976). The specification of an interaction site model is made complete by defining the positions of the sites within the molecule. Normally, these are located at the positions of the nuclei, with the bond lengths obtained from a standard source (CRC, 1984).

Rapid progress has been made in fitting the parameters for many classical pair potentials using *ab initio* quantum mechanical calculations. For example, symmetry-adapted perturbation theory, based on a density-functional approach, can be used to calculate separable and transferable parameters for the dispersion and electrostatic interactions (McDaniel and Schmidt, 2013). Calculations on monomers are used to estimate asymptotic properties such as charge and polarizability, while dimer calculations are used to estimate the parameters depending on charge density overlaps. The resulting parameters can be

used with simple functional forms in simulations and the technique has recently been applied to the parameterization and simulation of an ionic liquid (Son et al., 2016).

The site–site Lennard-Jones potentials include an anisotropic dispersion which has the correct r^{-6} radial dependence at long range. However, this is not the exact result for the anisotropic dispersion from second-order perturbation theory. The correct formula, in an appropriate functional form for use in a simulation, is given by Burgos et al. (1982). Its implementation requires an estimate of the polarizability and polarizability anisotropy of the molecule.

It is also possible to improve the accuracy of the overall repulsion–dispersion interaction by considering an anisotropic site–site potential in place of $v_{ab}(\mathbf{r}_{ab})$ in eqn (1.12). In other words, in a diatomic model of a chlorine molecule, the interatomic potential between chlorine atoms in different molecules would depend on r_{ab} and the angles between $\mathbf{r}_{ab}$ and intramolecular bonds. This type of model has been used to rationalize the liquid and solid structures of liquid Cl_2, Br_2, and I_2 (Rodger et al., 1988a,b).

The most straightforward way of representing electrostatic interactions is through partial charges as discussed in Section 1.3. To minimize the calculation of site–site distances they can be made to coincide with the Lennard-Jones sites, but this is not always desirable or possible; the only physical constraint on partial charge positions is that they should not lie outside the repulsive core region, since the potential might then diverge if molecules came too close. The magnitudes of the charges can be chosen to duplicate the known gas-phase electrostatic moments (Gray and Gubbins, 1984, Appendix D). Alternatively, the moments may be taken as adjustable parameters. For example, in a simple three-site model of N_2 representing only the quadrupole–quadrupole interaction, the best agreement with condensed phase properties is obtained with charges giving a quadrupole 10 %–15 % lower than the gas-phase value (Murthy et al., 1980). However, a sensible strategy is to begin with the gas-phase values, and alter the repulsive core parameters ϵ and σ before changing the partial charges.

Partial charges can also be developed using theoretical calculations. Bayly et al. (1993) have developed the widely used restrained electrostatic potential (RESP) method. In this technique:

(a) a molecule is placed in a 3D grid of points;

(b) the electrostatic potential is calculated at each grid point, outside the repulsive core, using a quantum mechanical calculation;

(c) a charge at each atom of the molecules is adjusted to reproduce the electrostatic potential at the grid points as accurately as possible.

Typically, accurate enough quantum mechanical estimates of the electrostatic field can be obtained using the 6-31G* level of the Gaussian code (Frisch et al., 2009). In order to make this fitting procedure robust and to obtain charges that are transferable between different molecules, it is necessary to minimize the magnitude of the charges that will fit the field. This is achieved using a hyperbolic restraint function in the minimization that pulls the magnitude of the charges towards zero.

Distributed multipoles and polarizabilities, for molecules containing up to about 60 atoms, can be calculated from first principles using the CAMCASP package developed by Stone and co-workers (Misquitta and Stone, 2013).

1.4.3 Adjusting the model potential

The first-guess potential can be used to calculate a number of properties in the gas, liquid, and solid phases; comparison of these results with experiment may be used to refine the potential, and the cycle can be repeated if necessary. The second virial coefficient is given by

$$B(T) = -\frac{2\pi}{\Omega^2}\int_0^\infty r_{ij}^2 \mathrm{d}r_{ij} \int \mathrm{d}\Omega_i \int \mathrm{d}\Omega_j \exp\left[-v(r_{ij},\ \Omega_i,\ \Omega_j)/k_\mathrm{B}T\right] - 1 \tag{1.36}$$

where $\Omega = 4\pi$ for a linear molecule and $\Omega = 8\pi^2$ for a non-linear one. This multidimensional integral (four-dimensional for a linear molecule and six-dimensional for a non-linear one) is easily calculated using a non-product algorithm (Murad, 1978). Experimental values of $B(T)$ have been compiled by Dymond and Smith (1980). Trial and error adjustment of the Lennard-Jones ϵ and σ parameters should be carried out, with any bond lengths and partial charges held fixed, so as to produce the closest match with the experimental $B(T)$. This will produce an improved potential, but still one that is based on pair properties.

The next step is to carry out a series of computer simulations of the liquid state, as described in Chapters 3 and 4. The densities and temperatures of the simulations should be chosen to be close to the orthobaric curve of the real system, that is, the liquid–vapour coexistence line. The output from these simulations, particularly the total internal energy and the pressure, may be compared with the experimental values. The coexisting pressures are readily available (Rowlinson and Swinton, 1982), and the internal energy can be obtained approximately from the known latent heat of evaporation. The energy parameters ϵ are adjusted to give a good fit to the internal energies along the orthobaric curve, and the length parameters σ altered to fit the pressures. If no satisfactory fit is obtained at this stage, the partial charges may be adjusted. It is also possible to adjust potential parameters to reproduce structural properties of the liquid, such as the site–site pair distribution functions (see Section 2.6), which can be extracted from coherent neutron diffraction studies using isotopic substitution (Cole et al., 2006; Zeidler et al., 2012).

Although the solid state is not the province of this book it offers a sensitive test of any potential model. Using the experimentally observed crystal structure, and the refined potential model, the lattice energy at zero temperature can be compared with the experimental value (remembering to add a correction for quantum zero-point motion). In addition, the lattice parameters corresponding to the minimum energy for the model solid can be compared with the values obtained by diffraction, and also lattice dynamics calculations (Neto et al., 1978) used to obtain phonons, librational modes, and dispersion curves of the model solid. Finally, we can ask if the experimental crystal structure is indeed the minimum energy structure for our potential. These constitute severe tests of our model-building skills (Price, 2008).

1.5 Force fields

In approaching the simulation of a complicated system, there might be 30 different atom types to consider and several hundred different intra- and inter-molecular potentials to fit. One would probably not want to build the potential model from scratch. Fortunately, it is

possible to draw on the considerable body of work that has gone into the development of consistent force fields over the last 50 years (Bixon and Lifson, 1967; Lifson and Warshel, 1968; Ponder and Case, 2003).

A force field, in the context of a computer simulation, refers to the functional forms used to describe the intra- and inter-molecular potential energy of a collection of atoms, and the corresponding parameters that will determine the energy of a given configuration. These functions and parameters have been derived from experimental work on single molecules and from accurate quantum mechanical calculations. They are often refined by the use of computer simulations to compare calculated condensed phase properties with experiment. This is precisely the same approach described in Section 1.4.3, but on a bigger scale, so that the transferable parameters developed can be used with many different molecules. Some examples of widely used force fields are given in Table 1.2. This list is representative and not complete. The individual force fields in the table are constantly being updated and extended. For example, the OPLS force field has been refined to allow for the modelling of carbohydrates (Kony et al., 2002) and the OPLS and AMBER force fields have been used as the basis of a new field for ionic liquids (Lopes et al., 2004). Extensions and versions are often denoted by the ffXX specification following the force field name. A short search of the websites of the major force fields will establish the latest version and the most recent developments.

Force fields are often divided into three classes. Class I force fields normally have a functional form of the type

$$\mathcal{V} = \sum_{\text{bonds}} \tfrac{1}{2}k_r(r_{ij} - r_0)^2 + \sum_{\text{angles}} \tfrac{1}{2}k_\theta(\theta_{ijk} - \theta_0)^2 + \sum_{\text{torsions}} \sum_{n} k_{\phi,n}[\cos(n\phi_{ijk\ell} + \delta_n) + 1] + \sum_{\substack{\text{non-bonded}\\ \text{pairs}}} \left[\frac{q_i q_j}{4\pi\epsilon_0 r_{ij}} + \frac{A_{ij}}{r_{ij}^{12}} - \frac{B_{ij}}{r_{ij}^{6}}\right]. \quad (1.37)$$

The first term in eqn (1.37) is a sum over all bonds, with an equilibrium bond-length r_0. There is one term for every pair ij of directly connected atoms. In some force fields the harmonic potential can be replaced by a more realistic functional form, such as the Morse potential, or the bonds can be fixed at their equilibrium values. The second term is a sum over all bond angles. There is one term for each set of three connected atoms ijk and it usually has a quadratic form. The third term is the sum over all torsions involving four connected atoms $ijk\ell$. In principle, this is an expansion in trigonometric functions with different values of n, the multiplicity (i.e. the number of minima in a rotation of 2π around the j–k bond); many force fields fix $n = 3$. This term can also include improper torsions, where the four atoms defining the angle are not all connected by covalent bonds; such terms serve primarily to enforce planarity around sp^2 centres and use a variety of functional forms (Tuzun et al., 1997). The fourth term is a sum over the non-bonded interactions (between molecules and within molecules). In particular, it describes the electrostatic and repulsion–dispersion interactions. It invariably excludes 1–2 and 1–3 pairs in the same molecule. Some force fields do include a non-bonded 1–4 interaction but the parameters A'_{ij}, B'_{ij} describing this interaction can be different from the values for atoms separated by more than three bonds (a scaling factor of 0.4 is used in the param19 force field of CHARMM (Brooks et al., 1983)). In some force fields, the r_{ij}^{-12}

Table 1.2 Force fields and their domains of application. This list is not complete and simply includes representative examples of some of the force fields commonly used in liquid-state simulations.

Force field	Class	Domain of Application	Source
OPLS	I	peptides, small organics	Jorgensen et al. (1996)
CHARMM22	I	proteins with explicit water	Mackerell et al. (1998)
CHARMM27	I	DNA, RNA, and lipids	Mackerell et al. (1998)
AMBER ff99	I	peptides, small organics, RESP charges	Wang et al. (2000)
GAFF	I	small organics, drug design	Wang et al. (2004)
GROMOS ffG45a3	I	lipids, micelles	Schuler et al. (2001)
COMPASS	II	small molecules, polymers	Sun (1998)
clayFF	II	hydrated minerals	Cygan et al. (2004)
MM4	II	small organics, coordination compounds	Allinger et al. (1996)
UFF	II	full Periodic Table (including actinides)	Rappe et al. (1992)
AMBER ff02	III	polarizable atoms	Cieplak et al. (2001)
AMOEBA	III	polarizable multipoles, distributed multipoles	Ponder et al. (2010)
MARTINI	III	coarse-grained, proteins, lipids, polymers	Marrink et al. (2007)
ReaxFF	III	chemical reactions	van Duin et al. (2001)

repulsion (associated with the Lennard-Jones potential) is replaced by an r_{ij}^{-9} repulsion which can produce better agreement with direct quantum calculations of the repulsion (Hagler et al., 1979; Halgren, 1992). The exponential form of the repulsion ($A\exp(-Br_{ij})$) was used in earlier versions of the AMBER force fields (MM2 and MM3) but has now been replaced by the r_{ij}^{-12} repulsion. The cross-interactions for the parameters in the repulsion–dispersion potential are often described using the Lorentz–Berthelot combining rules or an alternative such as the Slater–Kirkwood formula (Slater and Kirkwood, 1931). If these crossed interactions are important in the model they can be determined directly by fitting to experiment. In class I force fields, a simple Coulombic term is used to describe the interaction between the partial charges, which represent the electrostatic interactions between molecules.

Different parameters are required for different atoms in different environments, and all of the atom types in the model must be specified. For example, in the GROMOS force field ffG45a3 (Schuler et al., 2001), there are 12 types of C atoms, six Os, six Ns, four Cls, three Hs, two Ss, two Cus and one type for each of the remaining common atoms. The parameters $\{k_r, k_\theta, k_{\phi,n}, \delta_n, q_i, q_j, A_{ij}, B_{ij}\}$ are then specified for combinations of the atom types. For example, in a peptide chain, which contains C, N, and C_α atom types along the backbone (where C is a carbon additionally double-bonded to an oxygen and C_α is a carbon additionally connected to a hydrogen and a side chain) we would require k_r for the C–N stretch, a different k_r for the N–C_α stretch, k_θ for the C–N–C_α bend, $k_{\phi,n}$, for the C–N–C_α–C torsion, and additional parameters for the other bends and torsion in the backbone.

All-atom force fields provide parameters for every type of atom in a system, including hydrogen, while united-atom force fields treat the hydrogen and carbon atoms in each terminal methyl and each methylene bridge as a single interaction centre.

A class II force field normally adds cubic or anharmonic terms to the stretching potentials and defines explicit off-diagonal elements in the force constant matrix. Thus, the force field will contain terms of the form

$$\begin{aligned} v^{\text{str–str}}(r_{12}, r_{23}) &= k_{12,23}(r_{12} - r_{12,0})(r_{23} - r_{23,0}) \\ v^{\text{bend–str}}(\theta_{123}, r_{12}) &= k_{123,12}(\theta_{123} - \theta_{123,0})(r_{12} - r_{12,0}) \end{aligned} \tag{1.38}$$

where r_{12} and r_{23} are two adjacent bonds in the molecule, which include the angle θ_{123}. These additional potentials represent the fact that bonds, angles and torsions are not independent in molecules. Most cross-terms involve two internal coordinates and Dinur and Hagler (1991) have used quantum mechanical calculations to show that the stretch–stretch, stretch–bend, bend–bend, stretch–torsion, and bend–bend–torsion are the important coupling terms. The cross-terms are essential to include in models when attempting to calculate accurate vibrational frequencies. Despite the additional complexity, Class II force fields, such as COMPASS and CFF, have been used to good effect in liquid-state simulations (Peng et al., 1997; Sun, 1998).

Class III force fields go beyond the basic prescription to include more accurate representations of the electrostatic interactions between molecules and the inclusion of polarizability (as discussed in Section 1.3.3). For example, the AMOEBA force field includes distributed multipoles and the atom polarizabilities with the Thole modification of the

interaction tensor. This class would also include coarse-grained force fields such as MARTINI used to model lipids, proteins, and carbohydrates (see Section 1.3.4) and force fields specifically designed to model chemical reactions such as ReaxFF. ReaxFF includes a set of relationships between the bond distance and the bond order of a particular covalent bond. Once the bond order is determined, the associated bond energy can be calculated. This procedure results in proper dissociation of bonds to separated atoms at the appropriate distances.

After many decades of force field development, there are still considerable differences between the predictions from even the Class I force fields. In an excellent review of the field, Ponder and Case (2003) compare simulations of a solvated dipeptide using CHARMM27, AMBER94, and OPLS-aa force fields to map the free energy of the dipeptide as a function of the two torsional angles, ψ and ϕ. All three force fields exhibit ψ–ϕ maps that are different from one another and different from the results of an *ab initio* simulation of the same problem. In contrast, in considering the liquid-state properties for butane, methanol, and N-methylacetamide, Kaminski and Jorgensen (1996) demonstrated reasonable agreement between the AMBER94 and OPLS force field, both of which had been fitted to liquid-state properties. In this study the MMFF94 force field, that had been optimized for gas-phase geometries, needed to be adjusted to obtain the same level of agreement when applied to the liquids. One important point is that it is not possible to mix and match different force fields. They have been optimized as a whole and one should not attempt to use parts of one field with parts of another. This means that devising force fields to simulate very different materials interacting with each other is a particular challenge. As an illustration, the steps taken to model the adsorption of biomolecules on the surface of metallic gold, in water, are discussed in Example 1.2.

It is difficult to make blanket recommendations concerning the use of particular force fields. Individual researchers will need to understand the kind of problems for which the force field has been optimized to know if it can be applied to their particular problem. One sensible strategy would be to check the effect of using a few of the more common force fields on the problem to understand the sensitivity of the results to this choice.

An important advantage of the force-field approach is that that particular fields are often associated with large simulation programs. The acronyms CHARMM, AMBER, and GROMOS can also stand for large molecular dynamics codes which have been designed to work with the particular forms of a field and there are many examples of other codes such as LAMMPS (Plimpton, 1995) and DL_POLY (Todorov and Smith, 2011) that can take standard force fields with some adjustments. There is also a huge industry of analysis and data manipulation programmes that have grown with the major force fields and codes.

Of course, using these programmes as black-boxes is never a good idea and we plan in this book to dig into the principles behind such codes. Equally, if one can take advantage of the many years of careful development that have gone into producing these packages in an informed way, an enormous range of complicated and important applications can be tackled fairly quickly.

Example 1.2 Peptide–gold potentials

Peptides, short chains of amino acids, may be designed so as to specifically favour adsorption on certain material surfaces. This underpins a range of possible bionanotechnology applications (Care et al., 2015). Understanding this selectivity and specificity is a great challenge to molecular simulation: clearly the adsorption free energy depends on many factors, including changes in peptide flexibility, its solvation, and displacement of the water layer at the surface. Measurement of adsorption free energies requires advanced simulation techniques (see Chapters 4 and 9); modelling the potential energy of interaction between the surface and individual amino acids is itself challenging, involving the cross-interaction between two very different materials (Di Felice and Corni, 2011; Heinz and Ramezani-Dakhel, 2016). Here we focus on recent attempts to model peptide interactions with the surface(s) of metallic gold.

A simple Lennard-Jones force field for a range of FCC metals, including gold, has been proposed (Heinz et al., 2008): ϵ_{AuAu} and σ_{AuAu} are chosen to reproduce various experimental bulk and surface properties, under ambient conditions. Water and peptide atom–Au parameters are obtained by standard combining rules. Feng et al. (2011) have used this potential to study the adsorption of individual amino acids on gold, while Cannon et al. (2015) have used it to highlight solvent effects in peptide adsorption. A different parameterization, similar in spirit, has been derived independently (Vila Verde et al., 2009; 2011). The whole method has been generalized to cover a range of other materials (Heinz et al., 2013). Compatibility with standard force fields, such as CHARMM, is an advantage of this approach; polarization of the metal, and chemisorption, however, are neglected.

A purely dispersive potential of this kind may have limitations when one considers structure: adsorption (of water molecules or peptide atoms) onto hollow sites on the surface is strongly favoured. On metallic surfaces, however, adsorption on top of surface atoms is often preferred, as indicated by first-principles simulations. In the GolP force field (Iori et al., 2009), dynamical polarization of gold atoms is represented by a rotating dipole, and virtual interaction sites are introduced to tackle the hollow-site adsorption problem. GolP is parameterized using extensive first-principles calculations and experimental data, with special consideration given to surface interactions with sp^2-hybridized carbons. An extension, GolP–CHARMM, reparameterized for compatibility with CHARMM, also allows consideration of different gold surfaces (Wright et al., 2013b,a), opening up the study of facet selectivity (Wright et al., 2015). In GolP, the gold atoms are held fixed during the simulation.

Tang et al. (2013) have compared GolP results with experimental studies of peptide adsorption, and with the force field of Heinz et al. (2008). While both models perform reasonably well in describing the trend in amino acid adsorption energies, there are areas such as the prediction of water orientation in the surface layer where GolP–CHARMM agrees better with first-principles simulations (Nadler and Sanz, 2012). This approach may allow one to separate the enthalpic contributions to the binding free energy, and ascribe them to individual residues (Corni et al., 2013; Tang et al., 2013).

1.6 Studying small systems

1.6.1 Introduction

Simulations are usually performed on a small number of molecules, $10 \leq N \leq 10\,000$. The size of the system is limited by the available storage on the host computer, and, more crucially, by the speed of execution of the program. The time taken for a double loop used to evaluate the forces or potential energy is proportional to N^2. Special techniques (see Chapter 5) may reduce this dependence to $O(N)$, for very large systems, but the force/energy loop almost inevitably dictates the overall speed and, clearly, smaller systems will always be less expensive. If we are interested in the properties of a very small liquid drop, or a microcrystal, then the simulation will be straightforward. The cohesive forces between molecules may be sufficient to hold the system together unaided during the course of a simulation, otherwise our set of N molecules may be confined by a potential representing a container, which prevents them from drifting apart (see Chapter 13). These arrangements, however, are not satisfactory for the simulation of bulk liquids. A major obstacle to such a simulation is the large fraction of molecules which lie on the surface of any small sample; for 1000 molecules arranged in a $10 \times 10 \times 10$ cube, $8^3 = 512$ lie in the interior, leaving 488 (nearly half!) on the cube faces. Even for $N = 100^3 = 10^6$ molecules, 6 % of them will lie on the surface. Whether or not the cube is surrounded by a containing wall, molecules on the surface will experience quite different forces from those in bulk.

1.6.2 Periodic boundary conditions.

The problem of surface effects can be overcome by implementing periodic boundary conditions (Born and von Karman, 1912). The cubic box is replicated throughout space to form an infinite lattice. In the course of the simulation, as a molecule moves in the original box, its periodic image in each of the neighbouring boxes moves in exactly the same way. Thus, as a molecule leaves the central box, one of its images will enter through the opposite face. There are no walls at the boundary of the central box, and no surface molecules. This box simply forms a convenient axis system for measuring the coordinates of the N molecules. A two-dimensional version of such a periodic system is shown in Fig. 1.13. The duplicate boxes are labeled A, B, C, etc., in an arbitrary fashion. As particle 1 moves through a boundary, its images 1_A, 1_B, etc. (where the subscript specifies in which box the image lies) move across their corresponding boundaries. The number density in the central box (and hence in the entire system) is conserved. It is not necessary to store the coordinates of all the images in a simulation (an infinite number!), just the molecules in the central box. When a molecule leaves the box by crossing a boundary, attention may be switched to the image just entering. It is sometimes useful to picture the basic simulation box (in our two-dimensional example) as being rolled up to form the surface of a three-dimensional torus or doughnut, when there is no need to consider an infinite number of replicas of the system, nor any image particles. This correctly represents the topology of the system, if not the geometry. A similar analogy exists for a three-dimensional periodic system, but this is more difficult to visualize!

It is important to ask if the properties of a small, infinitely periodic, system and the macroscopic system which it represents are the same. This will depend both on the range of the intermolecular potential and the phenomenon under investigation. For a fluid of

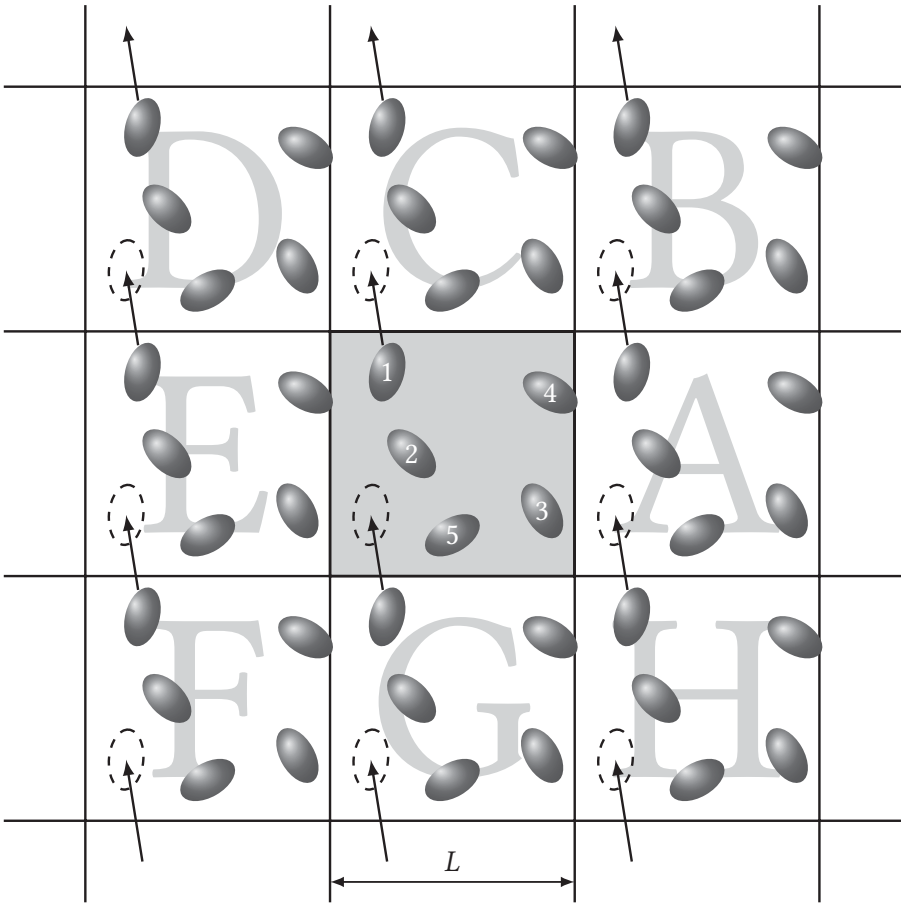

Fig. 1.13 A two-dimensional periodic system. Molecules can enter and leave each box across each of the four edges. In a three-dimensional example, molecules would be free to cross any of the six cube faces.

Lennard-Jones atoms it should be possible to perform a simulation in a cubic box of side $L \approx 6\,\sigma$ without a particle being able to 'sense' the symmetry of the periodic lattice. If the potential is long range (i.e. $v(r) \sim r^{-\nu}$ where ν is less than the dimensionality of the system) there will be a substantial interaction between a particle and its own images in neighbouring boxes, and consequently the symmetry of the cell structure is imposed on a fluid which is in reality isotropic. The methods used to cope with long-range potentials, for example in the simulation of charged ions ($v(r) \sim r^{-1}$) and dipolar molecules ($v(r) \sim r^3$), are discussed in Chapter 5. We know that even in the case of short-range potentials the periodic boundary conditions can induce anisotropies in the fluid structure (Mandell, 1976; Impey et al., 1981). These effects are pronounced for small system sizes ($N = 100$) and for properties such as the g_2 light scattering factor (see Chapter 2), which has a substantial long-range contribution. Pratt and Haan (1981) have developed theoretical methods for investigating the effects of boundary conditions on equilibrium properties.

The use of periodic boundary conditions inhibits the occurrence of long-wavelength fluctuations. For a cube of side L, the periodicity will suppress any density waves with a wavelength greater than L. Thus, it would not be possible to simulate a liquid close

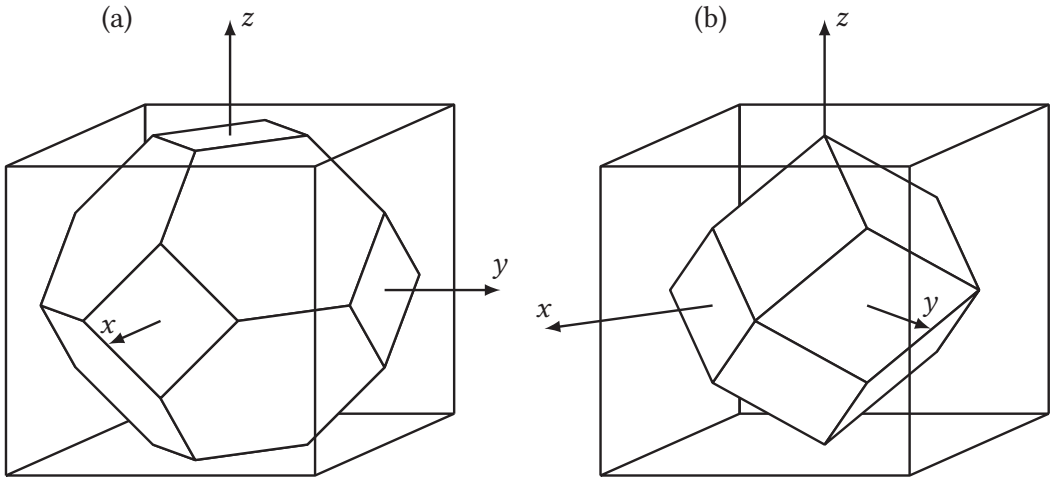

Fig. 1.14 Non-cubic, space-filling, simulation boxes. (a) The truncated octahedron and its containing cube; (b) the rhombic dodecahedron and its containing cube. The axes are those used in Code 1.4 and Code 1.5 of Section 1.6.4.

to the gas–liquid critical point, where the range of critical fluctuations is macroscopic. Furthermore, transitions which are known to be first order often exhibit the characteristics of higher-order transitions when modelled in a small box, because of the suppression of fluctuations. Examples are the nematic–isotropic transition in liquid crystals (Luckhurst and Simpson, 1982) and the solid–plastic-crystal transition for N_2 adsorbed on graphite (Mouritsen and Berlinsky, 1982). The same limitations apply to the simulation of long-wavelength phonons in model solids, where in addition, the cell periodicity picks out a discrete set of available wavevectors (i.e. $\mathbf{k} = (n_x, n_y, n_z)2\pi/L$, where n_x, n_y, n_z, are integers) in the first Brillouin zone (Klein and Weis, 1977). Periodic boundary conditions have also been shown to affect the rate at which a simulated liquid nucleates and forms a solid or glass when it is rapidly cooled (Honeycutt and Andersen, 1984).

Despite the preceding remarks, the common experience in simulation work is that periodic boundary conditions have little effect on the equilibrium thermodynamic properties and structures of fluids away from phase transitions and where the interactions are short-ranged. It is always sensible to check that this is true for each model studied. If the resources are available, it should be standard practice to increase the number of molecules (and the box size, so as to maintain constant density) and rerun the simulations. The cubic box has been used almost exclusively in computer simulation studies because of its geometrical simplicity. Of the four remaining semi-regular space-filling polyhedra, the rhombic dodecahedron (Wang and Krumhansl, 1972), and the truncated octahedron (Adams, 1979; 1980) have also been studied. These boxes are illustrated in Fig. 1.14. They are more nearly spherical than the cube, which may be useful for simulating liquids, whose structure is spatially isotropic. In addition, for a given number density, the distance between periodic images is larger than in the cube. This property is useful in calculating distribution functions and structure factors (see Chapters 2 and 8). As we shall see in Section 1.6.4, they are only slightly more complicated to implement in simulations than cubic boxes.

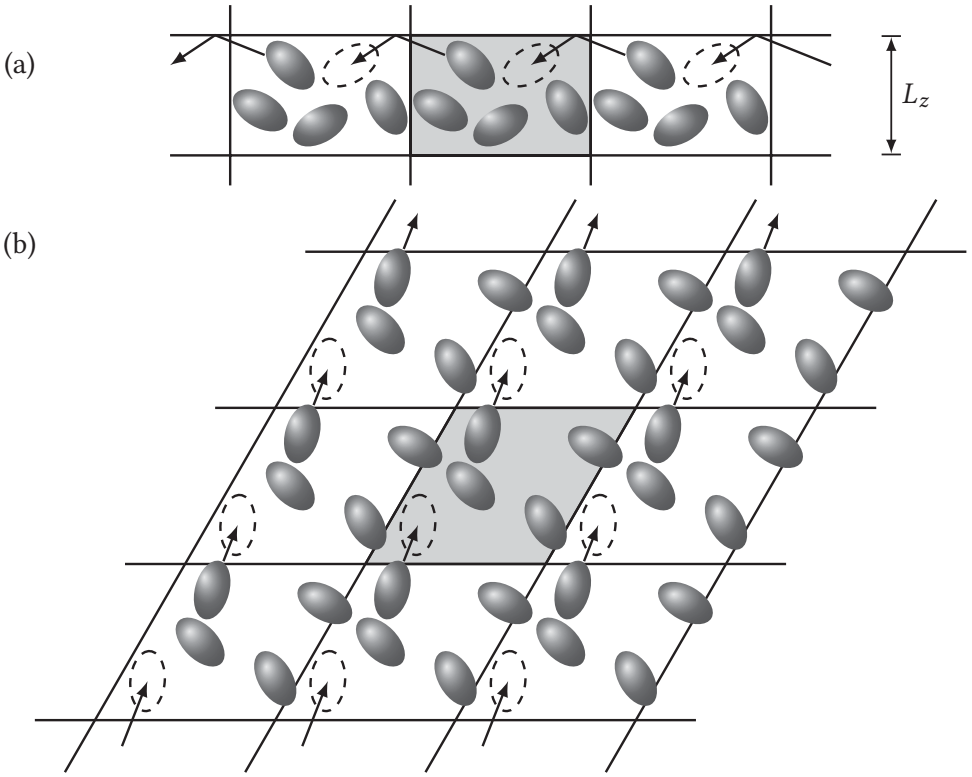

Fig. 1.15 Periodic boundary conditions used in the simulation of adsorption (see e.g. Severin and Tildesley, 1980). (a) A side view of the box. There is a reflecting boundary at height L_z. (b) A top view, showing the rhombic shape (i.e. the same geometry as the underlying graphite lattice). Periodic boundary conditions in this geometry are implemented in Code 1.6.

So far, we have tacitly assumed that there is no external potential, that is, no v_1, term in eqns (1.4) and (1.5). If such a potential is present, then either it must have the same periodicity as the simulation box, or the periodic boundaries must be abandoned. In some cases, it is not appropriate to employ periodic boundary conditions in each of the three coordinate directions. In the simulation of CH_4 on graphite (Severin and Tildesley, 1980) the simulation box, shown in Fig. 1.15, is periodic in the plane of the surface. In the z-direction, the graphite surface forms the lower boundary of the box, and the bulk of the adsorbate is in the region just above the graphite. Any molecule in the gas above the surface is confined by reversing its velocity should it cross a plane at a height L_z above the surface. If L_z is sufficiently large, this reflecting boundary will not influence the behaviour of the adsorbed monolayer. In the plane of the surface, the shape of the periodic box is a rhombus of side L. This conforms to the symmetry of the underlying graphite. Similar boxes have been used in the simulation of the electrical double layer (Torrie and Valleau, 1979), of the liquid–vapour surface (Chapela et al., 1977), and of fluids in small pores (Subramanian and Davis, 1979).

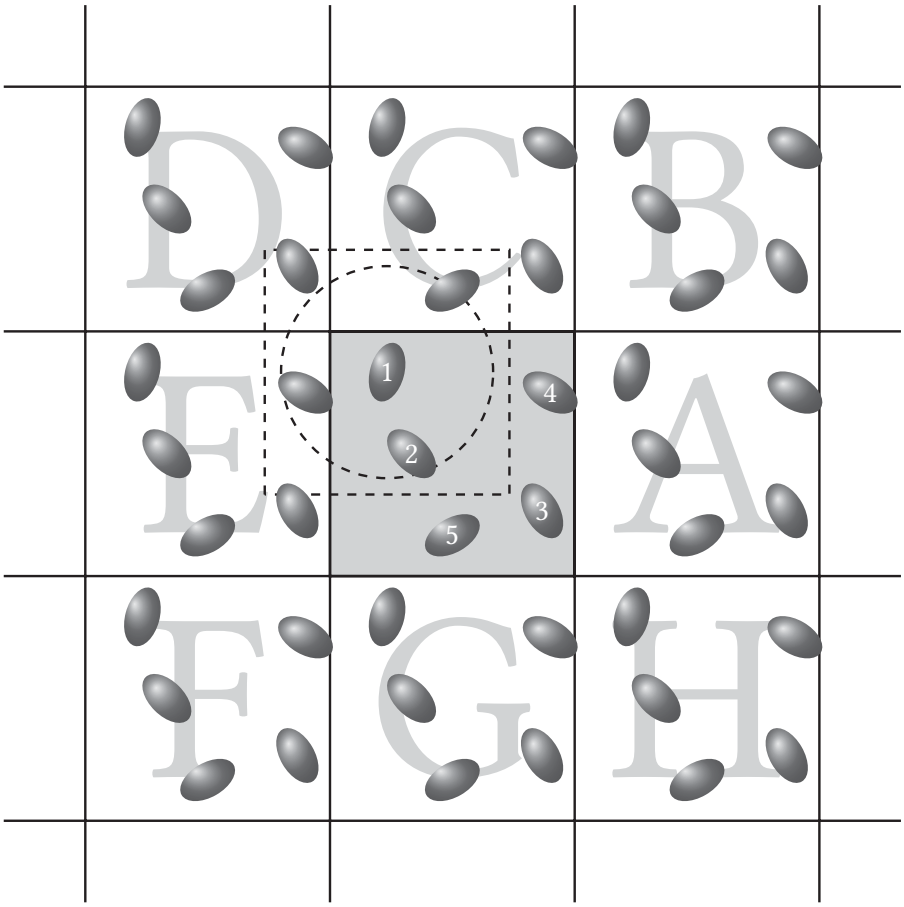

Fig. 1.16 The minimum image convention in a two-dimensional system. The central 'box' contains five molecules. The dashed 'box' constructed with molecule 1 at its centre also contains five molecules. The dashed circle represents the cutoff.

1.6.3 Potential truncation

Now we must turn to the question of calculating properties of systems subject to periodic boundary conditions. The heart of the MC and MD programs involves the calculation of the potential energy of a particular configuration, and, in the case of MD, the forces acting on all molecules. Consider how we would calculate the force on molecule 1, or those contributions to the potential energy involving molecule 1, assuming pairwise additivity. We must include interactions between molecule 1 and every other molecule i in the simulation box. There are $N - 1$ terms in this sum. However, in principle, we must also include all interactions between molecule 1 and images i_A, i_B, etc. lying in the surrounding boxes. This is an infinite number of terms, and of course is impossible to calculate in practice. For a short-range potential-energy function, we may restrict this summation by making an approximation. Consider molecule 1 to rest at the centre of a region which has the same size and shape as the basic simulation box (see Fig. 1.16). Molecule 1 interacts with all the molecules whose centres lie within this region, that is, with the closest periodic images of the other $N - 1$ molecules. This is called the 'minimum

image convention': for example, in Fig. 1.16, molecule 1 could interact with molecules 2, 3_D, 4_E, and 5_C. This technique, which is a natural consequence of the periodic boundary conditions, was first used in simulation by Metropolis et al. (1953).

In the minimum image convention, then, the calculation of the potential energy due to pairwise-additive interactions involves $\frac{1}{2}N(N-1)$ terms. This may still be a very substantial calculation for a system of (say) 1000 particles. A further approximation significantly improves this situation. The largest contribution to the potential and forces comes from neighbours close to the molecule of interest, and for short-range forces we normally apply a spherical cutoff. This means setting the pair potential $v(r)$ to zero for $r \geq r_c$, where r_c is the cutoff distance. The dashed circle in Fig. 1.16 represents a cutoff, and in this case molecules 2, 4_E and 5_C contribute to the force on 1, since their centres lie inside the cutoff, whereas molecule 3_D does not contribute. In a cubic simulation box of side L, the number of neighbours explicitly considered is reduced by a factor of approximately $4\pi r_c^3/3L^3$, and this may be a substantial saving. The introduction of a spherical cutoff should be a small perturbation, and the cutoff distance should be sufficiently large to ensure this. As an example, in the simulation of Lennard-Jones atoms the value of the pair potential at the boundary of a cutoff sphere of typical radius $r_c = 2.5\,\sigma$ is just 1.6 % of the well depth. Of course, the penalty of applying a spherical cutoff is that the thermodynamic (and other) properties of the model fluid will no longer be exactly the same as for (say) the non-truncated, Lennard-Jones fluid. As we shall see in Chapter 2, it is possible to apply long-range corrections to such results so as to recover, approximately, the desired information.

The cutoff distance must be no greater than $\frac{1}{2}L$ for consistency with the minimum image convention. In the non-cubic simulation boxes of Fig. 1.14, for a given density and number of particles, r_c may take somewhat larger values than in the cubic case. Looked at another way, an advantage of non-cubic boundary conditions is that they permit simulations with a given cutoff distance and density to be conducted using fewer particles. As an example, a simulation in a cubic box, with r_c set equal to $\frac{1}{2}L$, might involve $N = 256$ molecules; taking the same density, the same cutoff could be used in a simulation of 197 molecules in a truncated octahedron, or just 181 molecules in a rhombic dodecahedron.

1.6.4 Computer code for periodic boundaries

How do we handle periodic boundaries and the minimum image convention in a simulation program? Let us assume that, initially, the N molecules in the simulation lie within a cubic box of side L, with the origin at its centre, that is, all coordinates lie in the range $(-\frac{1}{2}L,\ \frac{1}{2}L)$. As the simulation proceeds, these molecules move about the infinite periodic system. When a molecule leaves the box by crossing one of the boundaries, it is usual to switch attention to the image molecule entering the box by simply adding L to, or subtracting L from, the appropriate coordinate. One simple way to do this uses an `IF` statement to test the positions immediately after the molecules have been moved (whether by MC or MD). For example,

```
IF ( r(1,i) >  box2 ) r(1,i) = r(1,i) - box
IF ( r(1,i) < -box2 ) r(1,i) = r(1,i) + box
```

where the first index 1 selects the x coordinate. Similar statements are applied to the y and z coordinates, or a vector assignment may be applied to all components at once

```
WHERE ( r(:,i) >  box2 ) r(:,i) = r(:,i) - box
WHERE ( r(:,i) < -box2 ) r(:,i) = r(:,i) + box
```

Here, box is a variable containing the box length L, and box2 is just $\frac{1}{2}L$. An alternative to the IF statement is to use arithmetic functions to calculate the correct number of box lengths to be added or subtracted. For example,

```
r(:,i) = r(:,i) - box * ANINT ( r(:,i) / box )
```

The function ANINT(x) returns the nearest integer to x, converting the result back to type REAL; thus ANINT(-0.49) has the value 0.0, whereas ANINT(-0.51) is −1.0. In Fortran, this function returns an array-valued result, computed component by component, if given an array argument. As we shall see in Chapter 5, there are faster ways of coding this up, especially for large system sizes.

By using these methods, we always have available the coordinates of the N molecules that currently lie in the 'central' box. It is not strictly necessary to do this; we could, instead, use uncorrected coordinates, and follow the motion of the N molecules that were in the central box at the start of the simulation. Indeed, as we shall see in Chapters 2 and 8, for calculation of transport coefficients it may be most desirable to have a set of uncorrected positions on hand. If it is decided to do this, however, care must be taken that the minimum image convention is correctly applied, so as to work out the vector between the two closest images of a pair of molecules, no matter how many 'boxes' apart they may be. This means, in general, adding or subtracting an integer number of box lengths (rather than just one box length).

The minimum image convention may be coded in the same way as the periodic boundary adjustments. Of the two methods just mentioned, the arithmetic formula is usually preferable, being simpler; the use of IF statements inside the inner loop may reduce program efficiency (see Appendix A). Immediately after calculating a pair separation vector, the following statements should be applied:

```
rij(:) = rij(:) - box * ANINT ( rij(:) / box )
```

This code is guaranteed to yield the minimum image vector, no matter how many 'box lengths' apart the original images may be. For cuboidal, rather than cubic, boxes, the variable box may be an array of three elements, holding the x, y, and z box lengths, without essentially changing the code.

The calculation of minimum image distances is simplified by the use of reduced units: the length of the box is taken to define the fundamental unit of length in the simulation. By setting $L = 1$, with particle coordinates nominally in the range $(-\frac{1}{2}, +\frac{1}{2})$, the minimum image correction becomes

```
rij(:) = rij(:) - ANINT ( rij(:) )
```

which is simpler, and faster, than the code for a general box length. This approach is an alternative to the use of the pair potential to define reduced units as discussed in Appendix B, and is more generally applicable. For this reason a simulation box of unit length is adopted in most of the examples given in this book.

Code 1.4 Periodic boundaries for truncated octahedron

This code snippet applies the truncated octahedron periodic boundary correction to a position vector $\mathbf{r}_i$, or equivalently the minimum image convention to a displacement vector $\mathbf{r}_{ij}$, provided as the array `r`. The box is centred at the origin and the containing cube is of unit length (see Fig. 1.14(a)). The Fortran `AINT` function rounds towards zero, producing a real-valued integer result: for example `AINT(-0.51)` and `AINT(0.51)` both have the value 0.0, whereas `AINT(-1.8)` is −1.0. The result of the Fortran `SIGN` function has the absolute value of its first argument and the sign of its second.

```
REAL, DIMENSION(3) :: r
REAL               :: corr
REAL, PARAMETER    :: r75 = 4.0 / 3.0

r(:) = r(:) - ANINT ( r(:) )
corr = 0.5 * AINT ( r75 * SUM ( ABS ( r(:) ) ) )
r(:) = r(:) - SIGN ( corr, r(:) )
```

Code 1.5 Periodic boundaries for rhombic dodecahedron

This code snippet applies the rhombic dodecahedron periodic boundary correction to a position vector $\mathbf{r}_i$, or equivalently the minimum image convention to a displacement vector $\mathbf{r}_{ij}$, provided as the array `r`. The box is centred at the origin and the side of the containing cube is $\sqrt{2}$ (see Fig. 1.14(b)).

```
REAL, DIMENSION(3) :: r
REAL               :: corr
REAL, PARAMETER    :: rt2 = SQRT(2.0), rrt2 = 1.0 / rt2

r(1) = r(1) - ANINT ( r(1) )
r(2) = r(2) - ANINT ( r(2) )
r(3) = r(3) - rt2 * ANINT ( rrt2 * r(3) )
corr = 0.5 * AINT ( ABS(r(1)) + ABS(r(2)) + rt2*ABS(r(3)) )
r(1) = r(1) - SIGN ( corr, r(1) )
r(2) = r(2) - SIGN ( corr, r(2) )
r(3) = r(3) - SIGN ( corr, r(3) ) * rt2
```

There are several alternative ways of coding the minimum image corrections, some of which rely on the images being in the same, central box (i.e. on the periodic boundary correction being applied whenever the molecules move). Some of these methods, for cubic boxes, are discussed in Appendix A. We have also mentioned the possibility of conducting simulations in non-cubic periodic boundary conditions. An implementation of the minimum image correction for the truncated octahedron (Adams, 1983a) is given

Code 1.6 Periodic boundaries for rhombus

Here we apply corrections for the rhombic box in two dimensions x, y. In most applications the molecules will be confined in the z direction by real walls rather than by periodic boundaries, so we assume that this coordinate may be left unchanged. The box is centred at the origin. The x axis lies along one side of the rhombus, which is of unit length (see Fig. 1.15). The acute angle of the rhombus is 60°.

```
REAL, DIMENSION(3) :: r
REAL, PARAMETER    :: rt3 = SQRT(3.0), rrt3 = 1.0 / rt3
REAL, PARAMETER    :: rt32 = rt3 / 2.0, rrt32 = 1.0 / rt32

r(1) = r(1) - ANINT ( r(1) - rrt3 * r(2) ) &
      &     - ANINT ( rrt32 * r(2) ) * 0.5
r(2) = r(2) - ANINT ( rrt32 * r(2) ) * rt32
```

in Code 1.4. A similar correction for the rhombic dodecahedron (Smith, 1983) appears in Code 1.5. This is a little more complicated than the code for the truncated octahedron, and the gain small, so that the latter is usually preferable. We also give in Code 1.6 the code for the two-dimensional rhombic box often used in surface simulation.

Now we turn to the implementation of a spherical cutoff, that is, we wish to set the pair potential (and all forces) to zero if the pair separation lies outside some distance r_c. It is easy to compute the square of the particle separation r_{ij} and, rather than waste time taking the square root of this quantity, it is fastest to compare this with the square of r_c which might be computed earlier and stored in a variable `r_cut_sq`. After computing the minimum image intermolecular vector, the following statements would be employed:

```
rij_sq = SUM ( rij(:) ** 2 )
IF ( rij_sq < r_cut_sq ) THEN
  ... compute i-j interaction ...
END IF
```

In a large system, it may be worthwhile to apply separate tests for the x, y, and z directions or some similar scheme.

```
IF ( ABS ( rij(1) ) < r_cut ) THEN
  IF ( ABS ( rij(2) ) < r_cut ) THEN
    IF ( ABS ( rij(3) ) < r_cut ) THEN
      rij_sq = SUM ( rij(:) ** 2 )
      IF ( rij_sq < r_cut_sq ) THEN
        ... compute i-j interaction ...
      END IF
    END IF
  END IF
END IF
```

The time saved in dropping out of this part of the program at any early stage must be weighed against the overheads of extra calculation and testing. In Chapter 5 we discuss the more complicated time-saving tricks used in the simulations of large systems.

1.6.5 Spherical boundary conditions

As an alternative to the standard periodic boundary conditions for simulating bulk liquids, a two-dimensional system may be embedded in the surface of a sphere without introducing any physical boundaries (Hansen et al., 1979), and the idea may be extended to consider a three-dimensional system as being the surface of a hypersphere (Kratky, 1980; Kratky and Schreiner, 1982). The spherical or hyperspherical system is finite: it cannot be considered as part of an infinitely repeating periodic system. In this case, non-Euclidean geometry is an unavoidable complication, and distances between particles are typically measured along the great circle geodesics joining them. However, the effects of the curved geometry will decrease as the system size increases, and such 'spherical boundary conditions' are expected to be a valid method of simulating bulk liquids. Interesting differences from the standard periodic boundary conditions, particularly close to any solid–liquid phase transition, will result from the different topology. Periodic boundaries will be biased in favour of the formation of a solid with a lattice structure which matches the simulation box. Spherical boundaries, on the other hand, are not consistent with periodic lattices, so the liquid state will be thermodynamically favoured in most simulations using this technique, and crystalline phases will inevitably contain defects. Similar considerations may apply to liquid-crystalline phases.

1.6.6 Periodic boundary conditions for three-body potentials

Finally, we note that some care is required when using the minimum image convention with three-body potentials such as the Axilrod–Teller potential (see Appendix C). This problem is illustrated in Fig. 1.17. In Fig. 1.17(a), atom 1 is at the centre of its box, of side L, and atoms 2 and 3_E are the two minimum images used in the calculation of the pair potential. However atom 3 is the minimum image of atom 2 and a straightforward application of the minimum image algorithm will lead to the incorrect triplet 123 rather than 123_E.

Attard (1992) has shown that this problem can be solved using the following statements for the separation vector

```
REAL, DIMENSION(3) :: rij, rik, rjk, tij, tik
tij(:) = box * ANINT ( rij(:) / box )
tik(:) = box * ANINT ( rik(:) / box )
rij(:) = rij(:) - tij(:)
rik(:) = rik(:) - tik(:)
rjk(:) = rjk(:) + tij(:) - tik(:)
```

Normally the three-body potential is set to zero if one side of the triangle is greater than $L/2$.

Some workers have taken a more brute-force approach (Sadus and Prausnitz, 1996; Marcelli and Sadus, 2012). If the potential cutoff r_c is set to $L/4$, the only triplets that contribute to the potential are those where all of the three atoms are within a box of side

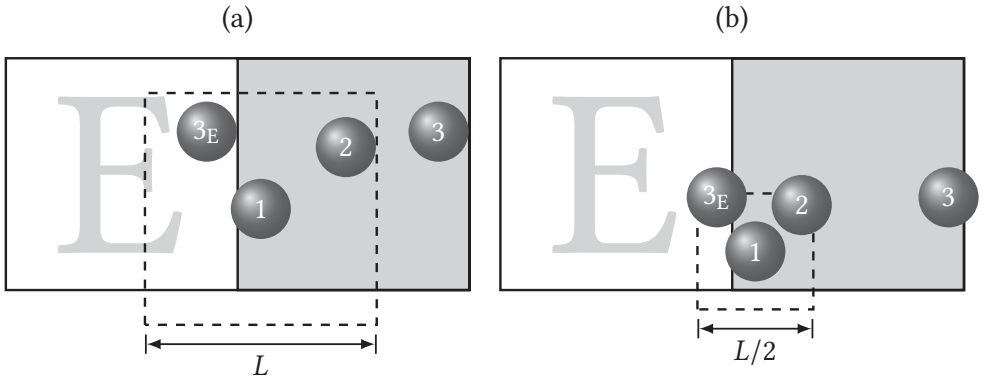

Fig. 1.17 Periodic boundary conditions and the minimum image convention for a triplet interaction: (a) an inconsistency in the triplet configuration for a cutoff of $L/2$; (b) a consistent triplet with a cutoff of $L/4$.

$L/2$ (as shown in Fig. 1.17(b)). Each of the atoms is then always the unique minimum image of the other two and the triplet is unambiguously determined with the normal minimum image calculation. This method works well. However, at a fixed density the simulation will need to include eight times as many atoms in circumstances where the additional calculation of the three-body force is particularly expensive.

2

Statistical mechanics

Computer simulation generates information at the microscopic level (atomic and molecular positions, velocities, etc.) and the conversion of this very detailed information into macroscopic terms (pressure, internal energy, etc.) is the province of statistical mechanics. It is not our aim to provide a text in this field since many excellent sources are available (Hill, 1956; McQuarrie, 1976; Landau and Lifshitz, 1980; Friedman, 1985; Chandler, 1987; Tuckerman, 2010; Swendsen, 2012; Hansen and McDonald, 2013). In this chapter, our aim is to summarize those aspects of the subject which are of most interest to the computer simulator.

2.1 Sampling from ensembles

Let us consider, for simplicity, a one-component macroscopic system; extension to a multicomponent system is straightforward. The thermodynamic state of such a system is usually defined by a small set of parameters (such as the number of particles N, the temperature T, and the pressure P). Other thermodynamic properties (density ρ, chemical potential μ, heat capacity C_V, etc.) may be derived through knowledge of the equations of state and the fundamental equations of thermodynamics. Even quantities such as the diffusion coefficient D, the shear viscosity η, and the structure factor $S(k)$ are state functions: although they clearly say something about the microscopic structure and dynamics of the system, their values are completely dictated by the few variables (e.g. NPT) characterizing the thermodynamic state, not by the very many atomic positions and momenta that define the instantaneous mechanical state. These positions and momenta can be thought of as coordinates in a multidimensional space: phase space. For a system of N atoms, this space has $6N$ dimensions. Let us use the abbreviation $\boldsymbol{\Gamma}$ for a particular point in phase space, and suppose that we can write the instantaneous value of some property $\mathcal{A}$ (it might be the potential energy) as a function $\mathcal{A}(\boldsymbol{\Gamma})$. The system evolves in time so that $\boldsymbol{\Gamma}$, and hence $\mathcal{A}(\boldsymbol{\Gamma})$ will change. It is reasonable to assume that the experimentally observable 'macroscopic' property $\mathcal{A}_{\rm obs}$ is really the time average of $\mathcal{A}(\boldsymbol{\Gamma})$ taken over a long time interval:

$$\mathcal{A}_{\rm obs} = \langle \mathcal{A} \rangle_{\rm time} = \Big\langle \mathcal{A}\big(\boldsymbol{\Gamma}(t)\big) \Big\rangle_{\rm time} = \lim_{t_{\rm obs}\to\infty} \frac{1}{t_{\rm obs}} \int_0^{t_{\rm obs}} \mathcal{A}\big(\boldsymbol{\Gamma}(t)\big)\, {\rm d}t. \tag{2.1}$$

The equations governing this time evolution, Newton's equations of motion in a simple classical system, are of course well known. They are just a system of ordinary differential

Computer Simulation of Liquids. Second Edition. M. P. Allen and D. J. Tildesley.
© M. P. Allen and D. J. Tildesley 2017. Published in 2017 by Oxford University Press.

equations: solving them on a computer, to a desired accuracy, is a practical proposition for, say, 10^5 particles, although not for a truly macroscopic number (e.g. 10^{23}). So far as the calculation of time averages is concerned, we clearly cannot hope to extend the integration of eqn (2.1) to infinite time, but might be satisfied to average over a long finite time τ_{obs}. This is exactly what we do in a molecular dynamics simulation. In fact, the equations of motion are usually solved on a step-by-step basis, that is, a large finite number τ_{obs} of timesteps, of length $\delta t = t_{\text{obs}}/\tau_{\text{obs}}$, are taken. In this case, we may rewrite eqn (2.1) in the form

$$\mathcal{A}_{\text{obs}} = \left\langle \mathcal{A} \right\rangle_{\text{time}} = \frac{1}{\tau_{\text{obs}}} \sum_{\tau=1}^{\tau_{\text{obs}}} \mathcal{A}\Big(\mathbf{\Gamma}(t)\Big). \tag{2.2}$$

In the summation, τ simply stands for an index running over the succession of timesteps. This analogy between the discrete τ and the continuous t is useful, even when, as we shall see in other examples, τ does not correspond to the passage of time in any physical sense.

The practical questions regarding the method are whether or not a sufficient region of phase space is explored by the system trajectory to yield satisfactory time averages within a feasible amount of computer time, and whether thermodynamic consistency can be attained between simulations with identical macroscopic parameters (density, energy, etc.) but different initial conditions (atomic positions and velocities). The answers to these questions are that such simulation runs are indeed within the power of modern computers, and that thermodynamically consistent results for liquid state properties can indeed be obtained, provided that attention is paid to the selection of initial conditions. We will turn to the technical details of the method in Chapter 3.

The calculation of time averages by MD is not the approach to thermodynamic properties implicit in conventional statistical mechanics. Because of the complexity of the time evolution of $\mathcal{A}\Big(\mathbf{\Gamma}(t)\Big)$ for large numbers of molecules, Gibbs suggested replacing the time average by the ensemble average. Here, we regard an ensemble as a collection of points $\mathbf{\Gamma}$ in phase space. The points are distributed according to a probability density $\rho(\mathbf{\Gamma})$. This function is determined by the chosen fixed macroscopic parameters (NPT, NVT, etc.), so we use the notation ρ_{NPT}, ρ_{NVT}, or, in general, ρ_{ens}. Each point represents a typical system at any particular instant of time. Each system evolves in time, according to the usual mechanical equations of motion, quite independently of the other systems. Consequently, in general, the phase space density $\rho_{\text{ens}}(\mathbf{\Gamma})$ will change with time. However, no systems are destroyed or created during this evolution, and Liouville's theorem, which is essentially a conservation law for probability density, states that $\mathrm{d}\rho/\mathrm{d}t = 0$ where $\mathrm{d}/\mathrm{d}t$ denotes the total derivative with respect to time (following a state $\mathbf{\Gamma}$ as it moves). As an example, consider a set of N atoms with Cartesian coordinates $\mathbf{r}_i$, and momenta $\mathbf{p}_i$, in the classical approximation. The total time derivative is

$$\frac{\mathrm{d}}{\mathrm{d}t} = \frac{\partial}{\partial t} + \sum_i \dot{\mathbf{r}}_i \cdot \boldsymbol{\nabla}_{\mathbf{r}_i} + \sum_i \dot{\mathbf{p}}_i \cdot \boldsymbol{\nabla}_{\mathbf{p}_i} \tag{2.3a}$$

$$= \frac{\partial}{\partial t} + \dot{\mathbf{r}} \cdot \boldsymbol{\nabla}_{\mathbf{r}} + \dot{\mathbf{p}} \cdot \boldsymbol{\nabla}_{\mathbf{p}}. \tag{2.3b}$$

In eqn (2.3a), $\partial/\partial t$ represents differentiation, with respect to time, of a function; $\boldsymbol{\nabla}_{\mathbf{r}_i}$, and $\boldsymbol{\nabla}_{\mathbf{p}_i}$, are derivatives with respect to atomic position and momentum respectively; and $\dot{\mathbf{r}}_i$,

$\dot{\mathbf{p}}_i$, signify the time derivatives of the position and momentum. Equation (2.3b) is the same equation written in a more compact way, and the equation may be further condensed by defining the Liouville operator L

$$\mathrm{i}L = \left(\sum_i \dot{\mathbf{r}}_i \cdot \boldsymbol{\nabla}_{\mathbf{r}_i} + \sum_i \dot{\mathbf{p}}_i \cdot \boldsymbol{\nabla}_{\mathbf{p}_i} \right) = \left(\dot{\mathbf{r}} \cdot \boldsymbol{\nabla}_{\mathbf{r}} + \dot{\mathbf{p}} \cdot \boldsymbol{\nabla}_{\mathbf{p}} \right) \tag{2.4}$$

so that $\mathrm{d}/\mathrm{d}t = \partial/\partial t + \mathrm{i}L$ and, using Liouville's theorem, we may write

$$\frac{\partial \rho_{\mathrm{ens}}(\boldsymbol{\Gamma}, t)}{\partial t} = -\mathrm{i}L\rho_{\mathrm{ens}}(\boldsymbol{\Gamma}, t). \tag{2.5}$$

This equation tells us that the rate of change of ρ_{ens} at a particular fixed point in phase space is related to the flows into and out of that point. This equation has a formal solution

$$\rho_{\mathrm{ens}}(\boldsymbol{\Gamma}, t) = \exp(-\mathrm{i}Lt)\, \rho_{\mathrm{ens}}(\boldsymbol{\Gamma}, 0) \tag{2.6}$$

where the exponential of an operator really means a series expansion

$$\exp(-\mathrm{i}Lt) = 1 - \mathrm{i}Lt - \tfrac{1}{2}L^2t^2 + \cdots . \tag{2.7}$$

The equation of motion of a function like $\mathcal{A}(\boldsymbol{\Gamma})$, which does not depend explicitly on time, takes a conjugate form (McQuarrie, 1976):

$$\dot{\mathcal{A}}\Big(\boldsymbol{\Gamma}(t)\Big) = \mathrm{i}L\mathcal{A}\Big(\boldsymbol{\Gamma}(t)\Big) \tag{2.8}$$

or

$$\mathcal{A}\Big(\boldsymbol{\Gamma}(t)\Big) = \exp(\mathrm{i}Lt)\mathcal{A}\Big(\boldsymbol{\Gamma}(0)\Big). \tag{2.9}$$

To be quite clear: in eqns (2.5) and (2.6) we consider the time-dependence of ρ_{ens} at a fixed point $\boldsymbol{\Gamma}$ in phase space; in eqns (2.8) and (2.9), $\mathcal{A}\Big(\boldsymbol{\Gamma}(t)\Big)$ is time-dependent because we are following the time evolution $\boldsymbol{\Gamma}(t)$ along a trajectory. This relationship is analogous to that between the Schrödinger and Heisenberg pictures in quantum mechanics.

If $\rho_{\mathrm{ens}}(\boldsymbol{\Gamma})$ represents an equilibrium ensemble, then its time-dependence completely vanishes, $\partial\rho_{\mathrm{ens}}/\partial t = 0$. The system evolution then becomes quite special. As each system leaves a particular state $\boldsymbol{\Gamma}(\tau)$ and moves on to the next, $\boldsymbol{\Gamma}(\tau + 1)$, another system arrives from state $\boldsymbol{\Gamma}(\tau - 1)$ to replace it. The motion resembles a long and convoluted conga line at a crowded party (see Fig. 2.1). There might be several such processions, each passing through different regions of phase space. However, if these are all connected into just one trajectory that passes through all the points in phase space for which ρ_{ens} is non-zero (i.e. the procession forms a single, very long, closed circuit) then each system will eventually visit all the state points. Such a system is termed 'ergodic' and the time taken to complete a cycle (the Poincaré recurrence time) is immeasurably long for a many-particle system (and for many parties as well it seems).

One way of answering the question 'was it a good party?' would be to interview one of the participants, and ask for their time-averaged impressions. This is essentially what we do in a molecular dynamics simulation, when a representative system evolves deterministically in time. However, as indicated in Fig. 2.1, this time average might not

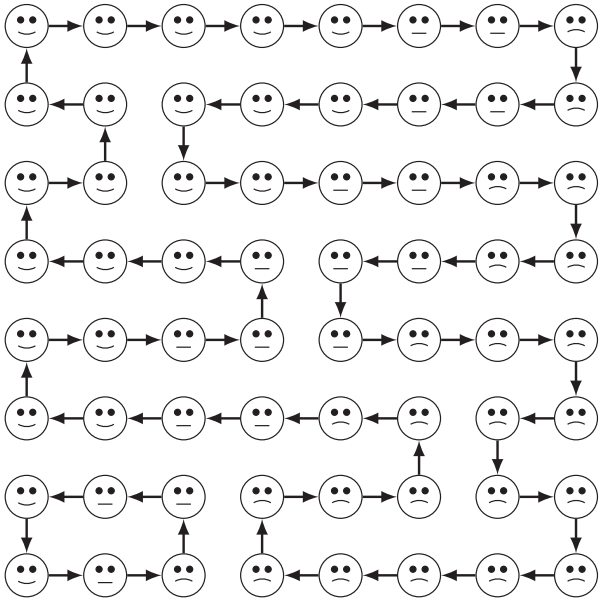

Fig. 2.1 A schematic representation of phase space. The circles represent different state points $(\mathbf{q}, \mathbf{p})$, and they are connected by a path representing the classical trajectory, analogous to a conga line at a party. Each state is characterized by some property (e.g. 'happiness' at the party). In an ergodic system, the single long trajectory would eventually pass through (or arbitrarily near) all states; in the bottom left corner of the diagram we symbolically indicate a disconnected region of six states which may or may not be practically important.

be representative of the whole trajectory: to be sure, it would have to be long enough to sample all the states. An alternative route to the average properties of our partygoers, would be to take photographs of all of them at the same time, assemble the complete collection of 'happy' and 'sad' faces, and take an average over them. This corresponds to replacing the time average in eqn (2.1) by an average taken over all the members of the ensemble, 'frozen' at a particular time:

$$\mathcal{A}_{\text{obs}} = \langle \mathcal{A} \rangle_{\text{ens}} = \left\langle \mathcal{A} \,\middle|\, \rho_{\text{ens}} \right\rangle = \sum_{\Gamma} \mathcal{A}(\Gamma)\rho_{\text{ens}}(\Gamma). \tag{2.10}$$

The $\langle \mathcal{A}|\rho \rangle$ notation reminds us of the dependence of the average on both $\mathcal{A}$ and ρ: this is important when taking a thermodynamic derivative of $\mathcal{A}_{\text{obs}}$ (we must differentiate both parts) or when considering time-dependent properties (when the Schrödinger–Heisenberg analogy may be exploited). Actually, we will be concerned with the practical question of efficient and thorough sampling of phase space, which is not quite the same as the rigorous definition of ergodicity (for a fuller discussion, see Tolman, 1938). In terms of our analogy of conga lines, there should not be a preponderance of independent closed circuits ('cliques') in which individuals can become trapped and fail fully to sample the available space (this is important in parties as well as in simulations). An MD simulation which started in the disconnected six-state region of Fig. 2.1, for example, would be disastrous. On the other hand, small non-ergodic regions are less likely to be dangerous and more likely to be recognized if they are unfortunately selected as starting points for

a simulation. In a similar way, regions of phase space which act as barriers and cause bottlenecks through which only a few trajectories pass can result in poor sampling by the relatively short simulation runs carried out in practice, even if the system is technically ergodic.

Finally, we might use a different kind of evolution to sample the states of the system: a random walk. This is the Monte Carlo approach: it may be more or less efficient than molecular dynamics. It also fits quite well the analogy of a party, in which the participants sample the different situations randomly, rather than systematically. Once again, trajectory averages are calculated over a finite duration, so these are not necessarily identical to full ensemble averages, and the approach might or might not alleviate some of the ergodicity issues.

It is sometimes convenient to use, in place of $\rho_{\text{ens}}(\boldsymbol{\Gamma})$, a 'weight' function $w_{\text{ens}}(\boldsymbol{\Gamma})$, which satisfies the following equations:

$$\rho_{\text{ens}}(\boldsymbol{\Gamma}) = Q_{\text{ens}}^{-1}\, w_{\text{ens}}(\boldsymbol{\Gamma}) \tag{2.11}$$

$$Q_{\text{ens}} = \sum_{\boldsymbol{\Gamma}} w_{\text{ens}}(\boldsymbol{\Gamma}) \tag{2.12}$$

$$\langle \mathcal{A} \rangle_{\text{ens}} = \sum_{\boldsymbol{\Gamma}} w_{\text{ens}}(\boldsymbol{\Gamma}) \mathcal{A}(\boldsymbol{\Gamma}) \Big/ \sum_{\boldsymbol{\Gamma}} w_{\text{ens}}. \tag{2.13}$$

The weight function is essentially a non-normalized form of $\rho_{\text{ens}}(\boldsymbol{\Gamma})$, with the partition function Q_{ens} (also called the sum over states) acting as the normalizing factor. Both w_{ens} and Q_{ens} contain an arbitrary multiplicative constant, whose choice corresponds to the definition of a zero of entropy. Q_{ens} is simply a function of the macroscopic properties defining the ensemble, and connection with classical thermodynamics is made by defining a thermodynamic potential Ψ_{ens} (see e.g. McQuarrie, 1976)

$$\Psi_{\text{ens}} = -\ln Q_{\text{ens}}. \tag{2.14}$$

This is the function that has a minimum value at thermodynamic equilibrium. For example, Ψ_{ens} might be the negative of the entropy S for a system at constant NVE, where V is the volume and E the total internal energy, or the Gibbs function G for a constant-NPT system, where P is the pressure and T the temperature.

Throughout the foregoing discussion, although we have occasionally used the language of classical mechanics, we have assumed that the states are discrete (e.g. a set of quantum numbers) and that we may sum over them. If the system were enclosed in a container, there would be a countably infinite set of quantum states. In the classical approximation, $\boldsymbol{\Gamma}$ represents the set of (continuously variable) particle positions and momenta, and we should replace the summation by a classical phase-space integral. w_{ens} and Q_{ens} are then usually defined with appropriate factors included to make them dimensionless, and to match up with the usual semiclassical 'coarse-grained' phase-space volume elements. On a computer, of course, all numbers are held to a finite precision and so, technically, positions and momenta are represented by discrete, not continuous, variables; we now have a countable and finite set of states. We assume that the distinction between this case and the classical limit is of no practical importance, and will use whichever representation is most convenient.

One conceivable approach to the computation of thermodynamic quantities, therefore, would be a direct evaluation of Q_{ens} for a particular ensemble, using eqn (2.12). This summation, over all possible states, is not feasible for many-particle systems: there are too many states, most of which have a very low weight due to non-physical overlaps between the repulsive cores of the molecules, rendering them unimportant. We would like to conduct the summation so as to exclude this large number of irrelevant states, and include only those with a high probability. Unfortunately, it is generally not possible to estimate Q_{ens} directly in this way. However, the underlying idea, that of generating (somehow) a set of states in phase space that are sampled from the complete set in accordance with the probability density $\rho_{\text{ens}}(\mathbf{\Gamma})$, is central to the Monte Carlo technique.

We proceed by analogy with molecular dynamics in the sense that the ensemble average of eqn (2.13) is replaced by a trajectory average like eqn (2.2). Newton's equations generate a succession of states in accordance with the distribution function ρ_{NVE} for the constant-NVE or microcanonical ensemble. Suppose we wish to investigate other ensembles; experiments in the laboratory, for example, are frequently performed under conditions of constant temperature and pressure, while it is often very convenient to consider inhomogeneous systems at constant chemical potential. For each such case, let us invent a kind of equation of motion, that is, a means of generating, from one state point $\mathbf{\Gamma}(\tau)$, a succeeding state point $\mathbf{\Gamma}(\tau + 1)$. This recipe need have no physical interpretation, and it could be entirely deterministic or could involve a stochastic, random, element. It might be derived by modifying the true equations of motion in some way, or it may have no relation whatever with normal dynamics.

To be useful, this prescription should satisfy some sensible conditions:

(a) the probability density $\rho_{\text{ens}}(\mathbf{\Gamma})$ for the ensemble of interest should not change as the system evolves;
(b) any 'reasonable' starting distribution $\rho(\mathbf{\Gamma})$ should tend to this stationary solution as the simulation proceeds;
(c) we should be able to argue that ergodicity holds, even though we cannot hope to prove this for realistic systems.

If these conditions are satisfied, then we should be able to generate, from an initial state, a succession of state points which, in the long term, are sampled in accordance with the desired probability density $\rho_{\text{ens}}(\mathbf{\Gamma})$. In these circumstances, the ensemble average will be equal to a kind of 'time average':

$$\mathcal{A}_{\text{obs}} = \langle \mathcal{A} \rangle_{\text{ens}} = \frac{1}{\tau_{\text{obs}}} \sum_{\tau=1}^{\tau_{\text{obs}}} \mathcal{A}\Big(\mathbf{\Gamma}(\tau)\Big). \tag{2.15}$$

Here τ is an index running over the succession of τ_{obs} states or trials generated by our prescription; in a practical simulation, τ_{obs} would be a large finite number. This is exactly what we do in Monte Carlo simulations. The trick, of course, lies in the generation of the trajectory through phase space, and the different recipes for different ensembles will be discussed in Chapter 4. In general, because only a finite number of states can be generated in any one simulation, Monte Carlo results are subject to the same questions of initial condition effects and satisfactory phase space exploration as are molecular dynamics results.

2.2 Common statistical ensembles

Let us consider four ensembles in common use: the microcanonical, or constant-NVE, ensemble just mentioned, the canonical, or constant-NVT, ensemble, the isothermal–isobaric constant-NPT ensemble, and the grand canonical constant-μVT ensemble. For each ensemble, the aforementioned thermodynamic variables are specified, that is, fixed. Other thermodynamic quantities must be determined by ensemble averaging and, for any particular state point, the instantaneous values of the appropriate phase function will deviate from this average value, that is, fluctuations occur.

The probability density for the microcanonical ensemble is proportional to

$$\delta[\mathcal{H}(\mathbf{\Gamma}) - E]$$

where $\mathbf{\Gamma}$ represents the set of particle positions and momenta (or quantum numbers), and $\mathcal{H}(\mathbf{\Gamma})$ is the Hamiltonian. The delta function selects those states of an N-particle system in a container of volume V that have the desired energy E. When the set of states is discrete, δ is just the Kronecker delta, taking values of 0 or 1; when the states are continuous, δ is the Dirac delta function. The microcanonical partition function may be written:

$$Q_{NVE} = \sum_{\mathbf{\Gamma}} \delta[\mathcal{H}(\mathbf{\Gamma}) - E] \tag{2.16}$$

where the summation takes due note of indistinguishability of particles. In the quasi-classical expression for Q_{NVE}, for an atomic system, the indistinguishability is handled using a factor of $1/N!$

$$Q_{NVE} = \frac{1}{N!}\frac{1}{h^{3N}} \int \mathrm{d}\mathbf{r}\, \mathrm{d}\mathbf{p}\, \delta[\mathcal{H}(\mathbf{r}, \mathbf{p}) - E]. \tag{2.17}$$

Here, $\int \mathrm{d}\mathbf{r}\, \mathrm{d}\mathbf{p}$ stands for integration over all $6N$ phase space coordinates. The appropriate thermodynamic potential is the negative of the entropy

$$-S/k_\mathrm{B} = -\ln Q_{NVE}. \tag{2.18}$$

The factor involving Planck's constant h in eqn (2.17) corresponds to the usual zero of entropy for the ideal gas (the Sackur–Tetrode equation).

For a classical system, Newton's equations of motion conserve energy and so provide a suitable method (but not the only method (Severin et al., 1978; Creutz, 1983)) for generating a succession of state points sampled from this ensemble, as discussed in the previous section. In fact, for a system not subjected to external forces, these equations also conserve total linear momentum $\mathbf{P}$, and so molecular dynamics probes a subset of the microcanonical ensemble, namely the constant-$NVE\mathbf{P}$ ensemble (for technical reasons, as we shall see in Chapter 3, total angular momentum is not conserved in most MD simulations). Since it is easy to transform into the centre-of-mass frame, the choice of $\mathbf{P}$ is not crucial, and zero momentum is usually chosen for convenience. Differences between the constant-NVE and constant-$NVE\mathbf{P}$ ensembles are minor: for the latter, an additional three constraints exist in that only $(N - 1)$ particle momenta are actually independent of each other.

The probability density for the canonical ensemble is proportional to

$$\exp[-\mathcal{H}(\mathbf{\Gamma})/k_{\mathrm{B}}T]$$

and the partition function is

$$Q_{NVT} = \sum_{\mathbf{\Gamma}} \exp[-\mathcal{H}(\mathbf{\Gamma})/k_{\mathrm{B}}T] \tag{2.19}$$

or, in quasi-classical form, for an atomic system

$$Q_{NVT} = \frac{1}{N!}\frac{1}{h^{3N}} \int \mathrm{d}\mathbf{r}\, \mathrm{d}\mathbf{p}\, \exp[-\mathcal{H}(\mathbf{r},\mathbf{p})/k_{\mathrm{B}}T]. \tag{2.20}$$

The appropriate thermodynamic function is the Helmholtz free energy A

$$A/k_{\mathrm{B}}T = -\ln Q_{NVT}. \tag{2.21}$$

In the canonical ensemble, all values of the energy are allowed, and energy fluctuations are non-zero. Thus, although $\rho_{NVT}(\mathbf{\Gamma})$ is indeed a stationary solution of the Liouville equation, the corresponding mechanical equations of motion are not a satisfactory method of sampling states in this ensemble, since they conserve energy: normal time evolution occurs on a set of independent constant-energy surfaces, each of which should be appropriately weighted, by the factor $\exp[-\mathcal{H}(\mathbf{\Gamma})/k_{\mathrm{B}}T]$. Our prescription for generating a succession of states must make provision for transitions between the energy surfaces, so that a single trajectory can probe all the accessible phase space, and yield the correct relative weighting. We shall encounter several ways of doing this in the later chapters.

Because the energy is always expressible as a sum of kinetic (**p**-dependent) and potential (**q**-dependent) contributions, the partition function factorizes into a product of kinetic (ideal gas) and potential (excess) parts

$$Q_{NVT} = \frac{1}{N!}\frac{1}{h^{3N}} \int \mathrm{d}\mathbf{p}\, \exp(-\mathcal{K}/k_{\mathrm{B}}T) \int \mathrm{d}\mathbf{q}\, \exp(-\mathcal{V}/k_{\mathrm{B}}T) = Q^{\mathrm{id}}_{NVT}\, Q^{\mathrm{ex}}_{NVT}. \tag{2.22}$$

Again, for an atomic system, we see (by taking $\mathcal{V} = 0$)

$$Q^{\mathrm{id}}_{NVT} = \frac{V^N}{N!\,\Lambda^{3N}} \tag{2.23}$$

Λ being the thermal de Broglie wavelength

$$\Lambda = (h^2/2\pi m k_{\mathrm{B}}T)^{1/2}. \tag{2.24}$$

The excess part is

$$Q^{\mathrm{ex}}_{NVT} = V^{-N} \int \mathrm{d}\mathbf{r}\, \exp[-\mathcal{V}(\mathbf{r})/k_{\mathrm{B}}T]. \tag{2.25}$$

Instead of Q^{ex}_{NVT}, we often use the configuration integral

$$Z_{NVT} = \int \mathrm{d}\mathbf{r}\, \exp[-\mathcal{V}(\mathbf{r})/k_{\mathrm{B}}T]. \tag{2.26}$$

Some workers include a factor $N!$ in the definition of Z_{NVT}. Although Q^{id}_{NVT} and Q^{ex}_{NVT} are dimensionless, the configuration integral has dimensions of V^N. As a consequence

of the separation of Q_{NVT}, all the thermodynamic properties derived from A can be expressed as a sum of ideal gas and configurational parts. In statistical mechanics, it is easy to evaluate ideal gas properties (Rowlinson, 1963), and we may expect most attention to focus on the configurational functions. In fact, it proves possible to probe just the configurational part of phase space according to the canonical distribution, using standard Monte Carlo methods. The corresponding trajectory through phase space has essentially independent projections on the coordinate and momentum sub-spaces. The ideal gas properties are added onto the results of configuration-space Monte Carlo simulations afterwards.

The probability density for the isothermal–isobaric ensemble is proportional to

$$\exp[-(\mathcal{H} + PV)/k_{\mathrm{B}}T].$$

Note that the quantity appearing in the exponent, when averaged, gives the thermodynamic enthalpy $H = \langle\mathcal{H}\rangle + P\langle V\rangle$. Now the volume V has joined the list of microscopic quantities ($\mathbf{r}$ and $\mathbf{p}$) comprising the state point. The appropriate partition function is

$$Q_{NPT} = \sum_{\Gamma}\sum_{V} \exp[-(\mathcal{H} + PV)/k_{\mathrm{B}}T] = \sum_{V} \exp(-PV/k_{\mathrm{B}}T)Q_{NVT}. \tag{2.27}$$

The summation over possible volumes may also be written as an integral, in which case some basic unit of volume V_0 must be chosen to render Q_{NPT} dimensionless. This choice is not practically important for our purposes, but has been discussed in detail elsewhere (Wood, 1968b; Attard, 1995; Koper and Reiss, 1996; Corti and Soto-Campos, 1998; Han and Son, 2001). In quasi-classical form, for an atomic system, we write:

$$Q_{NPT} = \frac{1}{N!}\frac{1}{h^{3N}}\frac{1}{V_0}\int \mathrm{d}V \int \mathrm{d}\mathbf{r}\,\mathrm{d}\mathbf{p}\ \exp[-(\mathcal{H} + PV)/k_{\mathrm{B}}T]. \tag{2.28}$$

The corresponding thermodynamic function is the Gibbs free energy G

$$G/k_{\mathrm{B}}T = -\ln Q_{NPT}. \tag{2.29}$$

The prescription for generating state points in the constant-NPT ensemble must clearly provide for changes in the sample volume as well as energy. Once more, it is possible to separate configurational properties from kinetic ones, and to devise a Monte Carlo procedure to probe configuration space only. The configuration integral in this ensemble is

$$Z_{NPT} = \int \mathrm{d}V\ \exp(-PV/k_{\mathrm{B}}T) \int \mathrm{d}\mathbf{r}\ \exp[-\mathcal{V}(\mathbf{r})/k_{\mathrm{B}}T]. \tag{2.30}$$

Again some definitions include $N!$ and V_0 as normalizing factors.

The density function for the grand canonical ensemble is proportional to

$$\exp[-(\mathcal{H} - \mu N)/k_{\mathrm{B}}T]$$

where μ is the specified chemical potential. Now the number of particles N is a variable, along with the coordinates and momenta of those particles. The grand canonical partition function is

$$Q_{\mu VT} = \sum_{N}\sum_{\Gamma} \exp[-(\mathcal{H} - \mu N)/k_{\mathrm{B}}T] = \sum_{N} \exp(\mu N/k_{\mathrm{B}}T)Q_{NVT}. \tag{2.31}$$

In quasi-classical form, for an atomic system,

$$Q_{\mu VT} = \sum_N \frac{1}{N!}\frac{1}{h^{3N}} \exp(\mu N/k_\mathrm{B}T) \int \mathrm{d}\mathbf{r}\,\mathrm{d}\mathbf{p}\ \exp(-\mathcal{H}/k_\mathrm{B}T). \tag{2.32}$$

Although it is occasionally useful to pretend that N is a continuous variable, for most purposes we sum, rather than integrate, in eqns (2.31) and (2.32). The appropriate thermodynamic function is just $-PV/k_\mathrm{B}T$:

$$-PV/k_\mathrm{B}T = -\ln Q_{\mu VT}. \tag{2.33}$$

Whatever scheme we employ to generate states in the grand ensemble, clearly it must allow for addition and removal of particles. Once more, it is possible to invent a Monte Carlo method to do this and, moreover, to probe just the configurational part of phase space; however, it turns out to be necessary to include the form of the kinetic partition function in the prescription used.

So far the discussion has been limited to one-component systems but each of the ensembles considered can be readily extended to multi-component mixtures. For example in the grand ensemble, the density function for a c-component mixture containing N_i particles of type i is proportional to

$$\left[\prod_{i=1}^{c} \frac{\exp\left(\mu_i N_i/k_\mathrm{B}T\right)}{N_i!}\right] \exp(-\mathcal{H}/k_\mathrm{B}T) \tag{2.34}$$

where μ_i is the chemical potential of species i and $\mathcal{H}$ is the Hamiltonian of the c-component mixture. In quasi-classical form, for an atomic system, the grand partition function is

$$Q_{\mu_1,\mu_2,\ldots\mu_n VT} = \sum_{N_1,N_2\ldots N_n} \frac{1}{h^{3N}}\left[\prod_{i=1}^{c} \frac{1}{N_i!}\exp(\mu_i N_i/k_\mathrm{B}T)\right] \int \mathrm{d}\mathbf{r}\,\mathrm{d}\mathbf{p}\ \exp(-\mathcal{H}/k_\mathrm{B}T). \tag{2.35}$$

The appropriate thermodynamic function is

$$-PV/k_\mathrm{B}T = -\ln Q_{\mu_1,\mu_2,\ldots\mu_n VT}. \tag{2.36}$$

It is also useful to study mixtures in the semi-grand ensemble (Kofke and Glandt, 1988). Here the total number of particles is fixed at N but the identities of the individual particles can change. The chemical potential of an arbitrary species, say 1, is defined as μ_1 and the $c-1$ chemical potential differences, $(\mu_2-\mu_1)\ldots(\mu_n-\mu_1)$, are fixed. When V and T are also fixed, the probability density is proportional to

$$\left[\prod_{i=1}^{c} \exp[(\mu_i-\mu_1)N_i/k_\mathrm{B}T]\right] \exp(-\mathcal{H}/k_\mathrm{B}T)$$

where $\mathcal{H}$ is the Hamiltonian for a system of N particles ($N = \sum_i N_i$) and where each particle is defined to have a specific identity from 1 to c. In quasi-classical form, for an

atomic system, the semi-grand partition function is

$$Q_{\{\mu_i|i\neq 1\}NVT} = \sum_{i_1=1}^{c} \cdots \sum_{i_N=1}^{c} \frac{1}{N!h^{3N}} \left[\prod_{i=1}^{c} \exp\Big((\mu_i - \mu_1) N_i / k_\mathrm{B} T \Big) \right] \int \mathrm{d}\mathbf{r}\, \mathrm{d}\mathbf{p}\ \exp(-\mathcal{H}/k_\mathrm{B}T) \quad (2.37)$$

where the sums are now over the particle identities (e.g. i_1 is the identity of particle 1). The corresponding thermodynamic potential is

$$-(PV - \mu_1 N)/k_\mathrm{B}T = -\ln Q_{\{\mu_i|i\neq 1\}NVT}. \quad (2.38)$$

It is also possible to develop a semi-grand ensemble at constant pressure rather than constant volume. In this case, the chemical potential difference is conveniently replaced by the fugacity fraction as the independent variable, as discussed in Section 4.7 (Kofke and Glandt, 1988; Frenkel and Smit, 2002). An important advantage of the semi-grand ensemble is that the chemical potential difference can be defined as a continuous function. For example, in a polydisperse fluid of hard spheres, the distribution $\mu(\sigma) - \mu_1$ as a function of the hard-sphere diameter σ would be fixed, and through the semi-grand ensemble we could predict the distribution of particle sizes.

It is possible to construct many more ensembles, some of which are of interest in computer simulation. When comparing molecular dynamics with Monte Carlo, it may be convenient to add the constraint of constant (zero) total momentum, that is, fixed centre of mass, to the constant-NVT ensemble. It is also permissible to constrain certain degrees of freedom (e.g. the total kinetic energy (Hoover, 1983b,a), or the energy in a particular chemical bond (Freasier et al., 1979)) while allowing others to fluctuate. Also, nonequilibrium ensembles may be set up (see Chapter 11). The possibilities are endless, the general requirements being that a phase-space density $\rho_\mathrm{ens}(\boldsymbol{\Gamma})$ can be written down, and that a corresponding prescription for generating state points can be devised. The remaining questions are ones of practicality.

Not all ensembles are of interest to the computer simulator. The properties of generalized ensembles, such as the constant-μPT ensemble, have been discussed (Hill, 1956). Here, only intensive parameters are specified: the corresponding extensive quantities show unbounded fluctuations, that is, the system size can grow without limit. Also, μ, P, and T are related by an equation of state, so, although this equation may be unknown, they are not independently variable. For these reasons, the simulation of the constant-μPT ensemble and related pathological examples is not a practical proposition. In all the ensembles dealt with in this book, at least one extensive parameter (usually N or V) is fixed to act as a limit on the system size.

Finally, it is by no means guaranteed that a chosen prescription for generating phase-space trajectories will correspond to any ensemble at all. It is easy to think of extreme examples of modified equations of motion for which no possible function $\rho_\mathrm{ens}(\boldsymbol{\Gamma})$ is a stationary solution. In principle, some care should be taken to establish which ensemble, if any, is probed by any novel simulation technique.

Example 2.1 Entropy and disorder

At the very least, molecular simulations provide an experimental route to check the predictions of statistical mechanics, as indicated in Fig. 1.2. In addition, however, simulations have provided the impetus to revise some basic ideas, especially in connection with the concept of entropy. Some of the earliest simulations (Wood and Jacobson, 1957; Alder and Wainwright, 1957) demonstrated that the hard-sphere system exhibited a phase transition between solid and liquid phases. Because there are no energetic terms in this model, the thermodynamic driving force must be the entropy: at sufficiently high density, the ordered, solid, phase has a higher entropy than the liquid. This result was not immediately accepted, as it required a rethinking of the definition of disorder, and its connection to the entropy. Roughly speaking, the loss in entropy, associated with the localization of particles around positions on a regular lattice, is more than compensated by the entropy gain associated with the increased free volume that may be explored by each particle around its lattice site. On compressing a disordered hard-sphere system, when the volume occupied by the spheres reaches $\eta \approx 64\,\%$, the free volume becomes zero (random close packing); the freezing transition occurs before this, at $\eta \approx 49\,\%$ (for comparison, in the FCC structure, close packing occurs at $\eta \approx 74\,\%$). Recent computer simulations of polyhedral hard particles have shown that shape-related entropic effects alone can give rise to a huge variety of solid structures (Damasceno et al., 2012; van Anders et al., 2014).

A more fundamental debate concerns the factor $N!$ appearing in eqns (2.17), (2.20), and usually associated with particle indistinguishability. In quantum mechanics, identical particles are indistinguishable as a matter of principle. However, our simulations are of classical, distinguishable (i.e. labelled) particles! Also, statistical mechanics is applied successfully to colloidal systems, for which the constituent particles are of mesoscopic size and clearly distinguishable, even when nearly monodisperse. Should the factor $N!$ be included or not? The question arises whenever two systems, under identical conditions, in a classical simulation or a colloidal experiment, are brought into contact and allowed to exchange particles: is the entropy additive (i.e. extensive) or is there an entropy of mixing term? The answer is that the factor $N!$ *should* be present, for N very similar but distinguishable particles, in order to obtain extensive entropy and Helmholtz free energy functions, and hence it is not intimately connected with quantum mechanics. This has been discussed in the context of simulations by Swendsen (2002) and for colloidal systems by Warren (1998) and Swendsen (2006) (see also Frenkel, 2014, and references therein). These considerations come from first principles, not computer experiments. However, interestingly, they are crucial in practical attempts to quantify the entropy of a granular system, in terms of the number of ways of realizing a jammed structure, extending ideas of Edwards and Oakeshott (1989) and Edwards (1990). Computer simulations (Asenjo et al., 2014) involving the preparation of jammed configurations by quenching equilibrated nearly-hard-sphere liquids, have confirmed the need to include the $N!$ term in order to define an extensive granular entropy, even for systems of distinguishable particles.

2.3 Transforming between ensembles

Since the ensembles are essentially artificial constructs, it would be reassuring to know that they produce average properties which are consistent with one another. In the thermodynamic limit (for an infinite system size) and as long as we avoid the neighbourhood of phase transitions, this is believed to be true for the commonly used statistical ensembles (Fisher, 1964). Since we will be dealing with systems containing a finite number of particles, it is of some interest to see, in a general way, how this result comes about. The method of transformation between ensembles is standard (Hill, 1956; Lebowitz et al., 1967; Münster, 1969; Landau and Lifshitz, 1980) and a useful summary for several ensembles of interest has appeared (Graben and Ray, 1993). We merely outline the procedure here; nonetheless, the development is rather formal, and this section could be skipped on a first reading.

We shall be interested in transforming from an ensemble in which an extensive thermodynamic variable F is fixed to one in which the intensive conjugate variable f is constant. Typical conjugate pairs are (β, E), $(\beta P, V)$, $(-\beta\mu, N)$, where $\beta = 1/k_{\mathrm{B}}T$. If the old partition function and characteristic thermodynamic potential are Q_F, and Ψ_F, respectively, then the new quantities are given by

$$Q_f = \int \mathrm{d}F' \exp(-F'f) Q_{F'} \tag{2.39}$$

$$\Psi_f = \Psi_F + Ff. \tag{2.40}$$

Equations (2.19)–(2.33) provide specific examples of these relations. Equation (2.40) corresponds to the Legendre transformation of classical thermodynamics. For example, when moving from a system at constant energy to one at constant temperature (i.e. constant β), the characteristic thermodynamic potential changes from $-S/k_{\mathrm{B}}$ to $-S/k_{\mathrm{B}} + \beta E = \beta A$. Similarly, on going to constant temperature and pressure, the thermodynamic potential becomes $\beta A + \beta PV = \beta G$.

The average $\langle \mathcal{A} \rangle_f$ calculated in the constant-f ensemble is related to the average $\langle \mathcal{A} \rangle_F$ calculated at constant F by (Lebowitz et al., 1967)

$$\langle \mathcal{A} \rangle_f = \exp(\Psi_f) \int \mathrm{d}F' \exp(-\Psi_{F'} - F'f) \langle \mathcal{A} \rangle_{F'}. \tag{2.41}$$

The equivalence of ensembles relies on the behaviour of the integrand of this equation for a large system: it becomes very sharply peaked around the mean value $F' = \langle F \rangle_f$. In the thermodynamic limit of infinite system size, we obtain simply

$$\langle \mathcal{A} \rangle_f = \langle \mathcal{A} \rangle_F \tag{2.42}$$

where it is understood that $F = \langle F \rangle_f$. Thus, the averages of any quantity calculated in, say, the constant-NVE ensemble and the constant-NVT ensemble, will be equal in the thermodynamic limit, as long as we choose E and T consistently so that $E = \langle E \rangle_{NVT}$. In

fact, there are some restrictions on the kinds of functions $\mathcal{A}$ for which eqn (2.42) holds. $\mathcal{A}$ should be, essentially, a sum of single-particle functions,

$$\mathcal{A} = \sum_{i=1}^{N} \mathcal{A}_i \tag{2.43}$$

or, at least, a sum of independent contributions from different parts of the fluid, which may be added up in a similar way. All of the thermodynamic functions are of this short-ranged nature, insofar as they are limited by the range of intermolecular interactions. For long-ranged (e.g. dielectric) properties and long-ranged (e.g. Coulombic) forces, this becomes a more subtle point.

The situation for a finite number of particles is treated by expanding the integrand of eqn (2.41) about the mean value $\langle F\rangle_f$. If we write $F' = \langle F\rangle_f + \delta F'$ then we obtain (Lebowitz et al., 1967):

$$\langle \mathcal{A}\rangle_f = \langle \mathcal{A}\rangle_{F=\langle F\rangle_f} + \frac{1}{2}\left(\frac{\partial^2}{\partial F^2}\langle \mathcal{A}\rangle_F\right)_{F=\langle F\rangle_f} \langle \delta F^2\rangle_f + \cdots . \tag{2.44}$$

The correction term, which is proportional to the mean-square fluctuations $\langle \delta F^2\rangle$ of the quantity F in the constant-f ensemble, is expected to be relatively small since, as mentioned earlier, the distribution of F values should be very sharply peaked for a many-particle system. This fluctuation term may be expressed as a straightforward thermodynamic derivative. Since F and f are conjugate variables, we have

$$\langle F\rangle_f = -\partial \Psi_f/\partial f \tag{2.45}$$

$$\langle \delta F^2\rangle_f = \partial^2 \Psi_f/\partial f^2 = -\partial \langle F\rangle_f/\partial f. \tag{2.46}$$

We may write this simply as $-(\partial F/\partial f)$. Equation (2.44) is most usefully rearranged by taking the last term across to the other side, and treating it as a function of f through the relation $F = \langle F\rangle_f$. Thus

$$\begin{aligned}
\langle \mathcal{A}\rangle_F &= \langle \mathcal{A}\rangle_f - \frac{1}{2}\langle \delta F^2\rangle_f \frac{\partial^2}{\partial F^2}\langle \mathcal{A}\rangle_f \\
&= \langle \mathcal{A}\rangle_f + \frac{1}{2}\frac{\partial F}{\partial f}\frac{\partial^2}{\partial F^2}\langle \mathcal{A}\rangle_f \\
&= \langle \mathcal{A}\rangle_f + \frac{1}{2}\frac{\partial}{\partial f}\frac{\partial}{\partial F}\langle \mathcal{A}\rangle_f \\
&= \langle \mathcal{A}\rangle_f + \frac{1}{2}\frac{\partial}{\partial f}\left(\frac{\partial f}{\partial F}\right)\frac{\partial}{\partial f}\langle \mathcal{A}\rangle_f .
\end{aligned} \tag{2.47}$$

Bearing in mind that F is extensive and f intensive, the small relative magnitude of the correction term can be seen explicitly: it decreases as $O(N^{-1})$.

Although the fluctuations are small, they are nonetheless measurable in computer simulations. They are of interest because they are related to thermodynamic derivatives

(like the specific heat or the isothermal compressibility) by equations such as eqn (2.46). In general, we define the root mean square (RMS) deviation $\sigma(\mathcal{A})$ by the equation

$$\sigma^2(\mathcal{A}) = \langle \delta\mathcal{A}^2 \rangle_{\text{ens}} = \langle \mathcal{A}^2 \rangle_{\text{ens}} - \langle \mathcal{A} \rangle_{\text{ens}}^2 \tag{2.48}$$

where

$$\delta\mathcal{A} = \mathcal{A} - \langle \mathcal{A} \rangle_{\text{ens}}. \tag{2.49}$$

It is quite important to realize that, despite the $\langle \delta\mathcal{A}^2 \rangle$ notation, we are not dealing here with the average of a mechanical quantity like $\mathcal{A}$; the best we can do is to write $\sigma^2(\mathcal{A})$ as a difference of two terms, as in eqn (2.48). Thus, the previous observations on equivalence of ensembles do not apply: fluctuations in different ensembles are not the same. As an obvious example, energy fluctuations in the constant-NVE ensemble are (by definition) zero, whereas in the constant-NVT ensemble, they are not. The transformation technique may be applied to obtain an equation analogous to eqn (2.47) (Lebowitz et al., 1967). In the general case of the covariance of two variables $\mathcal{A}$ and $\mathcal{B}$ the result is

$$\langle \delta\mathcal{A}\delta\mathcal{B} \rangle_F = \langle \delta\mathcal{A}\delta\mathcal{B} \rangle_f + \left(\frac{\partial f}{\partial F} \right) \left(\frac{\partial}{\partial f} \langle \mathcal{A} \rangle_f \right) \left(\frac{\partial}{\partial f} \langle \mathcal{B} \rangle_f \right). \tag{2.50}$$

Now the correction term is of the same order as the fluctuations themselves. Consider, once more, energy fluctuations in the microcanonical and canonical ensembles, that is, let $\mathcal{A} = \mathcal{B} = F = E$ and $f = \beta = 1/k_{\text{B}}T$. Then on the left of eqn (2.50) we have zero, and on the right we have $\sigma^2(E)$ at constant-NVT and a combination of thermodynamic derivatives which turn out to equal $(\partial E/\partial\beta) = -k_{\text{B}}T^2C_V$ where C_V is the constant-volume heat capacity.

2.4 Simple thermodynamic averages

A consequence of the equivalence of ensembles is that, provided a suitable phase function can be identified in each case, the basic thermodynamic properties of a model system may be calculated as averages in any convenient ensemble. Accordingly, we give in this section expressions for common thermodynamic quantities, omitting the subscripts which identify particular ensembles. These functions are usually derivatives of one of the characteristic thermodynamic functions Ψ_{ens}. Examples are $P = -(\partial A/\partial V)_{NT}$ and $\beta = (1/k_{\text{B}}T) = (1/k_{\text{B}})(\partial S/\partial E)_{NV}$.

The kinetic, potential, and total internal energies may be calculated using the phase functions of eqns (1.1)–(1.3).

$$E = \langle \mathcal{H} \rangle = \langle \mathcal{K} \rangle + \langle \mathcal{V} \rangle. \tag{2.51}$$

The kinetic energy is a sum of contributions from individual particle momenta, while evaluation of the potential contribution involves summing over all pairs, triplets, etc. of molecules, depending upon the complexity of the function as discussed in Chapter 1.

The temperature and pressure may be calculated using the virial theorem, which we write in the form of 'generalized equipartition' (Münster, 1969):

$$\langle p_k \partial \mathcal{H}/\partial p_k \rangle = k_B T \tag{2.52a}$$

$$\langle q_k \partial \mathcal{H}/\partial q_k \rangle = k_B T \tag{2.52b}$$

for any generalized coordinate q_k or momentum p_k. These expressions are valid (to $O(N^{-1})$) in any ensemble.

Equation (2.52a) is particularly simple when the momenta appear as squared terms in the Hamiltonian. For example, in the atomic case, we may sum up $3N$ terms of the form $p_{i\alpha}^2/m_i$, to obtain

$$\left\langle \sum_{i=1}^{N} \left| \mathbf{p}_i \right|^2 / m_i \right\rangle = 2\langle \mathcal{K} \rangle = 3Nk_B T. \tag{2.53}$$

This is the familiar equipartition principle: an average energy of $k_B T/2$ per degree of freedom. It is convenient to define an instantaneous 'kinetic temperature' function

$$\mathcal{T} = 2\mathcal{K}/3Nk_B = \frac{1}{3Nk_B} \sum_{i=1}^{N} \left| \mathbf{p}_i \right|^2 / m_i \tag{2.54}$$

whose average is equal to T. Obviously, this is not a unique definition. For a system of rigid molecules, described in terms of centre-of-mass positions and velocities together with orientational variables, the angular velocities may also appear in the definition of $\mathcal{T}$. Alternatively, it may be useful to define separate 'translational' and 'rotational' temperatures each of which, when averaged, gives T. In eqn (2.52a) it is assumed that the independent degrees of freedom have been identified and assigned generalized coordinates q_k, and momenta p_k. For a system of N atoms, subject to internal molecular constraints, the number of degrees of freedom will be $3N - N_c$ where N_c is the total number of independent internal constraints (fixed bond lengths and angles) defined in the molecular model. Then, we must replace eqn (2.54) by

$$\mathcal{T} = \frac{2\mathcal{K}}{(3N - N_c)k_B} = \frac{1}{(3N - N_c)k_B} \sum_{i=1}^{N} \left| \mathbf{p}_i \right|^2 / m_i. \tag{2.55}$$

We must also include in N_c, any additional global constraints on the ensemble. For example, in the 'molecular dynamics' constant-$NVE\mathbf{P}$ ensemble, we must include the three extra constraints on centre-of-mass motion.

Equations (2.52) are examples of the general form

$$\left\langle \mathcal{A} \frac{\partial \mathcal{H}}{\partial q_k} \right\rangle = k_B T \left\langle \frac{\partial \mathcal{A}}{\partial q_k} \right\rangle, \qquad \left\langle \mathcal{A} \frac{\partial \mathcal{H}}{\partial p_k} \right\rangle = k_B T \left\langle \frac{\partial \mathcal{A}}{\partial p_k} \right\rangle,$$

valid for any dynamical variable $\mathcal{A}$, which may be easily derived in the canonical ensemble (see e.g. Landau and Lifshitz, 1958, p100, eqn (33.14)). These are generally termed 'hypervirial' relations (Hirschfelder, 1960). Setting $\mathcal{A} = \partial \mathcal{H}/\partial q_k = \partial \mathcal{V}/\partial q_k$ gives an alternative

way of calculating the temperature from purely configurational properties, independent of the momenta. For example, for a simple atomic system

$$k_{\mathrm{B}}T = \frac{\left\langle (\partial \mathcal{V}/\partial r_{i\alpha})^2 \right\rangle}{\langle \partial^2 \mathcal{V}/\partial r_{i\alpha}^2 \rangle} = \frac{\langle f_{i\alpha}^2 \rangle}{\langle \partial^2 \mathcal{V}/\partial r_{i\alpha}^2 \rangle}. \tag{2.56}$$

Naturally, in a simulation it is usual to average this expression over all atoms i and all coordinate directions α, when the numerator becomes the mean-square force and the denominator becomes the average Laplacian of the potential. This 'configurational temperature' is useful in Monte Carlo simulations, in which the momenta do not appear (Rugh, 1997), and comparing it with the usual kinetic expression, (2.54), or with the prescribed temperature, is a useful check that a simulation is working properly (Butler et al., 1998). More details of how to calculate the configurational temperature appear in Appendix F.

The pressure may be calculated via eqn (2.52b). If we choose Cartesian coordinates, and use Hamilton's equations of motion (see Chapter 3), it is easy to see that each coordinate derivative in eqn (2.52b) is the negative of a component of the force $\mathbf{f}_i$ on some molecule i, and we may write, summing over N molecules,

$$-\tfrac{1}{3}\left\langle \sum_{i=1}^{N} \mathbf{r}_i \cdot \boldsymbol{\nabla}_{\mathbf{r}_i} \mathcal{V} \right\rangle = \tfrac{1}{3}\left\langle \sum_{i=1}^{N} \mathbf{r}_i \cdot \mathbf{f}_i^{\mathrm{tot}} \right\rangle = -Nk_{\mathrm{B}}T. \tag{2.57}$$

We have used the symbol $\mathbf{f}_i^{\mathrm{tot}}$ because this represents the sum of intermolecular forces and external forces. The latter are related to the external pressure, as can be seen by considering the effect of the container walls on the system:

$$\tfrac{1}{3}\left\langle \sum_{i=1}^{N} \mathbf{r}_i \cdot \mathbf{f}_i^{\mathrm{ext}} \right\rangle = -PV. \tag{2.58}$$

If we define the 'internal virial' $\mathcal{W}$

$$-\tfrac{1}{3}\sum_{i=}^{N} \mathbf{r}_i \cdot \boldsymbol{\nabla}_{\mathbf{r}_i} \mathcal{V} = \tfrac{1}{3}\sum_{i=1}^{N} \mathbf{r}_i \cdot \mathbf{f}_i = \mathcal{W} \tag{2.59}$$

where now we restrict attention to intermolecular forces, then

$$PV = Nk_{\mathrm{B}}T + \langle \mathcal{W} \rangle. \tag{2.60}$$

This suggests that we define an instantaneous 'pressure' function (Cheung, 1977)

$$\mathcal{P} = \rho k_{\mathrm{B}} \mathcal{T} + \mathcal{W}/V = \mathcal{P}^{\mathrm{id}} + \mathcal{P}^{\mathrm{ex}} \tag{2.61}$$

whose average is simply P. Again, this definition is not unique; apart from the different ways of defining $\mathcal{W}$ which we shall see later, it may be most convenient (say in a constant-temperature ensemble) to use

$$\mathcal{P}' = \rho k_{\mathrm{B}} T + \mathcal{W}/V = \langle \mathcal{P}^{\mathrm{id}} \rangle + \mathcal{P}^{\mathrm{ex}} \tag{2.62}$$

instead. Both $\mathcal{P}$ and $\mathcal{P}'$ give P when averaged, but their fluctuations in any ensemble will, in general, be different. Note that the preceding derivation is not really valid for the

infinite periodic systems used in computer simulation: there are no container walls and no external forces. Nonetheless, the result is the same (Erpenbeck and Wood, 1977).

For pairwise interactions, $\mathcal{W}$ is more conveniently expressed in a form which is explicitly independent of the origin of coordinates. This is done by writing $\mathbf{f}_i$ as the sum of forces $\mathbf{f}_{ij}$ on atom i due to atom j

$$\sum_i \mathbf{r}_i \cdot \mathbf{f}_i = \sum_i \sum_{j \neq i} \mathbf{r}_i \cdot \mathbf{f}_{ij} = \tfrac{1}{2} \sum_i \sum_{j \neq i} \big(\mathbf{r}_i \cdot \mathbf{f}_{ij} + \mathbf{r}_j \cdot \mathbf{f}_{ji} \big). \tag{2.63}$$

The second equality follows because the indices i and j are equivalent. Newton's third law $\mathbf{f}_{ij} = -\mathbf{f}_{ji}$ is then used to switch the force indices

$$\sum_i \mathbf{r}_i \cdot \mathbf{f}_i = \tfrac{1}{2} \sum_i \sum_{j \neq i} \mathbf{r}_{ij} \cdot \mathbf{f}_{ij} = \sum_i \sum_{j > i} \mathbf{r}_{ij} \cdot \mathbf{f}_{ij} \tag{2.64}$$

where $\mathbf{r}_{ij} = \mathbf{r}_i - \mathbf{r}_j$ and the final form of the summation is usually more convenient. It is essential to use the $\mathbf{r}_{ij} \cdot \mathbf{f}_{ij}$ form in a simulation that employs periodic boundary conditions. So we have at last

$$\mathcal{W} = \tfrac{1}{3} \sum_i \sum_{j > i} \mathbf{r}_{ij} \cdot \mathbf{f}_{ij} = -\tfrac{1}{3} \sum_i \sum_{j > i} \mathbf{r}_{ij} \cdot \boldsymbol{\nabla}_{\mathbf{r}_{ij}} v(r_{ij}) = -\tfrac{1}{3} \sum_i \sum_{j > i} w(r_{ij}) \tag{2.65}$$

where the intermolecular pair virial function $w(r)$ is

$$w(r) = r \frac{\mathrm{d}v(r)}{\mathrm{d}r}. \tag{2.66}$$

Like $\mathcal{V}$, $\mathcal{W}$ is limited by the range of the interactions, and hence $\langle \mathcal{W} \rangle$ should be a well-behaved, ensemble-independent function in most cases.

For molecular fluids we may write

$$\mathcal{W} = \tfrac{1}{3} \sum_i \sum_{j > i} \mathbf{r}_{ij} \cdot \mathbf{f}_{ij} = -\tfrac{1}{3} \sum_i \sum_{j > i} \mathbf{r}_{ij} \cdot \big(\boldsymbol{\nabla}_{\mathbf{r}_{ij}} \mathcal{V} \big)_{\Omega_i, \Omega_j} = -\tfrac{1}{3} \sum_i \sum_{j > i} w(r_{ij}) \tag{2.67}$$

where $\mathbf{r}_{ij}$ is the vector between the molecular centres. Here we have made it clear that the pair virial is defined as a position derivative at constant orientation of the molecules

$$w(r_{ij}) = r_{ij} \left(\frac{\partial\, v(r_{ij}, \Omega_i, \Omega_j)}{\partial\, r_{ij}} \right)_{\Omega_i, \Omega_j}. \tag{2.68}$$

The pressure function $\mathcal{P}$ is defined through eqn (2.61) as before. For interaction site models, we may treat the system as a set of atoms, and use eqns (2.65), (2.66), with the summations taken over distinct pairs of sites ia and jb (compare eqn (1.12)). When doing this, however, it is important to include all intramolecular contributions (forces along the bonds for example) in the sum. Alternatively, the molecular definition, eqns (2.67), (2.68) is still valid. In this case, for computational purposes, eqn (2.68) may be rewritten in the form

$$w(r_{ij}) = \sum_a \sum_b \frac{w_{ab}(r_{ab})}{r_{ab}^2} (\mathbf{r}_{ab} \cdot \mathbf{r}_{ij}) \tag{2.69}$$

where $\mathbf{r}_{ab} = \mathbf{r}_{ia} - \mathbf{r}_{jb}$ is the vector between the sites and $w_{ab}(r_{ab})$ is the site–site pair virial function. This is equivalent to expressing $\mathbf{f}_{ij}$ in eqn (2.67) as the sum of all the site–site

forces acting between the molecules. Whether the atomic or molecular definition of the virial is adopted, the ensemble average $\langle \mathcal{W} \rangle$ and hence $\langle \mathcal{P} \rangle = P$ should be unaffected. In inhomogeneous systems, the pressure is a tensor; see Section 2.12.

In systems with discontinuous interactions, such as the hard-sphere model, the usual expressions for the pressure cannot be applied. As we shall see in Chapter 3, in MD simulations of hard particles, we solve the classical equations of motion for the motion in between discrete collisions; at the moment of collision, an impulse acts between the two colliding particles, and changes their momenta. This is responsible for the non-ideal contribution to the pressure. The virial expression (2.65) can be recast into a form involving a sum over collisions, by time-averaging it:

$$\langle \mathcal{W} \rangle = \frac{1}{t_{\text{obs}}} \int_0^{t_{\text{obs}}} \mathrm{d}t \left(\tfrac{1}{3} \sum_i \sum_{j>i} \mathbf{r}_{ij} \cdot \mathbf{f}_{ij} \right) = \frac{1}{3t_{\text{obs}}} \sum_{\text{colls}} \mathbf{r}_{ij} \cdot \delta \mathbf{p}_{ij} \tag{2.70a}$$

where i and j represent a pair of molecules colliding at time t_{ij}, $\mathbf{r}_{ij}$ is the vector between the molecular centres at the time of collision, and

$$\delta \mathbf{p}_{ij} = \delta \mathbf{p}_i = -\delta \mathbf{p}_j = \int_{t_{ij}^-}^{t_{ij}^+} \mathrm{d}t \, \mathbf{f}_{ij} \tag{2.70b}$$

is the collisional impulse, that is, the change in momentum. The sum in eqn (2.70a) is over all collisions occurring in time t_{obs}, and the integral in eqn (2.70b) is over an infinitesimal time interval around t_{ij}. This expression may also be written in terms of the collision rate and the average of $\mathbf{r}_{ij} \cdot \delta \mathbf{p}_{ij}$ per collision. Equation (2.70a) replaces eqn (2.65) in the average pressure equation (2.60). Further details, including a discussion of the system-size dependence of these formulae may be found elsewhere (Alder and Wainwright, 1960; Hoover and Alder, 1967; Erpenbeck and Wood, 1977). In MC simulations of hard systems, a less direct approach must be used to estimate P, and this is discussed in Section 5.5.

Quantities such as $\langle N \rangle$ and $\langle V \rangle$ are easily evaluated in the simulation of ensembles in which these quantities vary, and derived functions such as the enthalpy are straightforwardly calculated. Now we turn to the question of evaluating entropy-related ('statistical') quantities such as the Gibbs and Helmholtz functions, the chemical potential μ, and the entropy itself. A direct approach is to conduct a simulation of the grand canonical ensemble, in which μ, or a related quantity, is specified. It must be said at the outset that there are some technical difficulties associated with grand canonical ensemble simulations, and we return to this in Chapter 4. There are also difficulties in obtaining these functions in the other common ensembles, since they are related directly to the partition function Q, not to its derivatives. To calculate Q would mean summing over all the states of the system. It might seem that we could use the formula

$$\exp\left(A^{\text{ex}}/k_{\text{B}}T\right) = {Q_{NVT}^{\text{ex}}}^{-1} = \left\langle \exp(\mathcal{V}/k_{\text{B}}T) \right\rangle_{NVT} \tag{2.71}$$

to estimate the excess statistical properties, but, in practice, the distribution ρ_{NVT} will be very sharply peaked around the largest values of $\exp(-\mathcal{V}/k_{\text{B}}T)$, that is, where $\exp(\mathcal{V}/k_{\text{B}}T)$ is comparatively small. Consequently, any simulation technique that samples according to the equilibrium distribution will be bound to give a poor estimate of A by this route. Special sampling techniques have been developed to evaluate averages of this type (Valleau

and Torrie, 1977) and we return to this in Chapter 9. It is comparatively easy to obtain free-energy differences for a given system at two different temperatures by integrating the internal energy along a line of constant density:

$$\left(\frac{A}{Nk_{\mathrm{B}}T}\right)_2 - \left(\frac{A}{Nk_{\mathrm{B}}T}\right)_1 = \int_{\beta_1}^{\beta_2} \left(\frac{E}{Nk_{\mathrm{B}}T}\right) \frac{\mathrm{d}\beta}{\beta} = -\int_{T_1}^{T_2} \left(\frac{E}{Nk_{\mathrm{B}}T}\right) \frac{\mathrm{d}T}{T}. \tag{2.72}$$

Alternatively, integration of the pressure along an isotherm may be used:

$$\left(\frac{A}{Nk_{\mathrm{B}}T}\right)_2 - \left(\frac{A}{Nk_{\mathrm{B}}T}\right)_1 = \int_{\rho_1}^{\rho_2} \left(\frac{PV}{Nk_{\mathrm{B}}T}\right) \frac{\mathrm{d}\rho}{\rho} = -\int_{V_1}^{V_2} \left(\frac{PV}{Nk_{\mathrm{B}}T}\right) \frac{\mathrm{d}V}{V}. \tag{2.73}$$

To use these expressions, it is necessary to calculate ensemble averages at state points along a reversible thermodynamic path. To calculate absolute free energies and entropies, it is necessary to extend the thermodynamic integration far enough to reach a state point whose properties can be calculated essentially exactly. In general, these calculations may be expensive, since accurate thermodynamic information is required for many closely spaced state points.

One fairly direct, and widely applicable, method for calculating μ is based on the thermodynamic identities

$$\exp(-\mu/k_{\mathrm{B}}T) = Q_{N+1}/Q_N = Q_N/Q_{N-1} \tag{2.74}$$

valid at large N for both the constant-NVT and constant-NPT ensembles. From these equations we can obtain expressions for the chemical potential in terms of a kind of ensemble average (Widom, 1963; 1982). If we define the excess chemical potential $\mu^{\mathrm{ex}} = \mu - \mu^{\mathrm{id}}$ then we can write

$$\mu^{\mathrm{ex}} = -k_{\mathrm{B}}T \ln\left\langle \exp(-\mathcal{V}_{\mathrm{test}}/k_{\mathrm{B}}T)\right\rangle \tag{2.75}$$

where $\mathcal{V}_{\mathrm{test}}$ is the potential energy which would result from the addition of a particle (at random) to the system. This is the 'test particle insertion' method of estimating μ. Eqn (2.75) also applies in the constant-μVT ensemble (Henderson, 1983). A slightly different formula applies for constant-NVE because of the kinetic temperature fluctuations (Frenkel, 1986):

$$\mu^{\mathrm{ex}} = -k_{\mathrm{B}}\langle \mathcal{T} \rangle \ln\left[\left\langle \mathcal{T} \right\rangle^{-3/2}\left\langle \mathcal{T}^{3/2} \exp(-\mathcal{V}_{\mathrm{test}}/k_{\mathrm{B}}T)\right\rangle\right] \tag{2.76a}$$

where $\mathcal{T}$ is the instantaneous kinetic temperature. Similarly, for the constant-NPT ensemble, it is necessary to include the fluctuations in the volume V (Shing and Chung, 1987):

$$\mu^{\mathrm{ex}} = -k_{\mathrm{B}}T \ln\left[\langle V\rangle^{-1}\left\langle V \exp(-\mathcal{V}_{\mathrm{test}}/k_{\mathrm{B}}T)\right\rangle\right]. \tag{2.76b}$$

In all these cases the 'test particle', the $(N + 1)$th, is not actually inserted: it is a 'ghost', that is, the N real particles are not affected by its presence. The Widom method can also be applied to inhomogeneous systems, see Section 2.12.

There is an alternative formula which applies to the removal of a test particle (selected at random) from the system (Powles et al., 1982). This 'test particle' is not actually removed:

it is a real particle and continues to interact normally with its neighbours. In practice, this technique does not give an accurate estimate of $\mu^{\rm ex}$, and for hard spheres (for example) it is completely unworkable (Rowlinson and Widom, 1982). We defer a detailed discussion of the applicability of these methods and more advanced techniques until Chapter 9.

2.5 Fluctuations

We now discuss the information that can be obtained from the RMS fluctuations calculated as indicated in eqn (2.48). The quantities of most interest are the constant-volume specific heat capacity $C_V = (\partial E/\partial T)_V$ or its constant-pressure counterpart $C_P = (\partial H/\partial T)_P$, the thermal expansion coefficient $\alpha_P = V^{-1}(\partial V/\partial T)_P$, the isothermal compressibility $\beta_T = -V^{-1}(\partial V/\partial P)_T$, the thermal pressure coefficient $\gamma_V = (\partial P/\partial T)_V$, and the adiabatic (constant-S) analogues of the last three. The relationship $\alpha_P = \beta_T\gamma_V$ means that only two of these quantities are needed to define the third. In part, formulae for these quantities can be obtained from standard theory of fluctuations (Landau and Lifshitz, 1980), but in computer simulations we must be careful to distinguish between properly defined mechanical quantities such as the energy or Hamiltonian $\mathcal{H}$, the kinetic temperature $\mathcal{T}$ or the instantaneous pressure $\mathcal{P}$, and thermodynamic concepts such as T and P, which can only be described as ensemble averages or as parameters defining an ensemble. Thus, a standard formula such as $\sigma^2(E) = \langle\delta E^2\rangle = k_{\rm B}T^2C_V$ can be used to calculate the specific heat in the canonical ensemble (provided we recognize that E really means $\mathcal{H}$), whereas the analogous simple formula $\sigma^2(P) = \langle\delta P^2\rangle = k_{\rm B}T/V\beta_T$ will not be so useful (since P is not the same as $\mathcal{P}$).

Fluctuations are readily computed in the canonical ensemble, and accordingly we start with this case. As just mentioned, the specific heat is given by the fluctuations in the energy:

$$\langle\delta\mathcal{H}^2\rangle_{NVT} = k_{\rm B}T^2C_V. \tag{2.77}$$

This can be divided into kinetic and potential contributions which are uncorrelated (i.e. $\langle\delta\mathcal{K}\delta\mathcal{V}\rangle_{NVT} = 0$):

$$\langle\delta\mathcal{H}^2\rangle_{NVT} = \langle\delta\mathcal{V}^2\rangle_{NVT} + \langle\delta\mathcal{K}^2\rangle_{NVT}. \tag{2.78}$$

The kinetic part can be calculated easily, for example in the case of a system of N atoms:

$$\langle\delta\mathcal{K}^2\rangle_{NVT} = \frac{3N}{2}(k_{\rm B}T)^2 = 3N/2\beta^2 \tag{2.79}$$

yielding the ideal gas part of the specific heat $C_V^{\rm id} = (3/2)Nk_{\rm B}$. For this case, then, potential-energy fluctuations are simply

$$\langle\delta\mathcal{V}^2\rangle_{NVT} = k_{\rm B}T^2\left(C_V - \tfrac{3}{2}Nk_{\rm B}\right). \tag{2.80}$$

Consideration of the cross-correlation of the potential-energy and virial fluctuations yields an expression for the thermal pressure coefficient γ_V (Rowlinson, 1969)

$$\langle\delta\mathcal{V}\delta\mathcal{W}\rangle_{NVT} = k_{\rm B}T^2\left(V\gamma_V - Nk_{\rm B}\right) \tag{2.81}$$

where $\mathcal{W}$ is defined in eqns (2.65)–(2.69). In terms of the pressure function defined in eqn (2.61) this becomes

$$\langle\delta\mathcal{V}\delta\mathcal{P}\rangle_{NVT} = k_{\rm B}T^2\left(\gamma_V - \rho k_{\rm B}\right) \tag{2.82}$$

once more valid for a system of N atoms. Equation (2.82) also applies if $\mathcal{P}$ is replaced by $\mathcal{P}'$ or by $\mathcal{P}^{\rm ex}$ (eqn (2.82)), which is more likely be available in a (configuration-space) constant-NVT Monte Carlo calculation. Similar formulae may be derived for molecular systems. When we come to consider fluctuations of the virial itself, we must define a further 'hypervirial' function

$$\mathcal{X} = \tfrac{1}{9}\sum_i \sum_{j>i} \sum_k \sum_{\ell>k} \left(\mathbf{r}_{ij}\cdot\boldsymbol{\nabla}_{\mathbf{r}_{ij}}\right)\left(\mathbf{r}_{k\ell}\cdot\boldsymbol{\nabla}_{\mathbf{r}_{k\ell}}\right)\mathcal{V} \tag{2.83}$$

which becomes, for a pairwise additive potential

$$\mathcal{X} = \tfrac{1}{9}\sum_i \sum_{j>i} x(r_{ij}) \tag{2.84}$$

where

$$x(r) = r\frac{\mathrm{d}w(r)}{\mathrm{d}r} \tag{2.85}$$

$w(r)$ being the intermolecular viral defined in eqn (2.66). It is then easy to show that

$$\langle \delta\mathcal{W}^2\rangle_{NVT} = k_{\rm B}T\left(Nk_{\rm B}T + \langle\mathcal{W}\rangle_{NVT} - \beta_T^{-1}V + \langle\mathcal{X}\rangle_{NVT}\right) \tag{2.86}$$

or

$$\langle \delta\mathcal{P}^2\rangle_{NVT} = \frac{k_{\rm B}T}{V}\left(\frac{2Nk_{\rm B}T}{3V} + \langle\mathcal{P}\rangle_{NVT} - \beta_T^{-1} + \frac{\langle\mathcal{X}\rangle_{NVT}}{V}\right). \tag{2.87}$$

The average $\langle\mathcal{X}\rangle$ is a non-thermodynamic quantity. Nonetheless, it can be calculated in a computer simulation, so eqns (2.86) and (2.87) provide a route to the isothermal compressibility β_T. Note that Cheung (1977) uses a different definition of the hypervirial function. In terms of the fluctuations of $\mathcal{P}'$, the analogous formula is

$$\langle \delta\mathcal{P}^{\rm ex2}\rangle_{NVT} = \langle \delta\mathcal{P}'^2\rangle_{NVT} = \frac{k_{\rm B}T}{V}\left(\langle\mathcal{P}'\rangle_{NVT} - \beta_T^{-1} + \frac{\langle\mathcal{X}\rangle_{NVT}}{V}\right) \tag{2.88}$$

and this would be the formula used most in constant-NVT simulations.

The desired fluctuation expressions for the microcanonical ensemble may best be derived from the preceding equations, by applying the transformation formula, eqn (2.50) (Lebowitz et al., 1967; Cheung, 1977) or directly (Ray and Graben, 1981). The equivalence of the ensembles guarantees that the values of simple averages (such as $\langle\mathcal{X}\rangle$) are unchanged by this transformation. In the microcanonical ensemble, the energy (of course) is fixed, but the specific heat may be obtained by examining fluctuations in the separate potential and kinetic components (Lebowitz et al., 1967). For N atoms,

$$\langle \delta\mathcal{V}^2\rangle_{NVE} = \langle \delta\mathcal{K}^2\rangle_{NVE} = \tfrac{3}{2}Nk_{\rm B}^2T^2\left(1 - \frac{3Nk_{\rm B}}{2C_V}\right). \tag{2.89}$$

Cross-correlation of the pressure function and (say) the kinetic energy may be used to obtain the thermal pressure coefficient:

$$\langle \delta\mathcal{P}\delta\mathcal{K}\rangle_{NVE} = \langle \delta\mathcal{P}\delta\mathcal{V}\rangle_{NVE} = \frac{Nk_{\rm B}^2T^2}{V}\left(1 - \frac{3V\gamma_V}{2C_V}\right). \tag{2.90}$$

Finally the expression for fluctuations of $\mathcal{P}$ in the microcanonical ensemble yields the isothermal compressibility, but the formula is made slightly more compact by introducing the adiabatic compressibility β_S, and using $\beta_S^{-1} = \beta_T^{-1} + TV\gamma_V^2/C_V$

$$\langle \delta \mathcal{P}^2 \rangle_{NVE} = \frac{k_B T}{V}\left(\frac{2Nk_B T}{3V} + \langle \mathcal{P} \rangle_{NVE} - \beta_S^{-1} + \frac{\langle \mathcal{X} \rangle_{NVE}}{V} \right). \tag{2.91}$$

In eqns (2.89)–(2.91) T is short for $\langle \mathcal{T} \rangle_{NVE}$. All these expressions are easily derived using the transformation technique outlined earlier, and they are all valid for systems of N atoms. The same expressions (to leading order in N) hold in the constant-$NVE\mathbf{P}$ ensemble probed by molecular dynamics. Analogous formulae for molecular systems may be derived in a similar way.

Conversion from the canonical to the isothermal–isobaric ensemble is easily achieved. Most of the formulae of interest are very simple since they involve well-defined mechanical quantities. At constant T and P, both volume and energy fluctuations may occur. The volume fluctuations are related to the isothermal compressibility

$$\langle \delta V^2 \rangle_{NPT} = Vk_B T\beta_T. \tag{2.92}$$

The simplest specific heat formula may be obtained by calculating the 'instantaneous' enthalpy $\mathcal{H} + PV$, when we see

$$\left\langle \delta(\mathcal{H} + PV)^2 \right\rangle_{NPT} = k_B T^2 C_P. \tag{2.93}$$

This equation can be split into the separate terms involving $\langle \delta \mathcal{H}^2 \rangle$, $\langle \delta V^2 \rangle$, and $\langle \delta \mathcal{H} \delta V \rangle$. Finally the thermal expansion coefficient may be calculated from the cross-correlations of 'enthalpy' and volume:

$$\left\langle \delta V \delta(\mathcal{H} + PV) \right\rangle_{NPT} = k_B T^2 V \alpha_P. \tag{2.94}$$

Other quantities may be obtained by standard thermodynamic manipulations. Finally, to reiterate, although P is fixed in these expressions, the functions $\mathcal{P}$ and $\mathcal{P}'$ defined in eqns (2.61)–(2.62) will fluctuate around the average value P.

In the grand canonical ensemble, energy, pressure, and number fluctuations occur. The number fluctuations yield the isothermal compressibility

$$\langle \delta N^2 \rangle_{\mu VT} = k_B T(\partial N/\partial \mu)_{VT} = \frac{N^2}{V} k_B T \beta_T. \tag{2.95}$$

Expressions for the other thermodynamic derivatives are a little more complicated (Adams, 1975). The simplest formula for a specific heat is obtained by considering (by analogy with the enthalpy) a function $\mathcal{H} - \mu N$:

$$\left\langle \delta(\mathcal{H} - \mu N)^2 \right\rangle_{\mu VT} = k_B T^2 C_{\mu V} = k_B T^2 \left(\frac{\partial \langle \mathcal{H} - \mu N \rangle}{\partial T} \right)_{\mu V} \tag{2.96}$$

and the usual specific heat C_V (i.e. C_{NV}) is obtained by thermodynamic manipulations:

$$C_V = \tfrac{3}{2} Nk_B + \frac{1}{k_B T^2}\left(\langle \delta \mathcal{V}^2 \rangle_{\mu VT} - \frac{\langle \delta \mathcal{V} \delta N \rangle_{\mu VT}^2}{\langle \delta N^2 \rangle_{\mu VT}} \right). \tag{2.97}$$

The thermal expansion coefficient may be derived in the same way:

$$\alpha_P = \frac{P\beta_T}{T} - \frac{\langle \delta\mathcal{V}\delta N\rangle_{\mu VT}}{Nk_{\mathrm{B}}T^2} + \frac{\langle \mathcal{V}\rangle_{\mu VT}\langle \delta N^2\rangle_{\mu VT}}{N^2k_{\mathrm{B}}T^2}. \tag{2.98}$$

Finally, the thermal pressure coefficient is given by

$$\gamma_V = \frac{Nk_{\mathrm{B}}}{V} + \frac{\langle \delta\mathcal{V}\delta N\rangle_{\mu VT}}{VT}\left(1 - \frac{N}{\langle \delta N^2\rangle_{\mu VT}}\right) + \frac{\langle \delta\mathcal{V}\delta\mathcal{W}\rangle_{\mu VT}}{Vk_{\mathrm{B}}T^2}. \tag{2.99}$$

Except within brackets $\langle\cdots\rangle$, N in these equations is understood to mean $\langle N\rangle_{\mu VT}$ and similarly P means $\langle\mathcal{P}\rangle_{\mu VT}$. As emphasized by Adams (1975), when these formulae are used in a computer simulation, it is advisable to cross-check them with the thermodynamic identity $\alpha_P = \beta_T\gamma_V$.

The impression may arise that particular thermodynamic derivatives (such as α_P) are best calculated by conducting a simulation in the corresponding ensemble (e.g. constant-NPT). This is not the case, and Lustig (2012) has provided a systematic approach to calculating such quantities in a wide variety of ensembles. Care must be taken in the application of any formulae to the zero-momentum ensemble usually employed in molecular dynamics (Çağin and Ray, 1988; Lustig, 1994a,b). Also, it is important to bear in mind that significant deviations from the thermodynamic limit will happen when the system size is small (Ray and Graben, 1991; Shirts et al., 2006; Uline et al., 2008).

2.6 Structural quantities

The structure of a simple monatomic fluid is characterized by a set of distribution functions for the atomic positions, the simplest of which is the pair distribution function $g_2(\mathbf{r}_i, \mathbf{r}_j)$, or $g_2(r_{ij})$ or simply $g(r)$. This function gives the probability of finding a pair of atoms a distance r apart, relative to the probability for a completely random distribution at the same density. To define $g(r)$, we integrate the configurational distribution function over the positions of all atoms except two, incorporating the appropriate normalization factors (McQuarrie, 1976; Hansen and McDonald, 2013). In the canonical ensemble

$$g(\mathbf{r}_1, \mathbf{r}_2) = \frac{N(N-1)}{\rho^2 Z_{NVT}} \int \mathrm{d}\mathbf{r}_3\mathrm{d}\mathbf{r}_4\cdots\mathrm{d}\mathbf{r}_N \exp[-\beta\mathcal{V}(\mathbf{r}_1, \mathbf{r}_2, \cdots\mathbf{r}_N)]. \tag{2.100}$$

Obviously the choice $i = 1$ and $j = 2$ is arbitrary in a system of identical atoms. An equivalent definition begins with the pair density

$$\rho^{(2)}(\mathbf{r}' + \mathbf{r}, \mathbf{r}') = \left\langle \sum_i \sum_{j\neq i} \delta(\mathbf{r}' + \mathbf{r} - \mathbf{r}_i)\delta(\mathbf{r}' - \mathbf{r}_j)\right\rangle$$

for positions separated by a vector $\mathbf{r}$. This is independent of $\mathbf{r}'$ in a homogeneous system (we discuss inhomogeneous systems in Section 2.12). $g(\mathbf{r})$ is defined as the ratio

$$g(\mathbf{r}) = \frac{\rho^{(2)}(\mathbf{r}' + \mathbf{r}, \mathbf{r}')}{\rho^2} = \frac{V^2}{N^2}\frac{1}{V}\int \mathrm{d}\mathbf{r}'\,\rho^{(2)}(\mathbf{r}' + \mathbf{r}, \mathbf{r}')$$

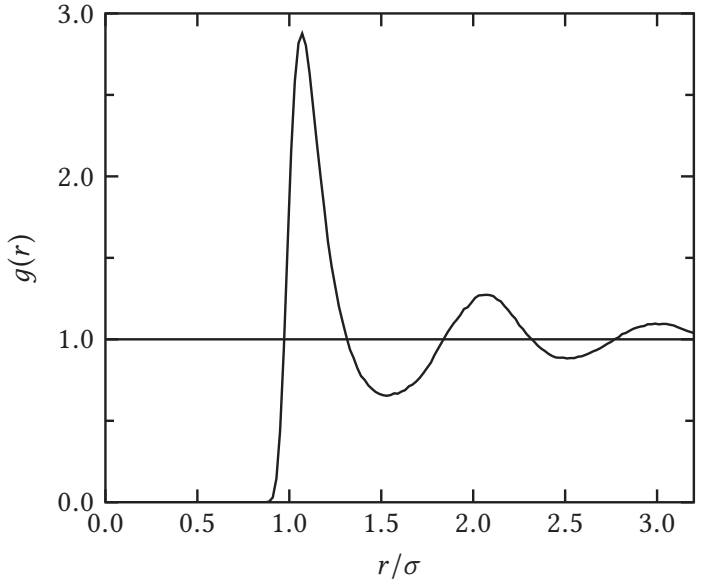

Fig. 2.2 Pair distribution function for the Lennard-Jones fluid (shifted, $r_c = 2.5\sigma$) close to its triple point ($T^* = 0.8$, $\rho^* = 0.8$).

where we average over $\mathbf{r}'$. The result of integrating over the delta functions is an ensemble average over pairs

$$g(r) = \frac{V}{N^2}\left\langle \sum_i \sum_{j\neq i} \delta(\mathbf{r} - \mathbf{r}_{ij}) \right\rangle, \quad \text{where } \mathbf{r}_{ij} = \mathbf{r}_i - \mathbf{r}_j, \tag{2.101}$$

and we note that the result depends only on $r = |\mathbf{r}|$ in an isotropic liquid. The pair distribution functions of simple model systems, such as hard spheres, may be predicted accurately by integral equation theories, and are frequently used as a basis for modelling the structure of a range of fluids (Hansen and McDonald, 2013); they may be easily calculated (Smith et al., 2008).

Equation (2.101) may be used in the evaluation of $g(r)$ by computer simulation; in practice, the delta function is replaced by a function which is non-zero in a small range of separations, and a histogram is compiled of all pair separations falling within each such range (see Chapter 8). Fig. 2.2 shows a typical pair distribution function for the Lennard-Jones liquid close to its triple point.

The pair distribution function is useful, not only because it provides insight into the liquid structure, but also because the ensemble average of any pair function may be expressed in the form

$$\left\langle a(\mathbf{r}_i, \mathbf{r}_j) \right\rangle = \frac{1}{V^2} \int \mathrm{d}\mathbf{r}_i \mathrm{d}\mathbf{r}_j \, g(\mathbf{r}_i, \mathbf{r}_j) a(\mathbf{r}_i, \mathbf{r}_j) \tag{2.102a}$$

or, in an isotropic fluid,

$$\langle \mathcal{A} \rangle = \left\langle \sum_i \sum_{j>i} a(r_{ij}) \right\rangle = \tfrac{1}{2} N\rho \int_0^\infty a(r) g(r) 4\pi r^2 \, \mathrm{d}r. \tag{2.102b}$$

For example, we may write the energy (assuming pair additivity)

$$E = \tfrac{3}{2}Nk_{\mathrm{B}}T + 2\pi N\rho \int_0^\infty r^2 v(r)g(r)\,\mathrm{d}r \tag{2.103}$$

or the pressure

$$PV = Nk_{\mathrm{B}}T - \tfrac{2}{3}\pi N\rho \int_0^\infty r^2 w(r)g(r)\,\mathrm{d}r \tag{2.104}$$

although in practice, a direct evaluation of these quantities, as discussed in Section 2.4, will usually be more accurate. Even the chemical potential may be related to $g(r)$

$$\mu = k_{\mathrm{B}}T\ln(\rho\Lambda^3) + 4\pi\rho \int_0^1 \mathrm{d}\xi \int_0^\infty r^2 v(r)g(r;\xi)\mathrm{d}r \tag{2.105}$$

with Λ given by eqn (2.24). As usual with the chemical potential, there is a twist: the formula involves a pair distribution function $g(r,\xi)$ which depends upon a parameter ξ coupling the two atoms, and it is necessary to integrate over ξ (McQuarrie, 1976).

The definition of the pair distribution function may be extended to the molecular case when the function $g(r_{ij},\Omega_i,\Omega_j)$ depends upon the separation between, and orientations of the molecules. This may be evaluated in a simulation by compiling histograms, as in the atomic case, but of course there is now the problem that many more variables are involved, and a very large, multidimensional table will be needed. A number of different approaches which give partial descriptions of the orientational ordering have been developed (Gray and Gubbins, 1984):

(a) sections through $g(r_{ij},\Omega_i,\Omega_j)$ are calculated as a function of r_{ij} for fixed relative orientations (Haile and Gray, 1980);
(b) $g(r_{ij},\Omega_i,\Omega_j)$ can be expressed as a spherical harmonic expansion, where the coefficients are functions of r_{ij} (Streett and Tildesley, 1976; Haile and Gray, 1980);
(c) a set of site–site distribution functions $g_{ab}(r_{ab})$ can be calculated in the same way as the atomic $g(r)$ for each type of site.

The first method proceeds by compiling histograms, just as for $g(r)$, but restricting the accumulation of data to pairs of molecules which are close to a few specific relative orientations. Thus for pairs of linear molecules, parallel configurations and T-shapes might be of interest.

The spherical harmonic expansion for a pair of linear molecules would take the form

$$g(r_{ij},\Omega_i,\Omega_j) = 4\pi \sum_{\ell=0}^{\infty}\sum_{\ell'=0}^{\infty}\sum_{m} g_{\ell\ell' m}(r_{ij})Y_{\ell m}(\Omega_i)Y_{\ell'\bar{m}}(\Omega_j) \tag{2.106}$$

where the functions $Y_{\ell m}(\Omega) \equiv Y_{\ell m}(\theta,\phi)$ are spherical harmonic functions of the polar angles defining the direction of the molecular axis, and $\bar{m} = -m$. The range of the sum over m values is either $(-\ell,\ell)$ or $(-\ell',\ell')$, whichever is the smaller. Note that the orientations are measured relative to the vector $\mathbf{r}_{ij}$ in each case. In a simulation, the coefficients $g_{\ell\ell' m}$ would be evaluated by averaging a product of spherical harmonics over a spherical shell around each molecule, as described in Chapter 8. The function $g_{000}(r)$ is the isotropic component, that is, the pair distribution function for molecular centres averaged over all

orientations. This approach is readily extended to non-linear molecules. The expansion can be carried out in a molecule-fixed frame (Streett and Tildesley, 1976) or in a space-fixed frame (Haile and Gray, 1980). The coefficients can be recombined to give the total distribution function, but this is not profitable for elongated molecules, since many terms are required for the series to converge. Certain observable properties are related to limited numbers of the harmonic coefficients. The angular correlation parameter of rank ℓ, g_ℓ, may be expressed in the molecule-fixed frame

$$g_\ell = 1 + \frac{4\pi\rho}{2\ell+1} \sum_{m=-\ell}^{\ell} (-1)^m \int_0^\infty g_{\ell\ell m}(r) r^2 \mathrm{d}r = 1 + \frac{1}{N} \left\langle \sum_i \sum_{j \neq i} P_\ell(\cos \gamma_{ij}) \right\rangle \tag{2.107}$$

where $P_\ell(\cos\gamma)$ is a Legendre polynomial and γ_{ij} is the angle between the axis vectors of molecules i and j. g_1 is related to the dielectric properties of polar molecules, while g_2 may be investigated by depolarized light scattering. Formulae analogous to eqns (2.106) and (2.107) may be written for non-linear molecules. These would involve the Wigner rotation matrices $\mathcal{D}^\ell_{mm'}(\Omega_i)$ instead of the spherical harmonics (Gray and Gubbins, 1984, Appendix 7). In liquid crystals, where the isotropic rotational symmetry is broken, these expansions involve many more terms (Zannoni, 2000).

As an alternative, a site–site description might be more appropriate. Pair distribution functions $g_{ab}(r_{ab})$ are defined for each pair of sites on different molecules, using the same definition as in the atomic case. The number of independent $g_{ab}(r_{ab})$ functions will depend on the complexity of the molecule. For example, in a three-site model of OCS, the isotropic liquid is described by six independent $g_{ab}(r_{ab})$ functions (for OO, OC, OS, CC, CS, and SS distances), whereas for a five-site model of CH_4, the liquid is described by three functions (CC, CH, HH). While less information is contained in these distribution functions than in the components of $g(r_{ij}, \Omega_i, \Omega_j)$, they have the advantage of being directly related to the structure factor of the molecular fluid (Lowden and Chandler, 1974) and hence to experimentally observable properties (for example neutron and X-ray scattering). We return to the calculation of these quantities in Chapter 8.

Finally, we turn to the definitions of quantities that depend upon wavevector rather than on position. In a simulation with periodic boundaries, we are restricted to wavevectors that are commensurate with the periodicity of the system, that is, with the simulation box. Specifically, in a cubic box, we may examine fluctuations for which $\mathbf{k} = (2\pi/L)(n_x, n_y, n_z)$ where L is the box length and n_x, n_y, n_z are integers. This is a severe restriction, particularly at low k. One quantity of interest is the spatial Fourier transform of the number density

$$\rho(\mathbf{k}) = \sum_{i=1}^{N} \exp(-\mathrm{i}\mathbf{k} \cdot \mathbf{r}_i). \tag{2.108}$$

Fluctuations in $\rho(\mathbf{k})$ are related to the structure factor $S(k)$

$$S(k) = N^{-1} \left\langle \rho(\mathbf{k}) \rho(-\mathbf{k}) \right\rangle \tag{2.109}$$

which may be measured by neutron or X-ray scattering experiments, and depends only on $k = |\mathbf{k}|$ in an isotropic system. Thus, $S(k)$ describes the Fourier components of the density

fluctuations in the liquid. It is related, through a three-dimensional Fourier transform (see Appendix D) to the pair distribution function

$$S(k) = 1 + \rho\hat{h}(k) = 1 + \rho\hat{g}(k) = 1 + 4\pi\rho \int_0^\infty r^2 \frac{\sin kr}{kr} g(r)\, \mathrm{d}r \tag{2.110}$$

where we have introduced the Fourier transform of the total correlation function $h(r) = g(r) - 1$, and have ignored a delta function contribution at $k = 0$. In a similar way, k-dependent orientational functions may be calculated and measured routinely in computer simulations.

2.7 Time correlation functions and transport coefficients

Correlations between two different quantities $\mathcal{A}$ and $\mathcal{B}$ are measured in the usual statistical sense, via the correlation coefficient $c_{\mathcal{AB}}$

$$c_{\mathcal{AB}} = \langle \delta\mathcal{A}\delta\mathcal{B}\rangle / \sigma(\mathcal{A})\sigma(\mathcal{B}) \tag{2.111}$$

with $\sigma(\mathcal{A})$ and $\sigma(\mathcal{B})$ given by eqn (2.48). Schwartz inequalities guarantee that the absolute value of $c_{\mathcal{AB}}$ lies between 0 and 1, with values close to 1 indicating a high degree of correlation. The idea of the correlation coefficient may be extended in a very useful way, by considering $\mathcal{A}$ and $\mathcal{B}$ to be evaluated at two different times. For an equilibrium system, the resulting quantity is a function of the time difference t: it is a 'time correlation function' $c_{\mathcal{AB}}(t)$. For identical phase functions, $c_{\mathcal{AA}}(t)$ is called an autocorrelation function and its time integral (from $t = 0$ to $t = \infty$) is a correlation time $t_{\mathcal{A}}$. These functions are of great interest in computer simulation because:

(a) they give a clear picture of the dynamics in a fluid;
(b) their time integrals $t_{\mathcal{A}}$ may often be related directly to macroscopic transport coefficients;
(c) their Fourier transforms $\hat{c}_{\mathcal{AA}}(\omega)$ may often be related to experimental spectra measured as a function of frequency ω.

Useful discussions of time correlation functions may be found in the references (Steele, 1969; 1980; Berne and Harp, 1970; McQuarrie, 1976; Hansen and McDonald, 2013). A few comments may be relevant here. The non-normalized correlation function is defined

$$C_{\mathcal{AB}}(t) = \left\langle \delta\mathcal{A}(t)\delta\mathcal{B}(0)\right\rangle_{\mathrm{ens}} = \left\langle \delta\mathcal{A}\big(\mathbf{\Gamma}(t)\big)\delta\mathcal{B}\big(\mathbf{\Gamma}(0)\big)\right\rangle_{\mathrm{ens}} \tag{2.112}$$

so that

$$c_{\mathcal{AB}}(t) = C_{\mathcal{AB}}(t)/\sigma(\mathcal{A})\sigma(\mathcal{B}) \tag{2.113a}$$

or

$$c_{\mathcal{AA}}(t) = C_{\mathcal{AA}}(t)/\sigma^2(\mathcal{A}) = C_{\mathcal{AA}}(t)/C_{\mathcal{AA}}(0). \tag{2.113b}$$

Just like $\langle \delta\mathcal{A}\delta\mathcal{B}\rangle$, $C_{\mathcal{AB}}(t)$ is different for different ensembles, and eqn (2.50) may be used to transform from one ensemble to another. The computation of $C_{\mathcal{AB}}(t)$ may be thought of as a two-stage process. First, we must select initial state points $\mathbf{\Gamma}(0)$, according to the desired distribution $\rho_{\mathrm{ens}}(\mathbf{\Gamma})$, over which we will subsequently average. This may be

done using any of the prescriptions mentioned in Section 2.1. Second, we must evaluate $\mathbf{\Gamma}(t)$. This means solving the true (Newtonian) equations of motion. By this means, time-dependent properties may be calculated in any ensemble. In practice, the mechanical equations of motion are almost always used for both purposes, that is, we use molecular dynamics to calculate the time correlation functions in the microcanonical ensemble.

Some attention must be paid to the question of ensemble equivalence, however, since the link between correlation functions and transport coefficients is made through linear response theory, which can be carried out in virtually any ensemble. This actually caused some confusion in the original derivations of the expressions for transport coefficients (Zwanzig, 1965). In the following, we make some general observations, and refer the reader elsewhere (McQuarrie, 1976; Frenkel and Smit, 2002; Tuckerman, 2010; Hansen and McDonald, 2013) for a fuller discussion.

Transport coefficients such as the diffusion coefficient, thermal conductivity, and shear and bulk viscosities appear in the equations of hydrodynamics, such as the mass and thermal diffusion equations and the Navier–Stokes equation. Accordingly, they describe the relaxation of dynamical variables on the macroscopic scale. Provided the long-time and large-length-scale limits are considered carefully, they can be expressed in terms of equilibrium time correlation functions of microscopically defined variables. Such relations are generally termed Green–Kubo formulae (Hansen and McDonald, 2013). Linear response theory can be used to provide an interpretation of these formulae in terms of the response of the system to a weak perturbation. By introducing such perturbations into the Hamiltonian, or directly into the equations of motion, their effect on the distribution function ρ_{ens} may be calculated. Generally, a time-dependent nonequilibrium distribution $\rho(t) = \rho_{\text{ens}} + \delta\rho(t)$ is produced. Hence, any nonequilibrium ensemble average (in particular, the desired response) may be calculated. By retaining the linear terms in the perturbation, and comparing the equation for the response with a macroscopic transport equation, we may identify the transport coefficient.

The Green–Kubo expression is usually written as the infinite time integral of an equilibrium time correlation function of the form

$$\gamma = \int_0^\infty \mathrm{d}t \left\langle \dot{\mathcal{A}}(t)\dot{\mathcal{A}}(0)\right\rangle \tag{2.114}$$

where γ is the transport coefficient, and $\mathcal{A}$ is the appropriate dynamical variable. Associated with any expression of this kind, there is an 'Einstein relation'

$$\left\langle \Big(\mathcal{A}(t) - \mathcal{A}(0)\Big)^2 \right\rangle = 2t\gamma, \quad \text{as } t \to \infty, \text{ or } \quad \gamma = \lim_{t\to\infty} \frac{\mathrm{d}}{\mathrm{d}t}\frac{1}{2}\left\langle \Big(\mathcal{A}(t) - \mathcal{A}(0)\Big)^2 \right\rangle \tag{2.115}$$

which holds at large t compared with the correlation time of $\mathcal{A}$. The connection between eqns (2.114) and (2.115) may be easily established by integration by parts. Note that only a few genuine transport coefficients exist; that is, for only a few 'hydrodynamic' variables $\mathcal{A}$ do eqns (2.114) and (2.115) give a non-zero γ (McQuarrie, 1976).

In computer simulations, transport coefficients may be calculated from equilibrium correlation functions, using eqn (2.114), by observing Einstein relations, eqn (2.115), or indeed going back to first principles and conducting a suitable nonequilibrium simulation. The details of the calculation via eqns (2.114), (2.115) will be given in Chapter 8, and we

will examine nonequilibrium methods in Chapter 11. For use in equilibrium molecular dynamics, we give here the equations for calculating thermal transport coefficients in the microcanonical ensemble, for a fluid composed of N identical molecules.

The diffusion coefficient D is given (in three dimensions) by

$$D = \frac{1}{3}\int_0^\infty \mathrm{d}t \left\langle \mathbf{v}_i(t) \cdot \mathbf{v}_i(0) \right\rangle \tag{2.116}$$

where $\mathbf{v}_i(t)$ is the centre-of-mass velocity of a single molecule. The corresponding Einstein relation, valid at long times, is

$$D = \lim_{t\to\infty} \frac{\mathrm{d}}{\mathrm{d}t}\frac{1}{6}\left\langle \left|\mathbf{r}_i(t) - \mathbf{r}_i(0)\right|^2 \right\rangle \tag{2.117}$$

where $\mathbf{r}_i(t)$ is the molecule position. There is also an equally valid 'intermediate' form:

$$D = \lim_{t\to\infty} \frac{1}{3}\left\langle \mathbf{v}_i(0) \cdot \left(\mathbf{r}_i(t) - \mathbf{r}_i(0)\right) \right\rangle. \tag{2.118}$$

In practice, these averages would be computed for each of the N particles in the simulation, the results added together, and divided by N, to improve statistical accuracy. Note that in the computation of eqns (2.117), (2.118), it is important not to switch attention from one periodic image to another, which is why it is sometimes useful to have available a set of particle coordinates which have not been subjected to periodic boundary conditions during the simulation (see Section 1.6 and Chapter 8).

The shear viscosity is given by

$$\eta = \frac{V}{k_\mathrm{B}T}\int_0^\infty \mathrm{d}t \left\langle \mathcal{P}_{\alpha\beta}(t)\mathcal{P}_{\alpha\beta}(0) \right\rangle \tag{2.119}$$

or

$$\eta = \lim_{t\to\infty} \frac{\mathrm{d}}{\mathrm{d}t}\frac{1}{2}\frac{V}{k_\mathrm{B}T}\left\langle \left(\mathcal{Q}_{\alpha\beta}(t) - \mathcal{Q}_{\alpha\beta}(0)\right)^2 \right\rangle. \tag{2.120}$$

Here

$$\mathcal{P}_{\alpha\beta} = \frac{1}{V}\left(\sum_i p_{i\alpha}p_{i\beta}/m_i + \sum_i r_{i\alpha}f_{i\beta} \right) \tag{2.121}$$

or

$$\mathcal{P}_{\alpha\beta} = \frac{1}{V}\left(\sum_i p_{i\alpha}p_{i\beta}/m_i + \sum_i \sum_{j>i} r_{ij\alpha}f_{ij\beta} \right) \tag{2.122}$$

is an off-diagonal ($\alpha \neq \beta$) element of the pressure tensor (compare the virial expression for the pressure function eqns (2.61) and (2.65)) and

$$\mathcal{Q}_{\alpha\beta} = \frac{1}{V}\sum_i r_{i\alpha}p_{i\beta}. \tag{2.123}$$

The negative of $\mathcal{P}_{\alpha\beta}$ is often called the stress tensor. These quantities are multi-particle properties, properties of the system as a whole, and no additional averaging over N particles is possible. Consequently η is subject to much greater statistical imprecision than

D. Some improvement is possible by averaging over different components $\alpha\beta = xy, yz, zx$, of $\mathcal{P}_{\alpha\beta}$. Just as for eqn (2.65), the origin-independent form, eqn (2.122), should be used rather than eqn (2.121), in periodic boundaries, and similar care needs to be taken in the calculation of $\mathcal{Q}_{\alpha\beta}(t) - \mathcal{Q}_{\alpha\beta}(0)$ in eqn (2.120).

The bulk viscosity is given by a similar expression:

$$\eta_V = \frac{V}{9k_\mathrm{B}T}\sum_{\alpha\beta}\int_0^\infty \mathrm{d}t\left\langle \delta\mathcal{P}_{\alpha\alpha}(t)\delta\mathcal{P}_{\beta\beta}(0)\right\rangle = \frac{V}{k_\mathrm{B}T}\int_0^\infty \mathrm{d}t\left\langle \delta\mathcal{P}(t)\delta\mathcal{P}(0)\right\rangle \tag{2.124a}$$

where we sum over $\alpha, \beta = x, y, z$ and note that $\mathcal{P} = \frac{1}{3}\operatorname{Tr}\boldsymbol{\mathcal{P}} = \frac{1}{3}\sum_\alpha \mathcal{P}_{\alpha\alpha}$. Rotational invariance leads to the equivalent expression

$$\eta_V + \tfrac{4}{3}\eta = \frac{V}{k_\mathrm{B}T}\int_0^\infty \mathrm{d}t\left\langle \delta\mathcal{P}_{\alpha\alpha}(t)\delta\mathcal{P}_{\alpha\alpha}(0)\right\rangle. \tag{2.124b}$$

Here the diagonal stresses must be evaluated with care, since a non-vanishing equilibrium average must be subtracted:

$$\delta\mathcal{P}_{\alpha\alpha}(t) = \mathcal{P}_{\alpha\alpha}(t) - \langle\mathcal{P}_{\alpha\alpha}\rangle = \mathcal{P}_{\alpha\alpha}(t) - P \tag{2.125a}$$

$$\delta\mathcal{P}(t) = \mathcal{P}(t) - \langle\mathcal{P}\rangle = \mathcal{P}(t) - P \tag{2.125b}$$

with $\mathcal{P}_{\alpha\beta}$ given by an expression like eqn (2.122). The corresponding Einstein relation is (Alder et al., 1970)

$$\eta_V + \tfrac{4}{3}\eta = \lim_{t\to\infty}\frac{\mathrm{d}}{\mathrm{d}t}\frac{1}{2}\frac{V}{k_\mathrm{B}T}\left\langle\left(\mathcal{Q}_{\alpha\alpha}(t) - \mathcal{Q}_{\alpha\alpha}(0) - Pt\right)^2\right\rangle. \tag{2.126}$$

The thermal conductivity λ_T can be written (Hansen and McDonald, 2013)

$$\lambda_T = \frac{V}{k_\mathrm{B}T^2}\int_0^\infty \mathrm{d}t\left\langle j^\epsilon_\alpha(t)j^\epsilon_\alpha(0)\right\rangle \tag{2.127}$$

or

$$\lambda_T = \lim_{t\to\infty}\frac{\mathrm{d}}{\mathrm{d}t}\frac{1}{2}\frac{V}{k_\mathrm{B}T^2}\left\langle\left(\delta\epsilon_\alpha(t) - \delta\epsilon_\alpha(0)\right)^2\right\rangle. \tag{2.128}$$

Here j^ϵ_α is a component of the energy current, that is, the time derivative of

$$\delta\epsilon_\alpha = \frac{1}{V}\sum_i r_{i\alpha}\left(\epsilon_i - \langle\epsilon_i\rangle\right). \tag{2.129}$$

The term $\sum_i r_{i\alpha}\langle\epsilon_i\rangle$ makes no contribution if $\sum_i r_{i\alpha} = 0$, as is the case in a normal one-component MD simulation. In calculating the energy per molecule ϵ_i, the potential energy of two molecules (assuming pairwise additive potentials) is taken to be divided equally between them:

$$\epsilon_i = p_i^2/2m_i + \tfrac{1}{2}\sum_{j\neq i} v(r_{ij}). \tag{2.130}$$

These expressions for η_V and λ_T are ensemble-dependent and the preceding equations hold for the microcanonical case only. A fuller discussion may be found in the standard texts (McQuarrie, 1976; Zwanzig, 1965).

Transport coefficients are related to the long-time behaviour of correlation functions. Short-time correlations, on the other hand, may be linked with static equilibrium ensemble averages by expanding in a Taylor series. For example, the velocity of particle i may be written

$$\mathbf{v}_i(t) = \mathbf{v}_i(0) + \dot{\mathbf{v}}_i(0)t + \tfrac{1}{2}\ddot{\mathbf{v}}_i(0)t^2 + \cdots . \tag{2.131}$$

Multiplying by $\mathbf{v}_i(0)$ and ensemble averaging yields

$$\Big\langle \mathbf{v}_i(t)\cdot\mathbf{v}_i(0)\Big\rangle = \langle v_i^2\rangle + \tfrac{1}{2}\langle \ddot{\mathbf{v}}_i\cdot\mathbf{v}_i\rangle t^2 + \cdots = \langle v_i^2\rangle - \tfrac{1}{2}\langle \dot{v}_i^2\rangle t^2 + \cdots . \tag{2.132}$$

The vanishing of the term linear in t, and the last step, where we set $\langle \ddot{\mathbf{v}}_i\cdot\mathbf{v}_i\rangle = -\langle \dot{\mathbf{v}}_i\cdot\dot{\mathbf{v}}_i\rangle$, follow from time-reversal symmetry and stationarity (McQuarrie, 1976). Thus, the short-time velocity autocorrelation function is related to the mean-square acceleration, that is, to the mean-square force. This behaviour may be used to define the Einstein frequency ω_{E}

$$\langle \mathbf{v}_i(t)\cdot\mathbf{v}_i(0)\rangle = \langle v_i^2\rangle\Big(1 - \tfrac{1}{2}\omega_{\mathrm{E}}^2 t^2 + \cdots\Big). \tag{2.133}$$

The analogy with the Einstein model, of an atom vibrating in the mean force field of its neighbours, with frequency ω_{E} in the harmonic approximation, becomes clear when we replace the mean-square force by the average potential curvature using

$$\langle f_{i\alpha}^2\rangle = -\Big\langle f_{i\alpha}\partial\mathcal{V}/\partial r_{i\alpha}\Big\rangle = -k_{\mathrm{B}}T\Big\langle \partial f_{i\alpha}/\partial r_{i\alpha}\Big\rangle = k_{\mathrm{B}}T\Big\langle \partial^2\mathcal{V}/\partial r_{i\alpha}^2\Big\rangle \tag{2.134}$$

which is another application of $\langle \mathcal{A}\,\partial\mathcal{H}/\partial q_k\rangle = k_{\mathrm{B}}T\langle\partial\mathcal{A}/\partial q_k\rangle$. The result is

$$\omega_{\mathrm{E}}^2 = \frac{\Big\langle f_i^2\Big\rangle}{m_i^2\Big\langle v_i^2\Big\rangle} = \frac{1}{3m_i}\Big\langle \nabla_{\mathbf{r}_i}^2\mathcal{V}\Big\rangle. \tag{2.135}$$

This may be easily evaluated for, say, a pairwise additive potential. Short-time expansions of other time correlation functions may be obtained using similar techniques. The temporal Fourier transform (see Appendix D) of the velocity autocorrelation function is proportional to the density of normal modes in a purely harmonic system, and is often loosely referred to as the 'density of states' in solids and liquids. The velocity autocorrelation function for the Lennard-Jones liquid near the triple point is illustrated in Fig. 2.3.

We can only mention briefly some other autocorrelation functions of interest in computer simulations. The generalization of eqn (2.109) to the time domain yields the intermediate scattering function $I(k,t)$.

$$I(k,t) = N^{-1}\Big\langle \rho(\mathbf{k},t)\rho(-\mathbf{k},0)\Big\rangle \tag{2.136}$$

with $\rho(\mathbf{k},t)$ defined by eqn (2.108). The temporal Fourier transform of this, the dynamic structure factor $S(k,\omega)$, in principle may be measured by inelastic neutron scattering. Spatially Fourier transforming $I(k,t)$ yields the van Hove function $G(r,t)$, a generalization of $g(r)$ which measures the probability of finding a particle at position r at time t, given that a particle was at the origin of coordinates at time 0. All of these functions may be divided into parts due to 'self' (i.e. single-particle) motion and due to 'distinct' (i.e. collective) effects. Other k-dependent variables may be defined, and their time correlation

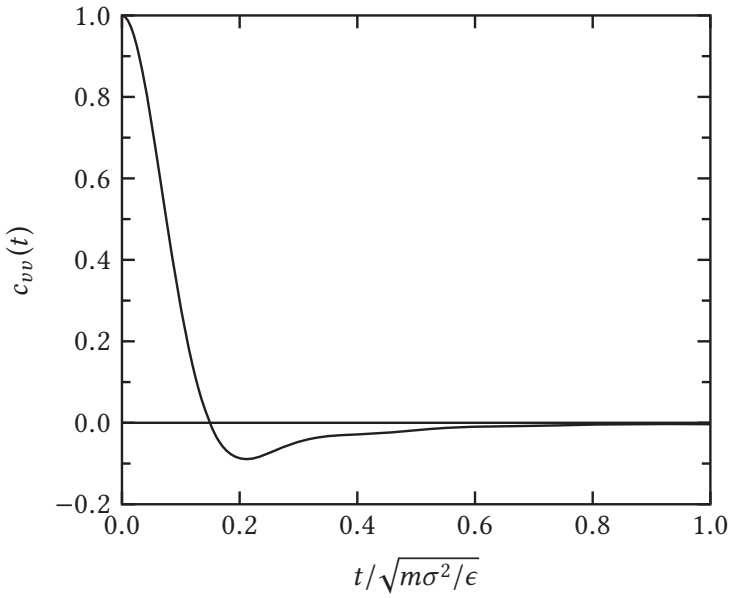

Fig. 2.3 The velocity autocorrelation function for the Lennard-Jones fluid (shifted potential, $r_c = 2.5\sigma$) close to its triple point ($T^* = 0.8$, $\rho^* = 0.8$).

functions are of great interest (Hansen and McDonald, 2013). For example, longitudinal and transverse momentum components may be defined

$$p^{\parallel}(\mathbf{k},t) = \frac{1}{V}\sum_i p_{ix}(t)\exp\Big(\mathrm{i}kx_i(t)\Big) \tag{2.137a}$$

$$p_1^{\perp}(\mathbf{k},t) = \frac{1}{V}\sum_i p_{iy}(t)\exp\Big(\mathrm{i}kx_i(t)\Big) \tag{2.137b}$$

$$p_2^{\perp}(\mathbf{k},t) = \frac{1}{V}\sum_i p_{iz}(t)\exp\Big(\mathrm{i}kx_i(t)\Big) \tag{2.137c}$$

where for convenience we take $\mathbf{k} = (k,0,0)$ in the x direction, and $x_i = r_{ix}$. These quantities are useful for discussing hydrodynamic modes in liquids. These functions may all be computed routinely in simulations, although, as always, the allowed k-vectors are restricted by small system sizes and periodic boundary conditions.

For systems of rigid molecules, the angular velocity $\boldsymbol{\omega}_i$ plays a role in reorientational dynamics analogous to that of $\mathbf{v}_i$ in translation (see Chapter 3). The angular velocity correlation function $\langle\boldsymbol{\omega}_i(t)\cdot\boldsymbol{\omega}_i(0)\rangle$ may be used to describe rotation. Time-dependent orientational correlations may be defined (Gordon, 1968; Steele, 1969; 1980) as straightforward generalizations of the quantities seen earlier. For a linear molecule, the time correlation function of rank-ℓ spherical harmonics is

$$c_\ell(t) = 4\pi\left\langle Y_{\ell m}\Big(\Omega_i(t)\Big)Y^*_{\ell m}\Big(\Omega_i(0)\Big)\right\rangle = \left\langle P_\ell\Big(\cos\delta\gamma(t)\Big)\right\rangle \tag{2.138}$$

where $\delta\gamma(t)$ is the magnitude of the angle turned through in time t. Note that, assuming an isotropic system, there are $2\ell+1$ rank-ℓ functions, all identical in form, corresponding to the different values of m.

Analogous formulae for non-linear molecules involve the Wigner rotation matrices. The starting point is the expansion of the probability density for rotation of the molecule through a set of Euler angles $\delta\Omega_i$ in time t:

$$\rho(\delta\Omega_i;t) = \sum_{\ell mm'} \frac{2\ell+1}{8\pi^2} c_{\ell mm'}(t) \mathcal{D}^{\ell *}_{mm'}(\delta\Omega_i)$$

which is equivalent to defining the key correlation functions

$$c_{\ell mm'}(t) = \left\langle \mathcal{D}^{\ell}_{mm'}\Big(\delta\Omega_i(t)\Big)\right\rangle.$$

The term on the right may be expressed in terms of the molecular orientations at time 0 and time t:

$$\mathcal{D}^{\ell}_{mm'}\Big(\delta\Omega_i(t)\Big) = \sum_{n=-\ell}^{\ell} \mathcal{D}^{\ell *}_{nm}\Big(\Omega_i(0)\Big)\mathcal{D}^{\ell}_{nm'}\Big(\Omega_i(t)\Big).$$

However, in an isotropic fluid, averaging over the initial distribution gives an identical result for each of these terms

$$\left\langle \mathcal{D}^{\ell}_{mm'}\Big(\delta\Omega_i(t)\Big)\right\rangle = (2\ell+1)\left\langle \mathcal{D}^{\ell *}_{nm}\Big(\Omega_i(0)\Big)\mathcal{D}^{\ell}_{nm'}\Big(\Omega_i(t)\Big)\right\rangle$$

independent of n, and so (Steele, 1980)

$$c_{\ell mm'}(t) = (2\ell+1)\left\langle \mathcal{D}^{\ell *}_{nm}\Big(\Omega_i(0)\Big)\, \mathcal{D}^{\ell}_{nm'}\Big(\Omega_i(t)\Big)\right\rangle. \tag{2.139}$$

When the symmetry of the phase is reduced, for example in liquid crystals, many more non-equivalent time correlation functions exist (Zannoni, 1994). These quantities are experimentally accessible and the relationships between them are of great theoretical interest. For example, first-rank autocorrelation functions may be related to infrared absorption, and second-rank functions to light scattering. Functions of all ranks contribute to inelastic neutron scattering spectra from molecular liquids.

2.8 Long-range corrections

As explained in Section 1.6, computer simulations frequently use a pair potential with a spherical cutoff at a distance r_c. It becomes useful to correct the results of simulations to compensate for the missing long-range part of the potential. Contributions to the energy, pressure, etc. for $r > r_c$ are frequently estimated by assuming that $g(r) \approx 1$ in this region, and using eqns (2.103)–(2.105)

$$E_{\text{full}} \approx E_c + E_{\text{LRC}} = E_c + 2\pi N\rho \int_{r_c}^{\infty} r^2 v(r)\, \mathrm{d}r \tag{2.140}$$

$$(PV)_{\text{full}} = (PV)_c + (PV)_{\text{LRC}} = (PV)_c - \tfrac{2}{3}\pi N\rho \int_{r_c}^{\infty} r^2 w(r)\, \mathrm{d}r \tag{2.141}$$

$$\mu_{\text{full}} = \mu_c + \mu_{\text{LRC}} = \mu_c + 4\pi\rho \int_{r_c}^{\infty} r^2 v(r)\, \mathrm{d}r \tag{2.142}$$

where E_{full}, $(PV)_{\text{full}}$, μ_{full} are the desired values for a liquid with the full potential, and E_{c}, $(PV)_{\text{c}}$, μ_{c} are the values actually determined from a simulation using a potential with a cutoff. For the Lennard-Jones potential, eqn (1.6), these equations become

$$E^*_{\text{LRC}} = \tfrac{8}{9}\pi N\rho^* r_{\text{c}}^{*-9} - \tfrac{8}{3}\pi N\rho^* r_{\text{c}}^{*-3} \tag{2.143}$$

$$P^*_{\text{LRC}} = \tfrac{32}{9}\pi \rho^{*2} r_{\text{c}}^{*-9} - \tfrac{16}{3}\pi \rho^{*2} r_{\text{c}}^{*-3} \tag{2.144}$$

$$\mu^*_{\text{LRC}} = \tfrac{16}{9}\pi \rho^* r_{\text{c}}^{*-9} - \tfrac{16}{3}\pi \rho^* r_{\text{c}}^{*-3} \tag{2.145}$$

where we use Lennard-Jones reduced units (see Appendix B). In the case of the constant-NVE and constant-NVT ensembles, these corrections can be applied to the results after a simulation has run. However, if the volume or the number of particles is allowed to fluctuate (e.g. in a constant-NPT or constant-μVT simulation) it is important to apply the corrections to the calculated instantaneous energies, pressures, etc. during the course of a simulation, since they will change as the density fluctuates: it is far more tricky to attempt to do this when the simulation is over.

For three-body potentials such as the Axilrod–Teller potential, the potential energy from the three-body term in a homogeneous fluid is

$$\langle \mathcal{V}_3 \rangle = \frac{\rho^3}{6} \iiint \mathrm{d}\mathbf{r}_1 \mathrm{d}\mathbf{r}_2 \mathrm{d}\mathbf{r}_3 \, v^{(3)}(r_{12}, r_{13}, r_{23}) \, g^{(3)}(\mathbf{r}_1, \mathbf{r}_2, \mathbf{r}_3). \tag{2.146}$$

In a simulation the three-body energy is calculated explicitly for

$$r_{12} \le r_{\text{c}} \text{ and } r_{13} \le r_{\text{c}} \text{ and } r_{23} \le r_{\text{c}}. \tag{2.147}$$

For the rest of the space, the long-range part, the three-body distribution function can be approximated using the superposition approximation

$$g^{(3)}(\mathbf{r}_1, \mathbf{r}_2, \mathbf{r}_3) \approx g^{(2)}(r_{12}) \, g^{(2)}(r_{13}) \, g^{(2)}(r_{23}). \tag{2.148}$$

There are six equivalent parts to this region, and the long-range correction is thus

$$\langle \mathcal{V}_3 \rangle_{\text{LRC}} = \rho^3 \iiint\limits_{\substack{r_{12} > r_{\text{c}} \\ r_{12} > r_{13} > r_{23}}} \mathrm{d}\mathbf{r}_1 \mathrm{d}\mathbf{r}_2 \mathrm{d}\mathbf{r}_3 \, v^{(3)}(r_{12}, r_{13}, r_{23}) \, g^{(2)}(r_{13}) \, g^{(2)}(r_{23}) \tag{2.149}$$

where we have explicitly considered the region in which $r_{12} > r_{\text{c}}$ and thus $g(r_{12}) = 1$ (Barker et al., 1971). Then transforming to bipolar coordinates we have

$$E_{3,\text{LRC}} = \langle \mathcal{V}_3 \rangle_{\text{LRC}} = 8\pi^2 \rho^2 N \int_{r_{\text{c}}}^{\infty} \mathrm{d}r_{12} \, r_{12} \int_0^{r_{12}} \mathrm{d}r_{13} \, r_{13} \int_{r_{12}-r_{13}}^{r_{13}} \mathrm{d}r_{23} \, r_{23} \, v^{(3)}(r_{12}, r_{13}, r_{23}) \, g^{(2)}(r_{13}) g^{(2)}(r_{23}) \tag{2.150}$$

which can be evaluated accurately using the kind of Monte Carlo integration method described in Section 4.2. Note that the approximate estimate of the three-body long-range correction requires the two-body radial distribution function for the fluid. This cannot

simply be set to one since both r_{13} and r_{23} can be less than r_c. For the specific case of the Axilrod–Teller potential, which is a homogeneous function of order 9 (Graben and Fowler, 1969)

$$(PV)_{3,\mathrm{LRC}} = 3E_{3,\mathrm{LRC}}. \tag{2.151}$$

For more general potentials the Monte Carlo evaluation of eqn (2.149) can be adapted to calculate the long-range correction for the pressure and the chemical potential.

2.9 Quantum corrections

Most of this book will deal with the computer simulation of systems within the classical approximation, although we turn in Chapter 13 to the attempts which have been made to incorporate quantum effects in simulations. Quantum effects in thermodynamics may be measured experimentally via the isotope separation factor, while tunnelling, superfluidity, etc. are clear manifestations of quantum mechanics.

Even within the limitations of a classical simulation, it is still possible to estimate quantum corrections of thermodynamic functions. This is achieved by expanding the partition function in powers of Planck's constant, $\hbar = h/2\pi$ (Wigner, 1932; Kirkwood, 1933). For a system of N atoms we have

$$Q_{NVT} = \frac{1}{\Lambda^{3N} N!} \int \mathrm{d}\mathbf{r} \left(1 - \frac{\beta\hbar^2}{24m} \sum_{i=1}^{N} \left[\boldsymbol{\nabla}_{\mathbf{r}_i} \beta\mathcal{V}(\mathbf{r})\right]^2\right) \exp[-\beta\mathcal{V}(\mathbf{r})] \tag{2.152}$$

where Λ is defined in eqn (2.24). The expansion accounts for the leading quantum-mechanical diffraction effects; other effects, such as exchange, are small for most cases of interest. Additional details may be found elsewhere (Landau and Lifshitz, 1980; McQuarrie, 1976). This leads to the following correction to the Helmholtz free energy, $\Delta A = A^{\mathrm{qu}} - A^{\mathrm{cl}}$

$$\Delta A_{\mathrm{trans}} = \tfrac{1}{24} N\hbar^2\beta^2 \left\langle f_i^2 \right\rangle / m. \tag{2.153}$$

Here, as in Section 2.7, $\langle f_i^2 \rangle$ is the mean-square force on one atom in the simulation. Obviously, better statistics are obtained by averaging over all N atoms. An equivalent expression is

$$\begin{aligned} \Delta A_{\mathrm{trans}} &= \frac{N\Lambda^2\rho}{48\pi} \int \mathrm{d}\mathbf{r}\, g(r) \nabla^2 v(r) \\ &= \frac{N\Lambda^2\rho}{12} \int_0^\infty r^2 g(r) \left(\frac{\mathrm{d}^2 v(r)}{\mathrm{d}r^2} + \frac{2}{r}\frac{\mathrm{d}v(r)}{\mathrm{d}r}\right) \mathrm{d}r \end{aligned} \tag{2.154}$$

assuming pairwise additive interactions. Additional corrections of order $\hbar^4$ can be estimated if the three-body distribution function g_3 can be calculated in a simulation (Hansen and Weis, 1969). Note that for hard systems, the leading quantum correction is of order $\hbar$: for hard spheres it amounts to replacing the hard sphere diameter σ by $\sigma + \Lambda/\sqrt{8}$ (Hemmer, 1968; Jancovici, 1969). By differentiating these equations, quantum corrections for the energy, pressure, etc. can easily be obtained.

Equation (2.153) is also the translational correction for a system of N molecules where it is understood that m now stands for the molecular mass and $\langle f_i^2 \rangle$ is the mean-square

force acting on the molecular centre of mass. Additional corrections must be applied for a molecular system, to take account of rotational motion (St. Pierre and Steele, 1969; Powles and Rickayzen, 1979). For linear molecules, with moment of inertia I, the additional term is (Gray and Gubbins, 1984)

$$\Delta A_{\text{rot}} = \tfrac{1}{24} N\hbar^2\beta^2\left\langle \tau_i^2 \right\rangle / I - N\hbar^2/6I \tag{2.155}$$

where $\langle \tau_i^2 \rangle$ is the mean-square torque acting on a molecule. The correction for the general asymmetric top, with three different moments of inertia I_{xx}, I_{yy}, and I_{zz}, is rather more complicated

$$\Delta A_{\text{rot}} = \tfrac{1}{24} N\hbar^2\beta^2\left(\frac{\left\langle \tau_{ix}^2 \right\rangle}{I_{xx}} + \frac{\left\langle \tau_{iy}^2 \right\rangle}{I_{yy}} + \frac{\left\langle \tau_{iz}^2 \right\rangle}{I_{zz}} \right) - \left[\frac{N\hbar^2}{24} \sum_{\text{cyclic}} \frac{2}{I_{xx}} - \frac{I_{xx}}{I_{yy}I_{zz}} \right] \tag{2.156}$$

where the sum is over the three cyclic permutations of x, y, and z. These results are independent of ensemble, and from them the quantum corrections to any other thermodynamic property can be calculated. Moreover, it is easy to compute the mean-square force and mean-square torque in a simulation.

Another, possibly more accurate, way of estimating quantum corrections has been proposed (Berens et al., 1983). In this approach, the velocity autocorrelation function is calculated and is Fourier transformed to obtain a spectrum, or density of states,

$$\begin{aligned} \hat{c}_{vv}(\omega) &= \int_{-\infty}^{\infty} \mathrm{d}t \, \exp(\mathrm{i}\omega t) \left\langle \mathbf{v}_i(t) \cdot \mathbf{v}_i(0) \right\rangle / \left\langle v_i^2 \right\rangle \\ &= \frac{m}{3k_{\text{B}}T} \int_{-\infty}^{\infty} \mathrm{d}t \, \exp(\mathrm{i}\omega t) \left\langle \mathbf{v}_i(t) \cdot \mathbf{v}_i(0) \right\rangle. \end{aligned} \tag{2.157}$$

Then, quantum corrections are applied to any thermodynamic quantities of interest, using the approximation that the system behaves as a set of harmonic oscillators, whose frequency distribution is dictated by the measured velocity spectrum. For each thermodynamic function a correction function, which would apply to a harmonic oscillator of frequency ω, may be defined. The total correction is then obtained by integrating over all frequencies. For the Helmholtz free energy, the correction is given by

$$\Delta A = 3Nk_{\text{B}}T \int_{-\infty}^{\infty} \frac{\mathrm{d}\omega}{2\pi} \, \hat{c}_{vv}(\omega) \, \ln\left(\frac{\exp\left(\frac{1}{2}\hbar\omega/k_{\text{B}}T\right) - \exp\left(-\frac{1}{2}\hbar\omega/k_{\text{B}}T\right)}{\hbar\omega/k_{\text{B}}T} \right) \tag{2.158}$$

which agrees with eqn (2.153) to $O(\hbar^2)$. The rationale here is that the harmonic approximation is most accurate for the high-frequency motions that contribute the largest quantum corrections, whereas the anharmonic motions are mainly of low frequency, and thus their quantum corrections are less important. Simulations comparing the simulated and experimental heat capacity (Waheed and Edholm, 2011) seem to confirm this for liquid water, but anharmonicity for ice near the melting point is significant, and the method overestimates the heat of vaporization. This approach has also been applied to liquid methanol (Hawlicka et al., 1989) and ammonia under extreme conditions (Bethkenhagen

et al., 2013). An alternative approach, however, is to incorporate quantum effects associated with light nuclei, such as hydrogen, into the simulation method directly using the path-integral approach (see Section 13.4).

Quantum corrections may also be applied to structural quantities such as $g(r)$. The formulae are rather complex and will not be given here, but they are based on the same formula eqn (2.152) for the partition function (Gibson, 1974). Again, the result is different for hard systems (Gibson, 1975a,b).

When it comes to time-dependent properties, there is one quantum correction which is essential to bring the results of classical simulation in line with experiment. Quantum mechanical autocorrelation functions obey the detailed balance condition

$$\hat{C}_{\mathcal{A}\mathcal{A}}(\omega) = \exp(\beta\hbar\omega)\hat{C}_{\mathcal{A}\mathcal{A}}(-\omega) \tag{2.159}$$

whereas, of course, classical autocorrelation functions are even in frequency (Berne and Harp, 1970). The effects of detailed balance are clearly visible in experimental spectra, for example in inelastic neutron scattering, which probes $S(k,\omega)$; in fact experimental results are often converted to the symmetrized form $\exp(\frac{1}{2}\hbar\beta\omega)S(k,\omega)$ for comparison with classical theories. Simple empirical measures have been advocated to convert classical time correlation functions into approximate quantum-mechanical ones. Both the 'complex time' substitutions

$$C_{\mathcal{A}\mathcal{A}}(t) \rightarrow C_{\mathcal{A}\mathcal{A}}(t - \tfrac{1}{2}i\hbar\beta) \qquad \text{(Schofield, 1960)} \tag{2.160}$$

$$\text{and} \quad C_{\mathcal{A}\mathcal{A}}(t) \rightarrow C_{\mathcal{A}\mathcal{A}}\left((t^2 - i\hbar\beta t)^{1/2}\right) \qquad \text{(Egelstaff, 1961)} \tag{2.161}$$

result in functions which satisfy detailed balance. The former is somewhat easier to apply, since it equates the symmetrized experimental spectrum with the classical simulated one, while the latter satisfies some additional frequency integral relations.

2.10 Constraints

In modelling large molecules such as proteins it may be necessary to include constraints in the potential model, as discussed in Section 1.3.3. This introduces some subtleties into the statistical mechanical description. The system of constrained molecules moves on a well-defined hypersurface in phase space. The generalized coordinates corresponding to the constraints and their conjugate momenta are removed from the Hamiltonian. This affects the form of the distribution function, and expressions for ensemble averages, in Cartesian coordinates (see Ryckaert and Ciccotti, 1983, Appendix). This system is not equivalent to a fluid where the constrained degrees of freedom are replaced by harmonic springs, even in the limit of infinitely strong force constants (Fixman, 1974; Pear and Weiner, 1979; Chandler and Berne, 1979).

To explore this difference more formally, we consider a set of N atoms grouped into molecules in some arbitrary way by harmonic springs. The Cartesian coordinates of the atoms are the $3N$ values $\mathbf{r} = \{r_{i\alpha}\}, i = 1, 2, \cdots N, \alpha = x, y, z$. The system can be described by $3N$ generalized coordinates $\mathbf{q}$ (i.e. the positions of the centre of mass of each molecule, their orientations, and vibrational coordinates). The potential energy of the system can be separated into a part, $\mathcal{V}_s$, associated with the 'soft' coordinates $\mathbf{q}^s$ (the translations,

rotations, and internal conversions) and a part $\mathcal{V}_\mathrm{h}$ associated with the 'hard' coordinates $\mathbf{q}^\mathrm{h}$ (bond stretching and possibly bond angle vibrations)

$$\mathcal{V}(\mathbf{q}) = \mathcal{V}_\mathrm{s}(\mathbf{q}^\mathrm{s}) + \mathcal{V}_\mathrm{h}(\mathbf{q}^\mathrm{h}). \tag{2.162}$$

If the force constants of the hard modes are independent of $\mathbf{q}^\mathrm{s}$ then the canonical ensemble average of some configurational property $\mathcal{A}(\mathbf{q}^\mathrm{s})$ is (Berendsen and van Gunsteren, 1984)

$$\langle \mathcal{A} \rangle_{NVT} = \frac{\int \mathcal{A}(\mathbf{q}^\mathrm{s}) \sqrt{\det(\mathbf{G})} \exp\left[-\beta \mathcal{V}_\mathrm{s}(\mathbf{q}^\mathrm{s})\right] \mathrm{d}\mathbf{q}^\mathrm{s}}{\int \sqrt{\det(\mathbf{G})} \exp\left[-\beta \mathcal{V}_\mathrm{s}(\mathbf{q}^\mathrm{s})\right] \mathrm{d}\mathbf{q}^\mathrm{s}} \tag{2.163}$$

where $\det(\mathbf{G})$ is the determinant of the mass-weighted metric tensor $\mathbf{G}$, which is associated with the transformation from Cartesian to generalized coordinates

$$G_{k\ell} = \sum_{i=1}^{N} \sum_{\alpha} m_i \frac{\partial r_{i\alpha}}{\partial q_k} \frac{\partial r_{i\alpha}}{\partial q_\ell}. \tag{2.164}$$

$\mathbf{G}$ involves all the generalized coordinates and is a $3N \times 3N$ matrix. If the hard degrees of freedom are actually constrained they are removed from the matrix $\mathbf{G}$:

$$\langle \mathcal{A} \rangle^\mathrm{s}_{NVT} = \frac{\int \mathcal{A}(\mathbf{q}^\mathrm{s}) \sqrt{\det(\mathbf{G}^\mathrm{s})} \exp\left[-\beta \mathcal{V}_\mathrm{s}(\mathbf{q}^\mathrm{s})\right] \mathrm{d}\mathbf{q}^\mathrm{s}}{\int \sqrt{\det(\mathbf{G}^\mathrm{s})} \exp\left[-\beta \mathcal{V}_\mathrm{s}(\mathbf{q}^\mathrm{s})\right] \mathrm{d}\mathbf{q}^\mathrm{s}} \tag{2.165}$$

where

$$G^\mathrm{s}_{k\ell} = \sum_{i=1}^{N} \sum_{\alpha} m_i \frac{\partial r_{i\alpha}}{\partial q^\mathrm{s}_k} \frac{\partial r_{i\alpha}}{\partial q^\mathrm{s}_\ell}. \tag{2.166}$$

$\mathbf{G}^\mathrm{s}$ is a sub-matrix of $\mathbf{G}$ and has the dimensions of the number of soft degrees of freedom. The simulation of a constrained system does not yield the same average as the simulation of an unconstrained system unless $\det(\mathbf{G})/\det(\mathbf{G}^\mathrm{s})$ is independent of the soft modes. In the simulation of large flexible molecules, it may be necessary to constrain some of the internal degrees of freedom, and in this case we would probably require an estimate of $\langle \mathcal{A} \rangle_{NVT}$ rather than $\langle \mathcal{A} \rangle^\mathrm{s}_{NVT}$. Fixman (1974) has suggested a solution to the problem of obtaining $\langle \mathcal{A} \rangle_{NVT}$ in a simulation employing constrained variables. A term,

$$\mathcal{V}_\mathrm{c} = \tfrac{1}{2} k_\mathrm{B} T \ln \det(\mathbf{H}) \tag{2.167}$$

is added to the potential $\mathcal{V}_\mathrm{s}$. $\det(\mathbf{H})$ is given by

$$\det(\mathbf{H}) = \det(\mathbf{G})/\det(\mathbf{G}^\mathrm{s}). \tag{2.168}$$

Substituting $\mathcal{V}_\mathrm{s} + \mathcal{V}_\mathrm{c}$ as the potential in eqn (2.165) we recover the unconstrained average of eqn (2.163). The separate calculation of $\mathbf{G}$ and $\mathbf{G}^\mathrm{s}$ to obtain their determinants is difficult. However, $\det(\mathbf{H})$ is the determinant of a simpler matrix

$$H_{k\ell} = \sum_{i=1}^{N} \sum_{\alpha} m_i \frac{\partial q^\mathrm{h}_k}{\partial r_{i\alpha}} \frac{\partial q^\mathrm{h}_\ell}{\partial r_{i\alpha}} \tag{2.169}$$

which has the dimensions of the number of constrained (hard) degrees of freedom.

As a simple example of the use of eqn (2.169) consider the case of a butane molecule (see Fig. 1.10). In our simplified butane, the four united atoms have the same mass m, the bond angles and torsional angles are free to change but the three bond lengths, C_1–C_2, C_2–C_3, and C_3–C_4 are fixed. The 3×3 matrix $\mathbf{H}$ is

$$\begin{pmatrix} 2m & -m\cos\theta & 0 \\ -m\cos\theta & 2m & -m\cos\theta' \\ 0 & -m\cos\theta' & 2m \end{pmatrix}$$

and

$$\det(\mathbf{H}) \propto \left(2 + \sin^2\theta + \sin^2\theta'\right). \tag{2.170}$$

Since θ and θ' can change, $\mathbf{H}$ should be included through eqn (2.167). However, it is possible to use a harmonic bond-angle potential, which keeps the bond angles very close to their equilibrium values. In this case $\mathbf{H}$ is approximately constant and might be neglected without seriously affecting $\langle\mathcal{A}\rangle_{NVT}$. If we had also constrained the bond angles in our model of butane, then $\det(\mathbf{H})$ would have been a function of the torsional angle ϕ as well as the θ angles. Thus $\mathbf{H}$ can change significantly when the molecule converts from the *trans* to the *gauche* state and $\mathcal{V}_c$ must be included in the potential (van Gunsteren, 1980). In the case of a completely rigid molecule, $\det(\mathbf{H})$ is a constant and need not be included. We shall discuss the consequences of constraining degrees of freedom at the appropriate points in Chapters 3 and 4.

2.11 Landau free energy

The idea of a free energy which depends on certain constrained 'order parameters', often termed a 'Landau' free energy because of its prominence in the Landau theory of phase transitions, is very common in molecular simulation. Consider a single parameter $q(\mathbf{r})$, a generalized coordinate, which can be written as a function of all the atomic positions $\mathbf{r}$. (In the most general case, it might also depend on momenta, but the configurational case is by far the most common). Then, quite generally, we may write the probability density function for q in the canonical ensemble

$$\rho(q) = \left\langle \delta[q - q(\mathbf{r})] \right\rangle = \frac{\int \mathrm{d}\mathbf{r}\, \delta[q - q(\mathbf{r})] \exp[-\beta\mathcal{V}(\mathbf{r})]}{\int \mathrm{d}\mathbf{r} \exp[-\beta\mathcal{V}(\mathbf{r})]} \equiv \frac{Q^{\mathrm{ex}}_{NVT}(q)}{Q^{\mathrm{ex}}_{NVT}}. \tag{2.171}$$

Here we have defined the numerator $Q^{\mathrm{ex}}_{NVT}(q)$ as the excess partition function of a system which is restricted to configurations for which the generalized coordinate $q(\mathbf{r})$ takes the value q. The function $\rho(q)$ is, of course, normalized such that $\int \mathrm{d}q\, \rho(q) = 1$. Taking logarithms, and identifying $A = -k_\mathrm{B}T \ln Q^{\mathrm{ex}}_{NVT}$, we may use $Q^{\mathrm{ex}}_{NVT}(q)$ to define a q-dependent Helmholtz free energy, which we usually write as $\mathcal{F}(q)$:

$$\mathcal{F}(q) = A - k_\mathrm{B}T \ln \rho(q) = A - k_\mathrm{B}T \ln\langle\delta[q - q(\mathbf{r})]\rangle. \tag{2.172}$$

The thermodynamic Helmholtz free energy is frequently omitted from this equation, since usually one is interested in changes in $\mathcal{F}(q)$ as a function of q. For example, in discussing phase transitions in the Ising model of ferromagnetic systems, below the critical point, q might be the overall magnetization of the system, and $\mathcal{F}(q)$ would typically have

a double-minimum structure corresponding to stable states with positive and negative values of q (Landau and Lifshitz, 1980; Chandler, 1987). As another example, q might be the coordinate of a molecule as it is moved from an aqueous phase into a non-aqueous phase, or a measure of 'crystallinity' in a nucleus of solid phase growing within a melt (Lynden-Bell, 1995). In many cases, the free-energy barrier between two states characterized by different values of q, is of primary interest. It is easy to extend these definitions to include several order parameters $\{q_i\}$ characterizing the system, in which case one would be interested in a Landau free-energy surface $\mathcal{F}(\{q_i\})$, and possibly in the typical trajectories followed by a system as it makes transitions between basins in this surface. Later chapters will give several examples of the use of simulations to measure these quantities, sometimes using special sampling methods to improve the efficiency. An interesting consequence of eqns (2.171) and (2.172) is that one can define a thermodynamic 'force'

$$-\frac{\mathrm{d}\mathcal{F}}{\mathrm{d}q} = \frac{k_\mathrm{B}T}{\rho(q)}\frac{\mathrm{d}\rho(q)}{\mathrm{d}q} = \left\langle -\frac{\mathrm{d}\mathcal{V}}{\mathrm{d}q} \right\rangle_q$$

where the average is to be taken in the restricted $q(\mathbf{r}) = q$ ensemble, and the quantity being averaged is the 'mechanical' force (the negative of the derivative of the potential energy $\mathcal{V}$ with respect to the coordinate q). Essentially the same definitions appear in the development of coarse-grained effective potentials, discussed in Section 12.7. In that case, the aim is to use the Landau free energy, written as a function of a reduced set of coordinates $\mathbf{q}$, in place of the full potential-energy function.

Often, phenomenological theories predict a particular form for $\mathcal{F}(q)$, which may be tested by simulation. Taking this further, theories may be based on a proposed free-energy *functional* $\mathcal{F}[q(\mathbf{r})]$ depending on an order parameter $q(\mathbf{r})$ which varies from place to place. Here, $\mathbf{r}$ is a position in the fluid, and to make contact with the microscopic description, it is necessary to have a suitable definition of q. For instance, a local property q_i of the molecules may be used to define a collective quantity

$$q(\mathbf{r}) \propto \sum_i q_i \delta(\mathbf{r} - \mathbf{r}_i).$$

Statistical mechanical theories of inhomogeneous systems often suppose that $\mathcal{F}$ depends on $q(\mathbf{r})$ through a local free-energy density $f(\mathbf{r}) = f(q(\mathbf{r}))$, together with terms involving gradients of q with respect to position

$$\mathcal{F}\left[q(\mathbf{r})\right] = \int \mathrm{d}\mathbf{r}\, f\Big(q(\mathbf{r})\Big) + \tfrac{1}{2}\kappa|\boldsymbol{\nabla} q(\mathbf{r})|^2$$

where κ is a phenomenological constant, and we shall see examples of this kind in the following sections.

2.12 Inhomogeneous systems

In most of this book, we will deal with homogeneous fluids, but the methods of liquid-state simulation have been extended with great advantage to consider the gas–liquid and solid–liquid interfaces in a variety of geometries. In this section we will illustrate the

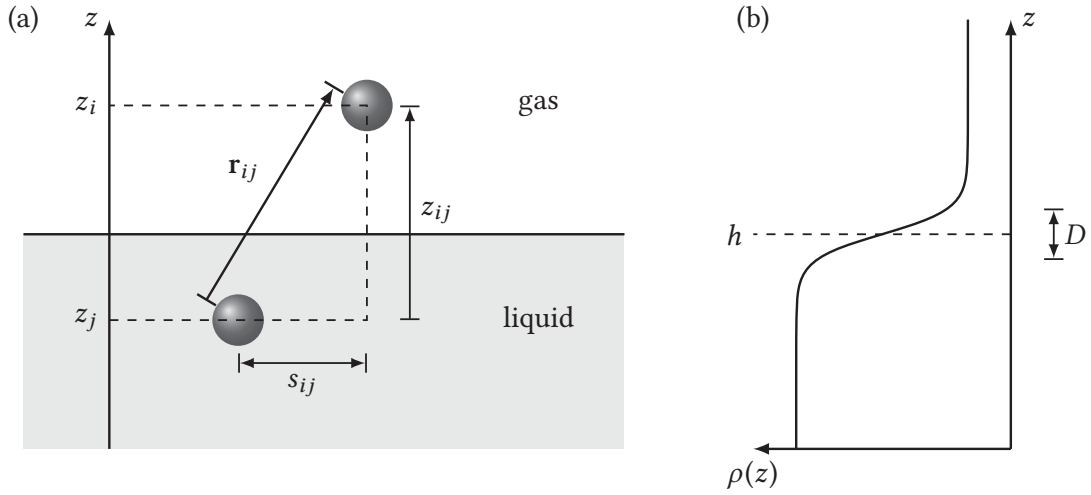

Fig. 2.4 (a) The geometry of the planar interface. (b) Density profile: h is the position (Gibbs dividing surface), and D the thickness, of the interface.

basic ideas with reference to the planar gas–liquid interface (see Fig. 2.4). For a more detailed review of the statistical mechanics of inhomogeneous systems see Rowlinson and Widom (1982), Nicholson and Parsonage (1982), Croxton (1980), and Safran (1994).

For an inhomogeneous fluid in the canonical ensemble, the singlet and pair density distribution functions for a fluid of N atoms at a temperature T are

$$\rho^{(1)}(\mathbf{r}_1) = N \frac{\int \cdots \int \exp(-\beta \mathcal{V})\, \mathrm{d}\mathbf{r}_2 \mathrm{d}\mathbf{r}_3 \cdots \mathbf{r}_N}{\int \cdots \int \exp(-\beta \mathcal{V})\, \mathrm{d}\mathbf{r}_1 \mathrm{d}\mathbf{r}_2 \mathrm{d}\mathbf{r}_3 \cdots \mathbf{r}_N} \tag{2.173}$$

and

$$\rho^{(2)}(\mathbf{r}_1, \mathbf{r}_2) = N(N-1) \frac{\int \cdots \int \exp(-\beta \mathcal{V})\, \mathrm{d}\mathbf{r}_3 \cdots \mathbf{r}_N}{\int \cdots \int \exp(-\beta \mathcal{V})\, \mathrm{d}\mathbf{r}_1 \mathrm{d}\mathbf{r}_2 \mathrm{d}\mathbf{r}_3 \cdots \mathbf{r}_N}. \tag{2.174}$$

For the planar gas–liquid interface, the cylindrical symmetry allows us to express these distribution functions in terms of the height of an atom, z_i, and the distance s_{ij} parallel to the planar interface between the atoms (see Fig. 2.4). Unlike the homogeneous fluid, the singlet particle density depends now on the position in the fluid.

In this case, $\rho^{(1)}$ and $\rho^{(2)}$ can be expressed in terms of the Dirac delta function as

$$\rho^{(1)}(z) = \frac{1}{\mathcal{A}} \left\langle \sum_{i=1}^{N} \delta(z - z_i) \right\rangle \tag{2.175}$$

and

$$\rho^{(2)}(z, z', s) = \frac{1}{\mathcal{A}} \left\langle \sum_{i=1}^{N} \sum_{j \neq i} \delta(z - z_i)\, \delta(z' - z_j) \delta(\mathbf{s} - \mathbf{s}_{ij}) \right\rangle \tag{2.176}$$

where $\delta(\mathbf{s})$ is a two-dimensional delta function in the surface vector $\mathbf{s} = (x, y)$, $s = |\mathbf{s}|$, and $\mathcal{A}$ is the surface area. Note that from this point, we omit the superscript (1) for the

single particle density. $\rho^{(2)}$ is simply related to the radial distribution function

$$\rho^{(2)}(z_1, z_2, s_{12}) = \rho(z_1)\,\rho(z_2)\,g^{(2)}(z_1, z_2, s_{12}). \tag{2.177}$$

In this geometry, $\rho^{(2)}(\mathbf{r}_1, \mathbf{r}_2)$ is often defined in terms of the variables $\{z_1, z_2, r_{12}\}$ where r_{12} is the interatomic separation. In this case (Nicholson and Parsonage, 1982),

$$\rho^{(2)}(z_1, z_2, s_{12}) s_{12} \mathrm{d}s_{12} \mathrm{d}z_1 \mathrm{d}z_2 = \rho^{(2)}(z_1, z_2, r_{12}) r_{12} \mathrm{d}r_{12} \mathrm{d}z_1 \mathrm{d}z_2. \tag{2.178}$$

The symmetry of the planar interface and the condition of hydrostatic equilibrium for the fluid

$$\boldsymbol{\nabla} \cdot \mathbf{P} = 0 \tag{2.179}$$

means that the pressure tensor $\mathbf{P}$ is diagonal and is a function only of z. The independent components are

$$P_{zz}(z) = P_{\mathrm{N}}, \quad \text{normal component, independent of } z, \text{ and} \tag{2.180a}$$

$$P_{xx}(z) = P_{yy}(z) = P_{\mathrm{T}}(z), \quad \text{tangential component, dependent on } z. \tag{2.180b}$$

Usually we define $P_{\mathrm{T}}(z) = \frac{1}{2}\Big(P_{xx}(z) + P_{yy}(z)\Big)$ in this geometry.

Extending the well-known virial equation for the pressure of a homogeneous fluid is not straightforward. There is no unique way of deciding whether the force between two atoms 1 and 2 contributes to the stress across a microscopic element of the fluid at a particular z. An obvious choice (Irving and Kirkwood, 1950) is to say that the forces contribute if the vector $\mathbf{r}_{12}$ intersects the element. There are infinitely many other different possible choices for the contour joining two atoms (Schofield and Henderson, 1982). They all lead to the same value of the normal pressure, but they give rise to different values of the tangential pressure.

With the Irving–Kirkwood (IK) choice, for a fluid with a pair additive potential $v(r)$, an atom at $\mathbf{r}_1$ experiences a force $-(\mathbf{r}_{12}/r_{12})v'(r_{12})$ from an atom at $\mathbf{r}_2$. The probability of there being two atoms at these positions is $\rho^{(2)}(\mathbf{r}_1, \mathbf{r}_2)$, which may be rewritten as $\rho^{(2)}(\mathbf{r} + \alpha\mathbf{r}_{12}, \mathbf{r} + (\alpha - 1)\mathbf{r}_{12})$ where $\alpha = |\mathbf{r} - \mathbf{r}_2|/r_{12}$. Then

$$\begin{aligned}\mathbf{P}(\mathbf{r}) &= \rho(\mathbf{r}) k_{\mathrm{B}} T \mathbf{1} - \tfrac{1}{2} \int \mathrm{d}\mathbf{r}_{12} \frac{\mathbf{r}_{12}\,\mathbf{r}_{12}}{r_{12}} v'(r_{12}) \int_0^1 \mathrm{d}\alpha\, \rho^{(2)}\Big(\mathbf{r} + \alpha\mathbf{r}_{12}, \mathbf{r} + (\alpha - 1)\mathbf{r}_{12}\Big) \\ &= \rho(\mathbf{r}) k_{\mathrm{B}} T \mathbf{1} - \tfrac{1}{2} \int \mathrm{d}\mathbf{r}_{12} \int \mathrm{d}\mathbf{r}_1 \frac{\mathbf{r}_{12}\,\mathbf{r}_{12}}{r_{12}} v'(r_{12}) \int_0^1 \mathrm{d}\alpha\, \rho^{(2)}(\mathbf{r}_1, \mathbf{r}_2) \delta(\mathbf{r} + \alpha\mathbf{r}_{12} - \mathbf{r}_1)\end{aligned} \tag{2.181}$$

where the first term is the ideal gas contribution and $\mathbf{r}_{12} = \mathbf{r}_1 - \mathbf{r}_2$. Eqn (2.181) is general, and for the planar interface, defining $z_{12} = z_1 - z_2$, it can be simplified to

$$\mathbf{P}(z) = \rho(z) k_{\mathrm{B}} T \mathbf{1} - \frac{1}{2\mathcal{A}} \int \mathrm{d}\mathbf{r}_1 \int \mathrm{d}\mathbf{r}_{12} \frac{\mathbf{r}_{12}\,\mathbf{r}_{12}}{r_{12}} v'(r_{12}) \int_0^1 \mathrm{d}\alpha\, \delta(z + \alpha z_{12} - z_1) \rho^{(2)}(z_1, \mathbf{r}_{12}). \tag{2.182}$$

The surface tension, γ, and the position of the surface of tension, z_s, can be calculated from the pressure tensor.

$$\gamma = \int_{-\infty}^{\infty} \mathrm{d}z \left[P_N(z) - P_T(z)\right] \tag{2.183a}$$

$$\gamma z_s = \int_{-\infty}^{\infty} \mathrm{d}z\, z\left[P_N(z) - P_T(z)\right] \tag{2.183b}$$

where the integral will be across one interface from far inside the gas to far inside the liquid. The surface tension is independent of the choice of contour discussed earlier in this section, whereas the surface of tension z_s depends on this choice and is therefore ill-defined from a microscopic perspective.

The surface tension can be obtained directly by calculating the change in the Helmholtz free energy, in the canonical ensemble (Buff, 1952), or the grand potential, in the grand canonical ensemble (Buff, 1955), with surface area at constant volume. In these derivations, all the particle coordinates are scaled as follows

$$\begin{aligned} x_i \to x_i' &= (1+\epsilon)^{1/2} x_i \approx (1+\tfrac{1}{2}\epsilon) x_i, \\ y_i \to y_i' &= (1+\epsilon)^{1/2} y_i \approx (1+\tfrac{1}{2}\epsilon) y_i, \\ z_i \to z_i' &= (1+\epsilon)^{-1} z_i \approx (1-\epsilon) z_i, \end{aligned}$$

where $\epsilon \ll 1$. This means that, to first order, the volume is constant and the change in interfacial area is $\Delta\mathcal{A} = \epsilon\mathcal{A}$. For a pair potential the result for the surface tension is

$$\begin{aligned} \gamma &= \frac{1}{4}\int_{-\infty}^{+\infty} \mathrm{d}z_1 \int \mathrm{d}\mathbf{r}_{12}\left(r_{12} - \frac{3z_{12}^2}{r_{12}}\right) v'(r_{12})\, \rho^{(2)}(\mathbf{r}_1, \mathbf{r}_2) \\ &= \frac{1}{2\mathcal{A}}\left\langle \sum_i \sum_{j>i} \left(r_{ij} - \frac{3z_{ij}^2}{r_{ij}}\right) v'(r_{ij}) \right\rangle. \end{aligned} \tag{2.184}$$

Eqn (2.184) is formally equivalent to eqn (2.183a) for the surface tension.

Finally the chemical potential, μ, in the interface can be calculated by the particle insertion method of Widom (1963)

$$\mu = k_B T \ln \Lambda^3 \rho(z) - k_B T \ln\left\langle \exp[-\beta v_{\mathrm{test}}(z)] \right\rangle \tag{2.185}$$

where Λ is the de Broglie wavelength of the atom and the first term is the ideal gas contribution to μ (compare with eqn (2.75)). $v_{\mathrm{test}}(z)$ is the potential energy of a test particle that is inserted into the fluid at a particular value of z and a random position in the xy plane. This particle does not influence the behaviour of other atoms in the system. Since the system is at equilibrium, μ must be independent of z (the potential distribution theorem). The density varies sharply around the interface, so that changes in the first and second terms in eqn (2.185) with z must cancel.

The interface between two phases will, in general, not be planar, due to fluctuations. Its height, that is, its z-coordinate, will be a function of x and y: we denote this $h(x, y)$. This is illustrated schematically in Fig. 14.3 and, as we shall see in Chapter 14, defining

$h(x, y)$ can be subtle. Suppose that this can be done. Capillary wave theory (Buff et al., 1965; Rowlinson and Widom, 1982; Safran, 1994) is based on a coarse-grained free energy, reflecting the increase in surface area associated with gradients of h:

$$\mathcal{F} = \tfrac{1}{2}\gamma \iint \mathrm{d}x\mathrm{d}y \left[\left(\frac{\partial h}{\partial x}\right)^2 + \left(\frac{\partial h}{\partial y}\right)^2\right] \tag{2.186}$$

where γ is the surface tension; this is expected to be valid for small gradients. Expanding in a Fourier series in the xy-plane, with $\mathbf{k} = (k_x, k_y)$, using Parseval's theorem (see Appendix D), and applying the equipartition principle to the resulting sum of independent Fourier modes gives:

$$\mathcal{F} = \frac{\gamma}{2\mathcal{A}} \sum_{\mathbf{k}} k^2 \left|\hat{h}(\mathbf{k})\right|^2 \quad \Rightarrow \quad \left\langle \left|\hat{h}(\mathbf{k})\right|^2 \right\rangle = \frac{\mathcal{A} k_\mathrm{B} T}{\gamma k^2}. \tag{2.187}$$

where $\mathcal{A}$ is the cross-sectional area. The resulting distribution of heights is Gaussian and the mean-square deviation is

$$\begin{aligned} \left\langle \delta h(x,y)^2 \right\rangle &= \left\langle h(x,y)^2 \right\rangle - \left\langle h(x,y) \right\rangle^2 = \frac{1}{\mathcal{A}} \iint_{\mathcal{A}} \mathrm{d}x\mathrm{d}y \left\langle h(x,y)^2 \right\rangle = \frac{1}{\mathcal{A}^2} \sum_{k_x, k_y} \left\langle \left|\hat{h}(\mathbf{k})\right|^2 \right\rangle \\ &\approx \frac{1}{(2\pi)^2} \iint \mathrm{d}k_x \mathrm{d}k_y \frac{k_\mathrm{B} T}{\gamma k^2} \approx \frac{k_\mathrm{B} T}{2\pi\gamma} \int_{2\pi/L}^{2\pi/a} \frac{\mathrm{d}k}{k} = \frac{k_\mathrm{B} T}{2\pi\gamma} \ln\left(\frac{L}{a}\right). \end{aligned} \tag{2.188}$$

In the second line, the sum over wavevectors is replaced by an integral. It is assumed that the coarse-grained description applies from a small length scale, a, usually taken to be of the order of molecular dimensions, up to L, where $\mathcal{A} = L^2$ (we have assumed a square cross-section). This capillary-wave variation is a major contribution to the observed density profile width D schematically indicated in Fig. 2.4(b); there is also an intrinsic contribution D_0 discussed further in Chapter 14. If one assumes that the two contributions are convoluted together (Semenov, 1993; 1994) the result is

$$\langle D \rangle^2 = D_0^2 + \frac{\pi}{2} \left\langle \delta h(x,y)^2 \right\rangle = D_0^2 + \frac{k_\mathrm{B} T}{4\gamma} \ln\left(\frac{L}{a}\right). \tag{2.189}$$

Equation (2.189) shows how this width increases with increasing transverse box dimensions. Observing these fluctuations gives us a way of determining the surface tension, as an alternative to eqn (2.184).

The ideas described in this section are readily extended to the solid–liquid interface, where the solid can be represented as a static external field or in its full atomistic detail using pair potentials, and for interfaces of different symmetry such as the spherical droplet. We return to this in Chapter 14.

2.13 Fluid membranes

Amphiphilic molecules, consisting of both hydrophobic and hydrophilic sections, may spontaneously self-assemble in water. Often the hydrophobic part consists of one or two hydrocarbon tails, and the hydrophilic part is a charged or polar head group. A variety of

phases may be observed, dependent upon composition and thermodynamic state: micelles, hexagonal arrangements of cylindrical assemblies, bicontinuous cubic phases, and the lamellar phase (Safran, 1994; Jones, 2002). The building block in this last case is the bilayer, consisting of two sheets of amphiphiles arranged tail-to-tail with the head groups on the outside, facing into layers of water. The bilayer itself is also found as the containing wall of spherical vesicles, which have water inside as well as outside. These are sometimes used as very simple models of biological cells, whose surrounding fluid membrane is typically a bilayer of phospholipid molecules, and simulation of these systems is a very active area (Sansom and Biggin, 2010).

The properties of planar bilayer membranes are, therefore, of interest, particularly their elasticity. Usually, a membrane is in a state of zero tension, and deformations away from planarity may be described by a coarse-grained Helfrich free energy (Helfrich, 1973), an integral over the membrane area $\mathcal{A}$

$$\mathcal{F} = \iint_{\mathcal{A}} \mathrm{d}\mathcal{A}\, \tfrac{1}{2}\kappa\Big(C_1 + C_2 - C_0\Big)^2 + \bar{\kappa} C_1 C_2 \tag{2.190}$$

where C_0 is the spontaneous curvature (zero for a symmetrical bilayer), C_1 and C_2 are the two principal curvatures of the membrane surface at a given point, κ is the bending modulus, and $\bar{\kappa}$ is the saddle splay modulus. In the limit of small gradients, a description in terms of the membrane height $h(x, y)$ may be adopted, and

$$\mathcal{F} = \iint \mathrm{d}x\mathrm{d}y\, \tfrac{1}{2}\kappa\Big(\nabla^2 h(x,y)\Big)^2 = \frac{\kappa}{2\mathcal{A}} \sum_{\mathbf{k}} k^4 \Big|\hat{h}(\mathbf{k})\Big|^2$$

where the Laplacian, and the wavevector, are both taken in the xy-plane. Hence, by equipartition of energy

$$\Big\langle \Big|\hat{h}(\mathbf{k})\Big|^2 \Big\rangle = \frac{\mathcal{A} k_{\mathrm{B}} T}{\kappa k^4}. \tag{2.191}$$

If the membrane is under tension, an appropriate term in k^2 must be included, as in eqn (2.187): however, this term would dominate at low k, so it is important that the tensionless state be maintained (see Section 14.6).

The moduli may also, in principle, be related to the pressure tensor profiles, in a manner analogous to equations (2.183) for the surface tension (Szleifer et al., 1990; Marsh, 2007; Ollila and Vattulainen, 2010). For the bilayer as a whole

$$\gamma = \int_{-\infty}^{\infty} \mathrm{d}z \, \Big[P_{\mathrm{N}} - P_{\mathrm{T}}(z)\Big] = 0, \tag{2.192a}$$

$$-\kappa C_0 = \int_{-\infty}^{\infty} \mathrm{d}z \, z\Big[P_{\mathrm{N}} - P_{\mathrm{T}}(z)\Big] = 0, \tag{2.192b}$$

$$\bar{\kappa} = \int_{-\infty}^{\infty} \mathrm{d}z \, z^2\Big[P_{\mathrm{N}} - P_{\mathrm{T}}(z)\Big], \tag{2.192c}$$

where the origin of coordinates $z = 0$ is chosen at the centre of the bilayer, and the pressure components are defined in eqns (2.180). (In the literature, the negative of the pressure, that is, the stress, is frequently used in these equations). The zeroth moment of

the pressure difference vanishes in the tensionless state, while the first moment vanishes by symmetry. The following equations apply to each monolayer constituting the bilayer

$$-\kappa^{\mathrm{m}} C_0^{\mathrm{m}} = \int_0^\infty \mathrm{d}z\, (z - z^{\mathrm{m}}) \Big[P_{\mathrm{N}} - P_{\mathrm{T}}(z) \Big], \tag{2.193a}$$

$$\bar{\kappa}^{\mathrm{m}} = \int_0^\infty \mathrm{d}z\, (z - z^{\mathrm{m}})^2 \Big[P_{\mathrm{N}} - P_{\mathrm{T}}(z) \Big]. \tag{2.193b}$$

The superscript 'm' indicates that these are properties of the separate monolayers. Here, z^{m} is the position of the monolayer 'neutral plane' relative to the mid-plane. The integrals may, in practice, be truncated once $|z|$ exceeds the monolayer thickness, since $P_{\mathrm{T}}(z) = P_{\mathrm{N}}$ in the bulk. The use of these formulae is limited by ambiguities in defining z^{m}, approximations needed to relate monolayer and bilayer properties, and by the fact that κ and C_0 appear together, not separately. Also, as mentioned earlier, the convention adopted for the pressure tensor will affect the profiles. As discussed further in Section 14.6, alternative approaches to the membrane elastic moduli are more reliable.

2.14 Liquid crystals

For liquid crystalline phases, extra care may be needed in measuring some of the standard properties discussed in previous sections, and there are some additional properties that uniquely characterize these phases. For recent reviews see Zannoni (2000), Care and Cleaver (2005), and Wilson (2005).

Liquid crystals have long-range orientational order, and some liquid crystal phases have long-range positional order in certain directions. The simplest case is the *nematic* phase, typically formed by highly elongated (rod-like) or very flat (disk-like) molecules, or by similarly shaped particles in colloidal suspension. The orientational order is characterized by both a magnitude S, the order parameter, and a direction, $\mathbf{n}$, usually called the *director*. The molecules may be irregularly shaped, but we assume that it is possible to identify a principal axis for each one, perhaps related to the inertia tensor, the polarizability tensor, or some other molecular property, and that S and $\mathbf{n}$ will be insensitive to this choice. Let $\mathbf{e}_i$ be the unit vector pointing along this axis. Irrespective of whether the molecules have head–tail symmetry or not, nematic ordering is a second-rank property, and S is given by the average second Legendre polynomial of the cosine of the angle between a typical molecule and the director:

$$S = \frac{1}{N} \sum_{i=1}^{N} \Big\langle P_2(\mathbf{e}_i \cdot \mathbf{n}) \Big\rangle = \left\langle \frac{1}{N} \sum_{i=1}^{N} \tfrac{3}{2} (\mathbf{e}_i \cdot \mathbf{n})^2 - \tfrac{1}{2} \right\rangle = \mathbf{n} \cdot \Big\langle \mathbf{Q} \Big\rangle \cdot \mathbf{n},$$

where we have defined the second-rank orientational order tensor

$$Q_{\alpha\beta} = \frac{1}{N} \sum_{i=1}^{N} Q^i_{\alpha\beta}, \quad \text{where} \quad Q^i_{\alpha\beta} = \tfrac{3}{2} e_{i\alpha} e_{i\beta} - \tfrac{1}{2} \delta_{\alpha\beta}, \quad \text{and } \alpha, \beta = x, y, z. \tag{2.194}$$

Typically $\mathbf{n}$ is unknown at the start of the calculation, but can be defined as the direction that maximizes the value of S. The problem is then reduced to a variational one, which

is solved by diagonalizing $\mathbf{Q}$ (Zannoni, 1979): S turns out to be the largest of the three eigenvalues, and $\mathbf{n}$ is the corresponding director. Because of the second-rank nature of the order, $-\mathbf{n}$ is equivalent to $\mathbf{n}$. Perfect orientational order corresponds to $S = 1$. For an isotropic liquid, $S = 0$, although in practice finite-size effects will result in fluctuations which make $S \sim N^{-1/2}$. Since $\mathbf{Q}$ is traceless, in a uniaxial nematic phase the other two eigenvalues will both be equal to $-\frac{1}{2}S$; once more, we expect finite-size effects to cause some small deviations (Eppenga and Frenkel, 1984).

Once the director has been determined, the single-particle orientational distribution function

$$\rho(\cos\theta) = \rho\Big(\mathbf{e}\cdot\mathbf{n}\Big) = \Big\langle \delta(\cos\theta - \cos\theta_i)\Big\rangle, \quad \text{where} \quad \int_{-1}^{1} \mathrm{d}\cos\theta\, \rho(\cos\theta) = 1$$

may be calculated by constructing a histogram of $\mathbf{e}_i \cdot \mathbf{n}$ values, averaged over particle index i. Alternatively, the function may be expanded in Legendre polynomials P_ℓ

$$\rho(\cos\theta) = \sum_{\ell=0,2,\ldots}^{\infty} \frac{2\ell+1}{2} S_\ell P_\ell(\cos\theta) \quad \text{where} \quad S_\ell = \Big\langle P_\ell(\cos\theta)\Big\rangle;$$

the coefficients are simulation averages of the indicated quantities. Only components with even values of ℓ are non-vanishing.

The pressure tensor in a nematic liquid crystal is isotropic, that is, diagonal with $\langle \mathcal{P}_{\alpha\beta}\rangle = P\delta_{\alpha\beta}$ (Allen and Masters, 1993, appendix). Most other properties are affected by the reduced symmetry. The molecular centre–centre pair distribution function will be a function of components of the separation vector $\mathbf{r}_{ij}$ resolved along and perpendicular to the director. The orientation dependence of pair correlations may be expanded in appropriate angular functions (Zannoni, 2000); the formula is more complicated than eqn (2.106), for isotropic fluids, but similar in concept.

Director fluctuations can be described by a coarse-grained free energy (Oseen, 1933; Frank, 1958) which involves the gradients of $\mathbf{n}$:

$$\mathcal{F} = \int_V \mathrm{d}\mathbf{r}\, \tfrac{1}{2}K_1\Big(\boldsymbol{\nabla}\cdot\mathbf{n}\Big)^2 + \tfrac{1}{2}K_2\Big(\mathbf{n}\cdot\boldsymbol{\nabla}\times\mathbf{n}\Big)^2 + \tfrac{1}{2}K_3\Big|\mathbf{n}\times\Big(\boldsymbol{\nabla}\times\mathbf{n}\Big)\Big|^2.$$

The quantities of interest are the Frank elastic constants K_1, K_2, and K_3. In a frame of reference where the equilibrium director is $\mathbf{n} = (0, 0, 1)$, this may be rewritten in terms of the deviations from equilibrium, $n_x(\mathbf{r})$ and $n_y(\mathbf{r})$. Taking Fourier components (as for the capillary waves of Section 2.12) with $\mathbf{k} = (k_x, 0, k_z)$ chosen in the xz-plane:

$$\mathcal{F} = \frac{1}{V}\sum_{k_x,k_y} \tfrac{1}{2}\Big(K_1k_x^2 + K_3k_z^2\Big)\Big|\hat{n}_x(k_x,k_z)\Big|^2 + \tfrac{1}{2}\Big(K_2k_x^2 + K_3k_z^2\Big)\Big|\hat{n}_y(k_x,k_z)\Big|^2.$$

Applying the equipartition principle

$$\Big\langle|\hat{n}_x|^2\Big\rangle = \frac{Vk_\mathrm{B}T}{K_1k_x^2 + K_3k_z^2}, \qquad \Big\langle|\hat{n}_y|^2\Big\rangle = \frac{Vk_\mathrm{B}T}{K_2k_x^2 + K_3k_z^2}. \tag{2.195}$$

In practice, these fluctuations are determined by measuring fluctuations in $\mathbf{Q}$. We define

$$Q_{\alpha\beta}(\mathbf{r}) = \frac{V}{N}\sum_{i=1}^{N} Q^i_{\alpha\beta}\,\delta(\mathbf{r}-\mathbf{r}_i), \qquad \hat{Q}_{\alpha\beta}(\mathbf{k}) = \frac{V}{N}\sum_{i=1}^{N} Q^i_{\alpha\beta}\,\exp(-\mathrm{i}\mathbf{k}\cdot\mathbf{r}_i).$$

For an axially symmetric phase it is easy to show $Q_{\alpha\beta}(\mathbf{r}) = \frac{3}{2}S[n_\alpha(\mathbf{r})n_\beta(\mathbf{r}) - \frac{1}{3}\delta_{\alpha\beta}]$, so for the off-diagonal elements of interest here $\hat{n}_\alpha(\mathbf{k}) = \hat{Q}_{z\alpha}(\mathbf{k})/(\frac{3}{2}S)$. The Frank elastic constants are obtained by fitting the director fluctuations to eqn (2.195) in the low-k limit (Allen et al., 1996; Humpert and Allen, 2015a).

Transport coefficients may be evaluated using time correlation functions or Einstein relations in the usual way, but taking into account the different symmetry cases (Sarman and Laaksonen, 2011); it is also possible to use nonequilibrium methods, of the general kind discussed in Chapter 11 (Sarman and Laaksonen, 2009a; 2015). The hydrodynamics of nematics is more complicated than that of simple liquids, and in particular the coupling between shear flow and director rotation is of great interest (Sarman and Laaksonen, 2009b; Humpert and Allen, 2015a,b).